Schweizerische Eidgenossenschaft
Confédération suisse
Confederazione Svizzera
Confederaziun svizra

Federal Department of the
Environment, Traffic, Energy and Communications DETEC

Swiss Federal Office of Energy SFOE
Sektion Cleantech

Final Report 28.11.2016

Demonstration of the Ability of Caverns for Compressed Air Storage with Thermal Energy Recuperation

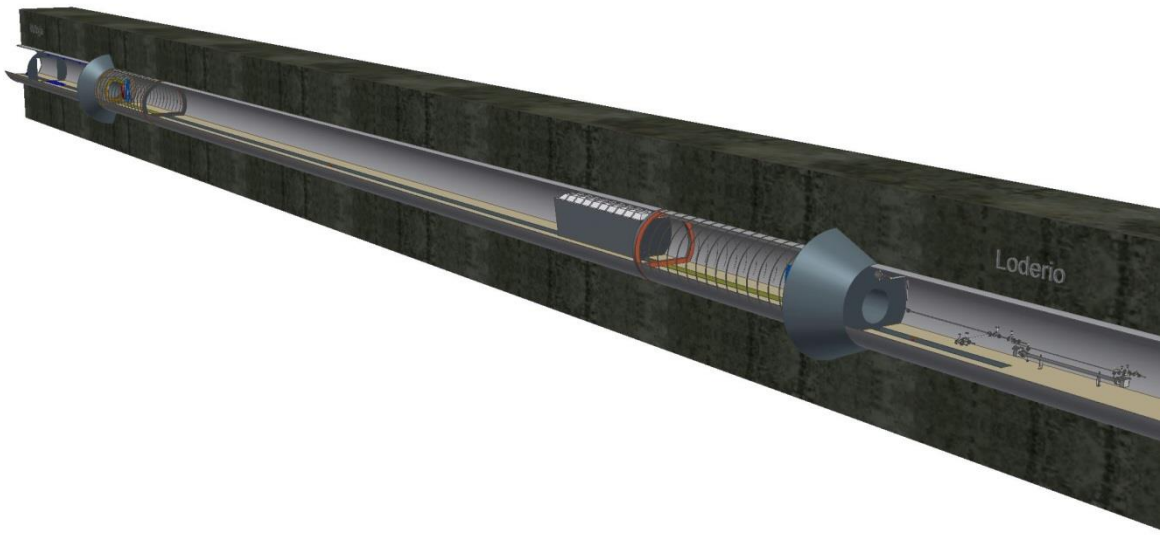

Date: November 28, 2016

Place: Biasca

Contracting body:

Swiss Federal Office of Energy SFOE
Pilot- and Demonstration Programme
CH-3003 Bern
www.bfe.admin.ch

Contractor:

ALACAES SA
Via Industria 10
CH-6710 Biasca
www.alacaes.com

Authors:

Giw Zanganeh, ALACAES SA, giw.zanganeh@alacaes.com

BFE-Programmleitung: Yasmine Calisesi, yasmine.calisesi@bfe.admin.ch
BFE-Projektbegleitung: Roland Brüniger, roland.brueniger@r-brueniger-ag.ch
BFE-Vertragsnummer: SI/501001-01

The authors only are responsible for the content and the conclusions of this report.

Zusammenfassung

Die weltweit erste Pilotanlage eines adiabatischen Druckluftspeichers wurde in den Schweizer Alpen gebaut und getestet, mit dem Ziel die Fähigkeit unbekleideter Kavernen für Druckluftspeicherung und Wärmerückgewinnung zu untersuchen. Die Anlage, die in einem unbenutztem Schutterstollen in den Tessiner Alpen realisiert wurde, wurde für 33 bar und 550 °C heisse Luft ausgelegt. Für die Druckluftspeicherung wurden 120 m des Tunnels mittels zwei 5 m dicke Betonzapfen abgeriegelt und ein Wärmespeicher wurde in dieser Druckzone gebaut. Ausser den beiden Betonzapfen, haben alle Komponenten der Anlage problemlos funktioniert und zufriedenstellende Resultate geliefert. Die Felsdeformierung war minimal und die Verluste vom Fels selber vernachlässigbar. Der Wärmespeicher konnte erfolgreich die Wärme der einströmenden Luft entnehmen und der ausströmenden Luft zurückgeben. Die Betonzapfen haben jedoch grössere Druckverluste verursacht. Die Gesamteffizienz der Anlage belief sich auf 65-79% und die thermische Effizienz des Wärmespeichers auf 75-89%. Die Resultate sind sehr zufriedenstellend in Bezug auf die von ALACAES entwickelten Technologien (der Wärmespeicher und deren Platzierung in der Druckzone) und für den Gebrauch von unbekleideten Kavernen für Druckluftspeicherung.

Abstract

The world’s first pilot plant of an adiabatic compressed air energy storage technology was built and tested in the Swiss Alps with the focus of assessing the ability of unlined caverns for compressed air storage with thermal energy recuperation. The plant was designed to store air at up to 33 bar and 550 °C using an unlined rock cavern. Therefore, 120 m of an unused tunnel was used by building two 5-m thick concrete plugs at the two ends. A proprietary thermal energy storage (TES) system was installed inside the pressure zone to store and release the heat. With exception of the main plugs, all components worked successfully. The rock deformation was negligible and no significant losses were measured from the rock itself. The TES performed as expected and effectively cooled down the incoming air and reheated it during discharging. However, the main plugs showed significant leakages. The plant efficiency was in the range of 65-79% and the TES had a thermal efficiency of 75-89%. The general conclusion of the project is highly favorable for ALACAES’ proprietary technologies, i.e. the thermal energy storage and its performance in a pressurized zone; and for use of unlined rock caverns for compressed air storage.

Riassunto

Il primo impianto pilota mondiale della tecnologia di stoccaggio adiabatico di aria compressa è stato costruito è testato nelle Alpi Svizzeri con lo scopo di esaminare l'adeguatezza di caverne rocciose senza rivestimento per lo stoccaggio di aria compressa e recupero di calore. L'impianto è stato disegnato per lo stoccaggio di aria fino a 33 bar e 550 °C sfruttando una galleria esistente nel canton Ticino. Per questo scopo, una zona di pressione è stata creata, costruendo due tamponi in calcestruzzo con una larghezza di 5 m ciascuno ed una distanza di 120 m fra uno e l'altro. Un stoccaggio termico è stato costruito all'interno della zona di pressione per immagazzinare il calore. Tranne i tamponi, tutti gli altri componenti hanno soddisfatto lo loro scopo senza alcun problema. La deformazione della roccia è stata trascurabile ed entro i limiti previsti e non ci sono state perdite significative dalla roccia stessa. Lo stoccaggio termico ha efficacemente immagazzinato e rilasciato il calore e quindi ha evitato che la temperatura della caverna stessa salisse. Comunque, i tamponi hanno avuto delle perdite importanti. L'efficienza globale dell'impianto è stato di 65-79% e l'efficienza termica dello stoccaggio termico di 75-89%. La conclusione generale è molto favorevole per le tecnologie proprietarie di ALACAES, che sono lo stoccaggio termico è il suo funzionamento all'interno della zona di pressione.

Table of Contents

1. Abbreviations

AA-CAES	Advanced Adiabatic Compressed Air Energy Storage
AET	Azienda Elettrica Ticinese
CAES	Compressed Air Energy Storage
CORE	Federal Energy Research Commission
EMPA	The Swiss Federal Laboratories for Materials Science and Technology
EPFL	École Polytechnique Fédérale de Lausanne
ETH Zurich	Swiss Federal Institute of Technology in Zurich
NFP/NRP	National Research Programme
PLC	Programmable Logic Controller
PREC	Professorship of Renewable Energy Carriers
PSI	Paul Scherrer Institute
SCADA	Supervisory Control And Data Acquisition
SCCER	Swiss Competence Center for Energy Research
SFOE	Swiss Federal Office of Energy
SUPSI	University of Applied Sciences and Arts of Southern Switzerland
TES	Thermal Energy Storage

2. Motivation

Electricity from solar and wind power facilities depends on short term and highly variable meteorological conditions without any firm generation, resulting in peak production periods that can exceed the market demand. Under some conditions electricity produced from wind farms and photovoltaic installations is placed on the market at negative prices due to temporal excess of production[1]. Moreover, it is expected that Germany's wind energy production will more than triple from 182 TWh in 2010 to 581 TWh in 2020[2]. In Switzerland by 2030 the electricity produced by renewable energy carriers has to be increased by 10%[3] with a strong growing trend in intermittent wind and solar power.

Further, the federal energy research Commission CORE asks for "innovative solutions from research and development institutions" and "corresponding pilot and demonstration projects". CORE gives high value to the "integration of Switzerland in the European energy market in all possible scenarios as a strong trading partner" in order to "guarantee the security of energy supply and to optimize the access to renewable energy sources such as wind, solar and geothermal from abroad"[4].

Deutsche Bank states in its report "Moderne Stromspeicher: Unverzichtbare Bausteine der Energiewende" that "on-demand renewable electricity" will become competitive in future and that the Compressed Air Energy Storage (CAES) concept has one of the lowest investment costs (700-1000€/kW)[5].

The ongoing significant investments in Switzerland, Austria and Germany to promote the construction of pumped hydro storage plants, even if temporarily reduced, emphasizes the importance of adequate and large scale storage solutions to satisfy the requirements of the European grid[6].

[1] Energiewirtschaftliches Institut an der Universität zu Köln: Analyse der Ursachen für negative Strompreise am 3./4. Oktober 2009 und möglicher Abhilfemaßnahmen
[2] The European Wind Energy Association Report: EU Energy policy after 2020
[3] Axpo Bericht: Erneuerbare Energien 2009
[4] Konzept der Energieforschung des Bundes 2013 – 2016
[5] Deutsche Bank, DB Research: Moderne Stromspeicher: Unverzichtbare Bausteine der Energiewende, Jan. 2012
[6] Schweiz, Deutschland und Österreich für Ausbau von Pumpspeicherkraftwerken (http://www.uvek.admin.ch/dokumentation/00474/00492/index.html?lang=de&msg-id=44382)

3. Project Goal

- Construction of a test plant to assess the feasibility of an advanced adiabatic compressed air energy storage (AA-CAES) system with thermal energy recuperation.
- For the test plant, a section of a dismissed tunnel excavated between Loderio and Pollegio for construction purposes of the Gotthard Basistunnel was used and adapted correspondingly. The geological conditions of the selected tunnel section might be considered representative for the crystalline portion of the Swiss Alps.
- The aim of the pilot plant is to test and evaluate the design and operational conditions of the different plant components including the behaviour of the rock massif under cyclic charging/discharging operation.

A future scale-up of the AA-CAES system could achieve efficiencies in the range of 75% and thus would be an attractive option to handle power fluctuations in the fast-growing electricity generation from wind and solar photovoltaics

4. Basics

In a CAES plant, electric energy is used to run a compressor or a series of compressors that deliver compressed air at 90-100 bar. During the compression stage, the air heats up according to the following equation:

$T_2 = T_1*(P_2/P_1)^{(n-1)/n}$ (1)

with:

T = Temperature [K]

P = Pressure [Pa]

n = Adiabatic coefficient (~1.4)

For instance, a pressure increase from ambient pressure (1 bar) to 35 bar corresponds to a temperature increase from ambient (25 °C) to 550 °C. The compressed air is then injected and stored in an underground cavern. However, before entering the cavern, the air needs to be cooled down to ambient temperatures in order to decrease the required volume as well as due to safety measures. In conventional CAES plants, isothermal compressors are used where the heat is removed by intercoolers and lost to the environment.

During the peak electricity demand the compressed air is extracted from the cavern and expanded in a turbine that drives a generator. During expansion, the air is cooled again according to equation (1). Starting from ambient temperatures this process would result in exhaust temperatures way below 0°C which would cause damages to the turbine blades. Hence, in the conventional and existing CAES plants, the air is preheated using a gas burner to guarantee safe operation of the turbine, associated with economic and environmental consequences (CO_2-emissions).

The discharging phase is usually carried out until a lower pressure limit in the cavern (for instance 70 bar) is reached. Hence the capacity of the plant is given by the energy that can be extracted between the upper and lower pressure limits.

ALACAES SA, a joint venture between Amberg Engineering AG, Lombardi SA – Ingegneri Consulenti and Airlight Energy Holding SA is aiming to develop an advanced adiabatic compressed air energy storage technology (AA-CAES), to be coupled with thermal storage systems (TES) to store the heat generated in the compression stage to be reused during the expansion stage. This approach will significantly increase the global efficiency of the process up to indicatively 75%, eliminating the need for gas burning and consequently the CO_2-emissions. The concept of the ALACAES plant, comprising the thermal energy storage, is shown in Fig. 4.1

In the ALACAES technology, the TES is placed inside the pressure zone. This has the crucial advantage that the pressure inside and outside the TES is in equilibrium and therefore, the TES tank does not have to bear any pressure except the one from the weight of the storage medium inside of it. This is an important point because the construction of a high-temperature pressure vessel is very complicated and expensive and therefore has a strong effect on the economics of the technology.
For the TES, the proven packed bed of rocks of Airlight Energy Holding SA was used, that was developed partially using funds of SFOE (TP Nr. 8100146-02). The first prototype has been built and tested in 2009/10 providing satisfactory results. Further, a lab-scale prototype has been built and used in collaboration with ETH Zurich to test different configurations in order to improve the efficiency of the TES.

Several doctorate theses at ETH Zurich are dedicated to the TES and AA-CAES design and numerical models have been developed to simulate its behavior[7][8][9][10].

Further, two nation-wide research projects are currently ongoing about the AA-CAES technology in which ALACAES is the main industrial partner: a project of the Swiss Competence Center for Energy Research (SCCER) in collaboration with ETH Zurich, EPFL Lausanne, PSI and SUPSI, as well as an NFP 70 project with the same academic partners.

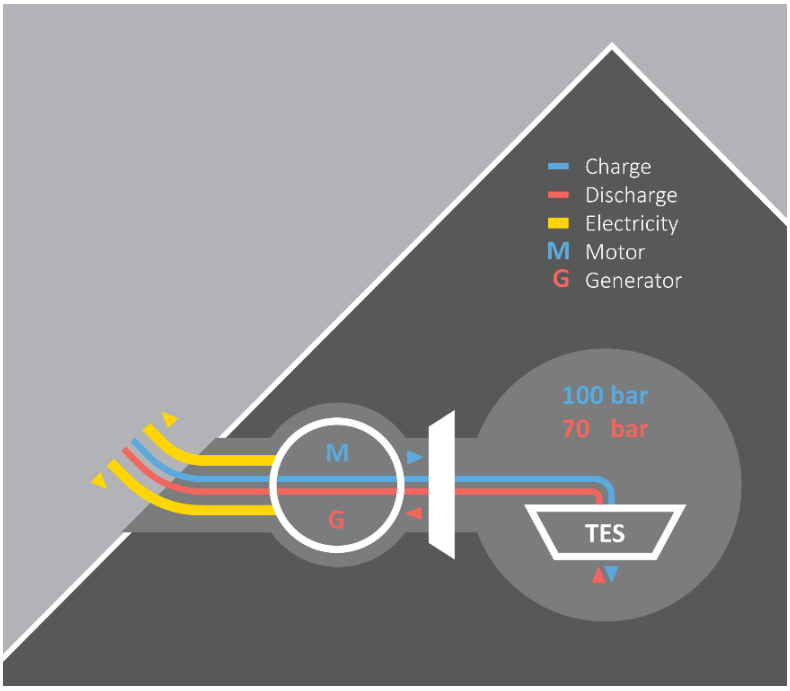

Fig. 4.1: Conceptual depiction of the ALACAES technology. “Motor” includes the compressor train, and “Generator” the expansion turbines.

[7] Hänchen et al., 2011, High-temperature thermal storage using a packed bed of rocks - heat transfer analysis and experimental validation, Applied Thermal Engineering, 31, 1798-1806.
[8] Zanganeh et al., 2011, A packed bed of rocks for high-temperature thermal storage of concentrating solar energy, Proceedings of the World Engineers’ Convention 2011, 4-9 September, Geneva, Switzerland
[9] Zavattoni S., Barbato M., Pedretti A., Zanganeh G., CFD Simulations of a Pebble Bed Thermal Energy Storage System Accounting for Porosity Variations Effects“, SolarPACES2011 Conference, 20-24 September 2011, Granada - Spain.
[10] Zanganeh, G., et al., 2012, Packed-bed thermal storage for concentrated solar power – Pilot-scale demonstration and industrial-scale design. Sol. Energy, Vol. 86, pp. 3084-3098

5. Plant Description

The plant is built in in a presently dismissed tunnel between Pollegio and Loderio (Canton of Ticino) used for muck transport during the excavation works of the Gotthard Basistunnel. The tunnel between Pollegio and Loderio has a total length of 3.16 km with a circular section of 5 m diameter. The main pressure chamber used for the ALACAES plant is 120 m long and starts approximately 800 m after the Loderio side portal (See Fig. 5.1).

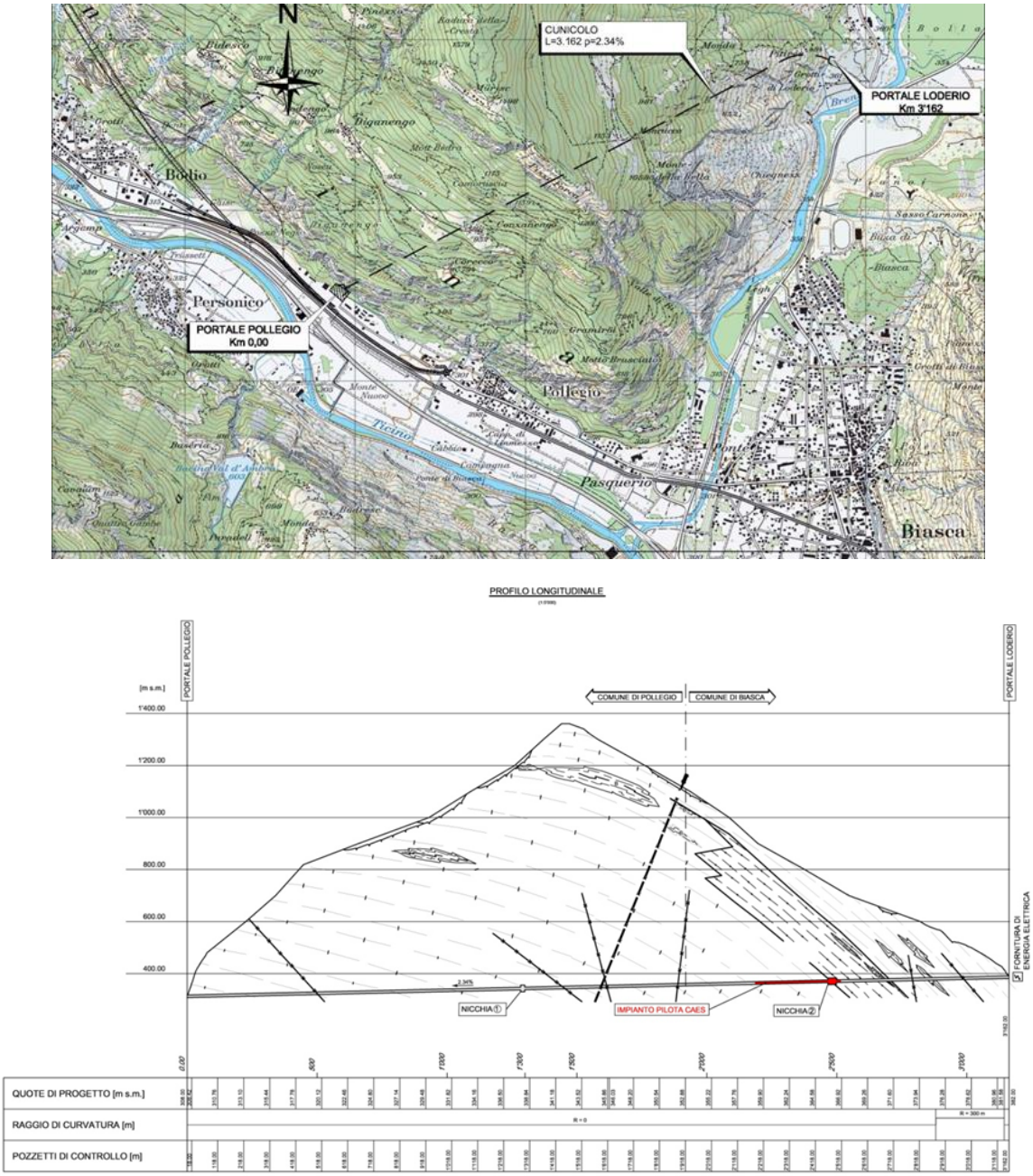

Fig. 5.1: Map view of the tunnel and location of pilot plant within the presently dismissed tunnel

The pilot plant and all of the civil and mechanical components were designed for a maximum operating pressure of 33 bar. This value was chosen to demonstrate the first stage of a commercial, scale-up AA-CAES plant, which would use an existing adiabatic compressor. The limit of commercially available adiabatic compressors is 33 bar and 530-550 °C (e.g. GT26 gas turbine by Alstom/GE). A further pressure increase in the plant would be done by an additional compressor (isothermal or adiabatic) after the air has been cooled down in the TES. Therefore, it was chosen to build the pilot plant to demonstrate this first stage. The findings from the pilot plant can then be used to extrapolate the conclusions to higher operating pressures using geological and rock-mechanics engineering. The TES is in equilibrium with the pressure chamber, and therefore, the pressure is not expected to have an influence on its performance.

The civil works (main plugs, secondary plugs, etc.) were designed by Lombardi SA – Ingegneri Consulenti and executed by Ferrari-LGV consortium. The construction site supervisor for the civil works was Dr. Mauro Pedretti. The mechanical and electrical installations as well as the TES and all the IT and communication concepts, were designed, installed and supervised by ALACAES and its affiliates. The geological monitoring concept was designed, installed and supervised by Amberg Engineering and its affiliates.

The following sections are organized in the physical order of the main plant sections as demonstrated in Fig. 5.2 and describe the installed components in each of these sections.

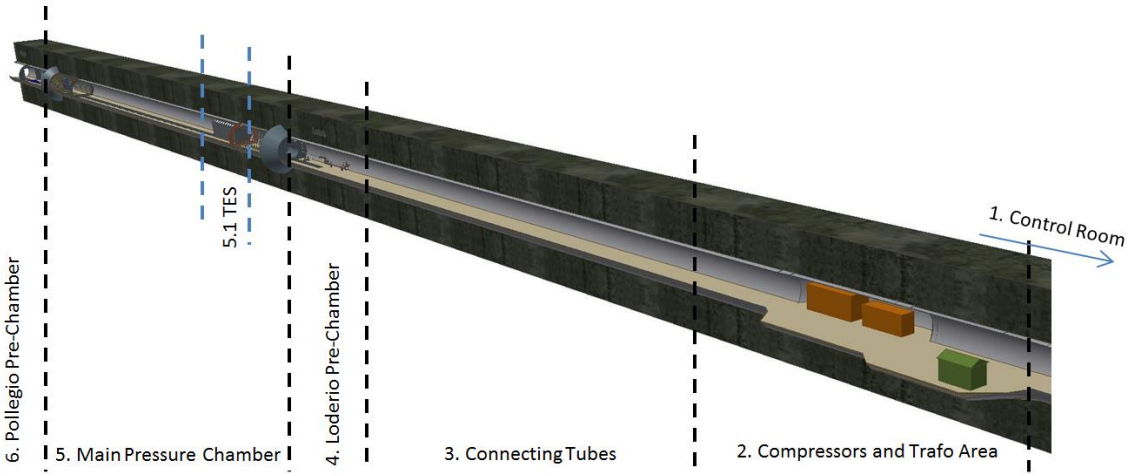

Fig. 5.2: Different sections of the pilot plant.

5.1. Control Room

The control room is the place from which all of the experiments will be executed and is placed outside of the tunnel for safety reasons. All measurement values including camera images are constantly

monitored and registered. If key parameters are surpassed – such as pressure or temperature values – an alarm is triggered and depending on the position and value of the parameter, actions will be taken automatically – shutting down the heater, opening the valves, etc. – in order to neutralize the alarm-causing parameter.

Two “nodes” are placed in the plant that handle the electronic installations via a Programmable Logic Controller (PLC). These nodes read and command all the installed instruments. Node 1 is placed on the Loderio side of the plant, while Node 2 is placed on the Pollegio side. The communication between the two nodes and the control room is done using fiber optic cables. Fig. 5.3 shows the electronic communication concept of the plant, while Fig. 5.4 depicts the control room itself. The Supervisory Control And Data Acquisition (SCADA) system has been setup using Movicon11 from Progea. For additional information please see Section 5.8.

A motion-sensitive security camera is placed at the Loderio portal that monitors the control room and surrounding area. Fig. 5.4 shows an image captured by this camera.

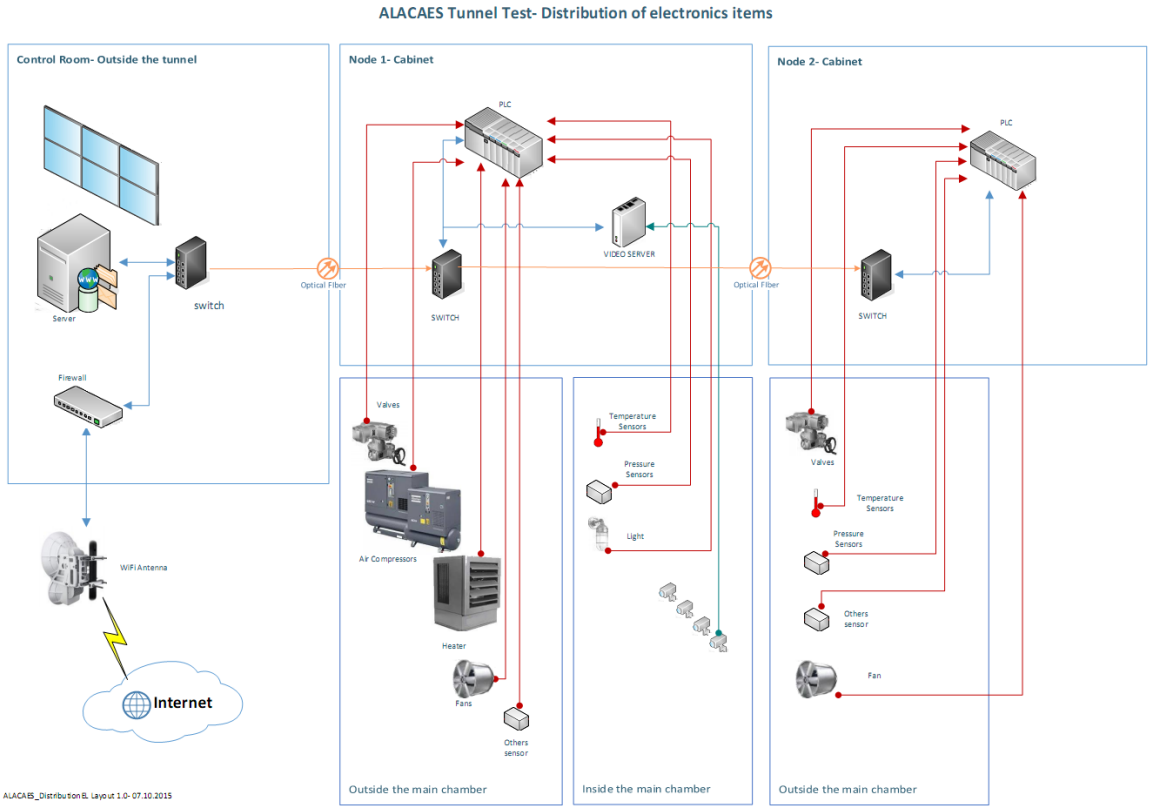

Fig. 5.3: Electronic communication concept of the pilot plant.

Fig. 5.4: The plant is remotely operated from the control room. The control room and its surrounding area are monitored by a security camera (captured image at bottom).

5.2. Compressors and Transformer Area

About 150 meters before the Loderio side main Plug and 650 m from the Loderio side portal, an enlargement exists in the tunnel cross section (See also Fig. 5.2) that was used to place the bulky components of the plant, such as the transformer, the electric boards, the emergency generator and the compressors. Fig. 5.5 shows the components placed on one side of the enlargement:

- The transformer that was provided by Azienda Elettrica Ticinese (AET) due to their interest in the project.
- The main electric board will supply electricity to all the plant components and hosts the programmable uninterruptible power supply that will start the generator in case of emergencies.

- The heater's electric board manages the electric supply and temperature regulation of the heater.
- The emergency generator will be activated automatically in case of emergency or current loss and will operate the necessary valves to put the plant into "safe mode".

Fig. 5.5: From left to right: the transformer supplying the electricity for the whole plant, the main electric board of the plant, the electric board of the heater, and the emergency generator.

Fig. 5.6 shows the compressor train that can provide air at up to 42 bar. The compressor (designated with the letter Z) achieves a pressure of up to 10 bar and the booster (designated with the letter D) will increase the pressure to the required operating pressure.

The compressor and transformer area is monitored by cameras. A typical image captured by these cameras can be seen in Fig. 5.7.

Fig. 5.6: The compressor train that supplies the pressurized air for the pilot plant.

Fig. 5.7: Images captured by the security cameras monitoring the transformer and compressor area.

5.3. Connecting Tubes

The pressurized air is transported from the compressor train to the Loderio side pre-chamber area using 2” steel tubes, as shown in Fig. 5.8.

Fig. 5.8: 2” tubes connect the outlet of the compressors to the Loderio pre-chamber.

5.4. Loderio Pre-Chamber

On the Loderio side pre-chamber, a series of piping systems is installed that is used to charge and discharge the plant. A schematic is shown in Fig. 5.9.

The heater is placed here to heat up the air and hence simulate - together with the compressor train - an adiabatic compressor. A bypass-pipe is installed in order to be able to run pressure-only tests, i.e. without addition of heat, in order to examine the rock behaviour. A non-return valve before the heater ensures that the compressor train is not damaged in case of valve failure.

On the charging side, a gate valve is placed in series with a globe valve as a redundancy. Using the globe valve, the mass flow can be regulated.

For discharging, a T-branch allows the air to enter two, parallel installed valves (one globe and one gate) for faster discharging rates. The discharging air enters an industrial silencer to be cooled down and diffused before entering the environment.

The piping section after the heater is insulated with ceramic wool and rock wool in order to reduce heat losses.

The whole piping is placed on rolling structures in order to allow for thermal expansion of the pipes.

The temperature and pressure are measured at several points in the piping system and the inlet and outlet mass flow rates are measured using differential pressure sensors and a Pitot tube.

The feeding pipe that passes through the main plug is actively (air cooling) and passively (microporous insulation) cooled in order to avoid over-heating of the concrete plug. The temperature around the feeding pipe is measured and monitored at several positions inside the concrete.

Further, cameras observe the installations and a fonometers registers the noise level after the silencer.

Fig. 5.10 and Fig. 5.9 depict the above described installations. These installations are also monitored by security cameras. An image captured by this camera is shown in Fig. 5.11.

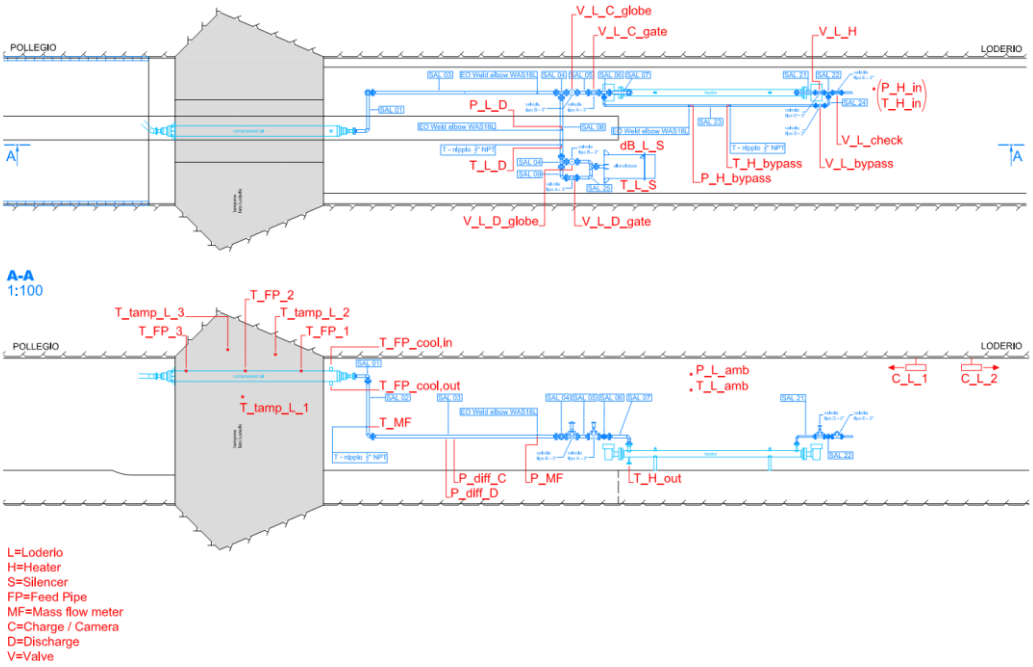

Fig. 5.9: Schematic of the air-flow process installations and sensors in the Loderio pre-chamber.

Fig. 5.10: Picture of the installed components on the Loderio side pre-chamber.

Fig. 5.11: An image captured by the Loderio side security camera

Node 1, the control panel that manages all of the instruments and sensors on the Loderio side and inside the main pressure chamber is placed in the vicinity of to the plug. A depiction is shown in Fig. 5.12.

Fig. 5.12: Node 1 electric board and control panel that manages all the instruments and sensors on the Loderio side, according to Fig. 5.3.

5.5. Main Chamber

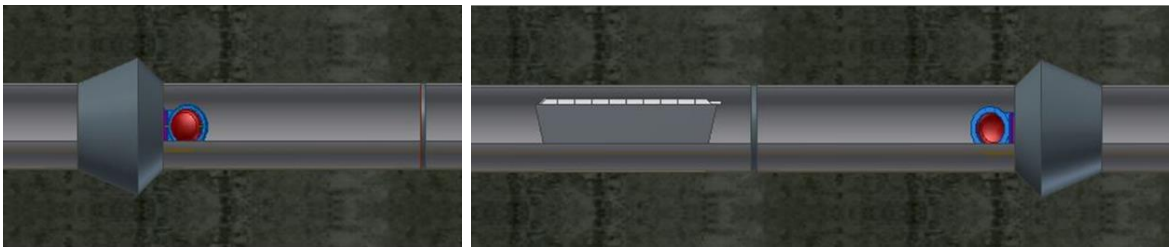

Fig. 5.13: Schematic of the main chamber depicting the concrete plugs, their steel access doors, and the Thermal Energy Storage (TES).

Concrete Plugs

The main pressure chamber is 120 m of the tunnel that is confined by two 5 m-thick concrete plugs. The plugs have a double-conical shape in order to distribute the pressure in the plant onto the mountain's rock massif (See Fig. 5.13). The plug area was widened using explosives to accommodate the plug shape (See Fig. 5.14).

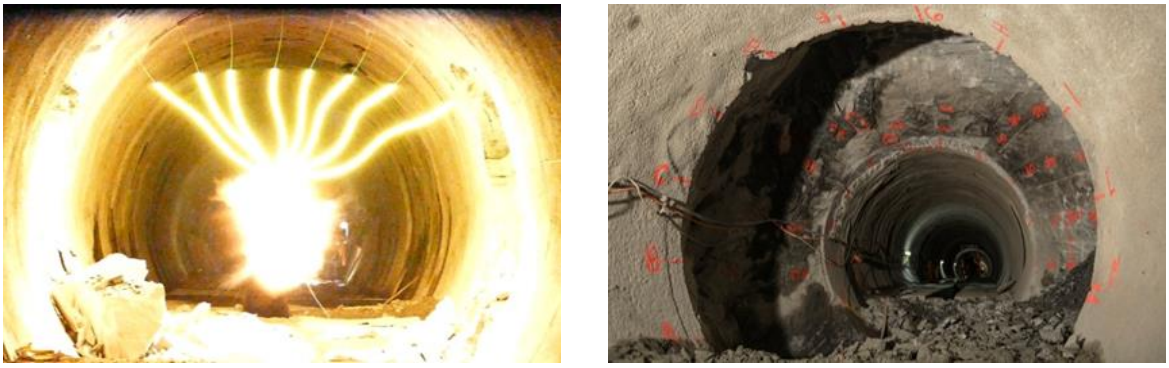

Fig. 5.14: Using explosives to widen the zone of the main concrete plugs and the resulting shape.

In order to understand the rock behavior during grouting (permeability, rock resistance, and fracture characteristics), Lugeon tests were performed with water as the testing fluid before the consolidation grouting. The results showed low permeability of the rock for water.

The consolidation grouting followed, for which three series of 16 radial boreholes were created, each 15 m deep inside the rock (See Fig. 5.15). The boreholes were then used to pump special micro-cement mixtures in the rock mass with a maximum pressure of 70 bar using the GIN methodology, filling eventual fissures in the rock (Fig. 5.16). This procedure is derived from dam construction and is supposed to create an impermeable screen around the main plug in order to decrease the probability of air leakage.

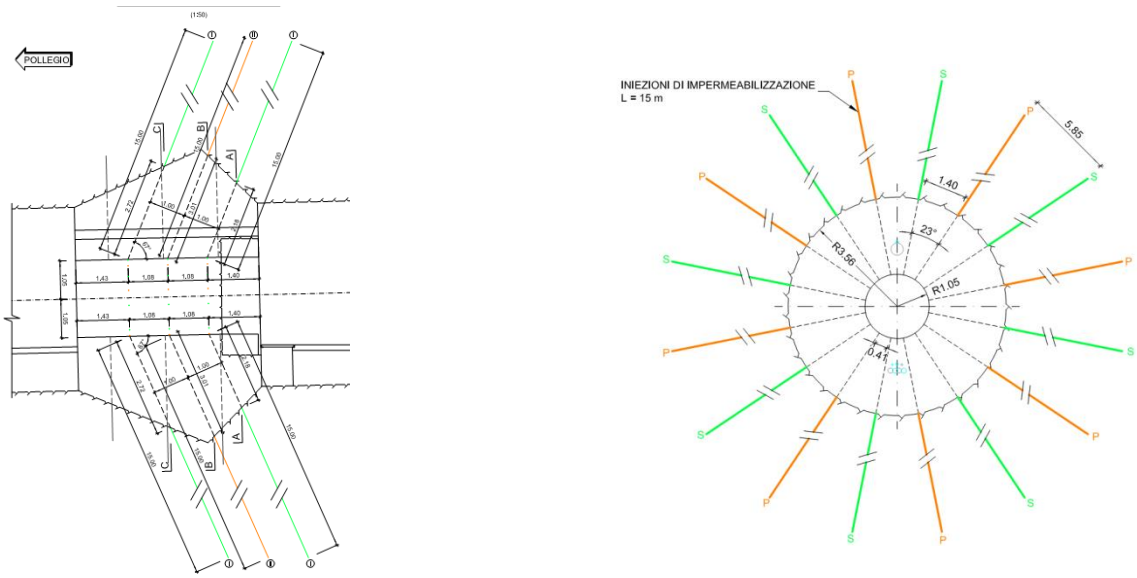

Fig. 5.15: Schematic of the boreholes for the consolidation grouting.

Fig. 5.16: The machine used for the consolidation grouting that can handle 4 injections simultaneously (left) and an injection taking place in the rock mass (right)

The plug area is then armored, a steel tube is placed in the middle of the plug to grant access, thermocouples, strain gauges and pressure cells (stress cells) are placed in the plug, and the volume is consequently filled with approximately 185 m3 of self-compacting concrete. Polystyrene tubes are placed between the boreholes of the consolidation grouting and the central cylinder that are removed after concreting and used to execute a second round of consolidation/contact grouting (See Fig. 5.17).

Fig. 5.17: Reinforcement and preparations to place the center tube that grants access to the plant (left) and the radially placed polystyrene cylinders between the center tube and the rocks (right). The polystyrene cylinders were removed after the concreting and the remaining holes were used to execute a final round of consolidation grouting.

The inside face of the plug (facing the pressure-zone) was closed using 8-mm thick steel plates that were seamlessly welded to each other. The internal steel lining of the plug is necessary to guarantee air-tightness.

The steel access doors are incorporated on the pressure side of the main plug in a second concreting phase. Pressure (stress) cells between the two concreting phases monitor the acting pressure between them.

The above steps were executed almost identically for both plugs.

Fig. 5.18: The steel door incorporated on the pressure side of the plug.

Central Canal

A central canal is dug in the tunnel that hosts a series of 4 pipelines carrying cavern water, plant water, signal cables and a current cable (See. Fig. 5.19). While the cavern water pipeline is open towards the pressure chamber, the other pipelines have an internal pressure equal to ambient pressure and an external pressure equal to the plant operating pressure. Therefore, the pipe thickness was calculated in-house using finite element analysis of the tubes under the operating conditions. Due to the external pressure acting on the tubes, commercial axial compensators could not be used as they are designed for internal pressure only. Therefore, special attention had to be paid to the piping temperature during operation to avoid thermal expansion and hence cracking of the pipes that could lead to a catastrophic failure of the plant.

Fig. 5.19: 3D depiction of the tubes in the center canal (left) and bolting of one of the pipelines.

Sealing Membranes

Two ring-like concrete structures were constructed at a distance of 15 m from each main plug. These intermediate plugs are used to hold a fire resistant, high-strength glass fiber membrane that will cover the rock surface between the main and the intermediate plug (See Fig. 5.20). This is the only area that has an impermeable lining in the tunnel in order to reduce air leakages through the plug area. The consolidation grouting presented above should, however, have the main contribution in avoiding air

leakages. The side of the intermediate plug that faces the main plug is made of steel plates to ensure further air-tightness of the zone

Fig. 5.20: Loderio Side (left) and Pollegio side (right) plugs and steel access doors. The white fire-resistant membrane covers the first 15 m after each plug in order to avoid air leakage from these areas.

Main Chamber Instruments

The schematic of the installed components and sensors in the main pressure chamber is shown in Fig. 5.21.

Two pressure sensors monitor the pressure and several resistance temperature detectors measure the air, rock and piping temperature as well as the temperature inside and around the TES.

4 pressure-resistant cameras and 5 pressure-resistant LED lights allow the monitoring of the main pressure chamber from the control room during the tests (see Fig. 5.22). Fig. 5.23 shows the images captured by the high pressure cameras.

The signal of the instruments in the pressure zone arrives via cables to flanges equipped with high-pressure connectors that are installed on the signal pipeline. These connectors transfer the signal from the high pressure zone to the ambient pressure zone without the possibility of air passage (see Fig. 5.22).

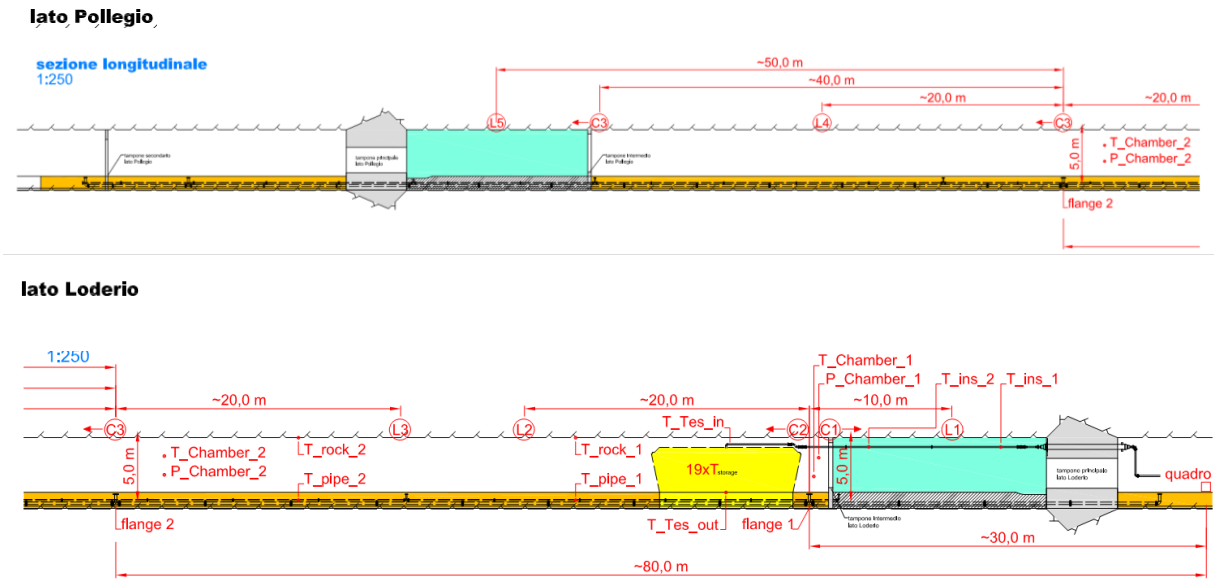

Fig. 5.21: Schematic of the main chamber and the installed sensors.

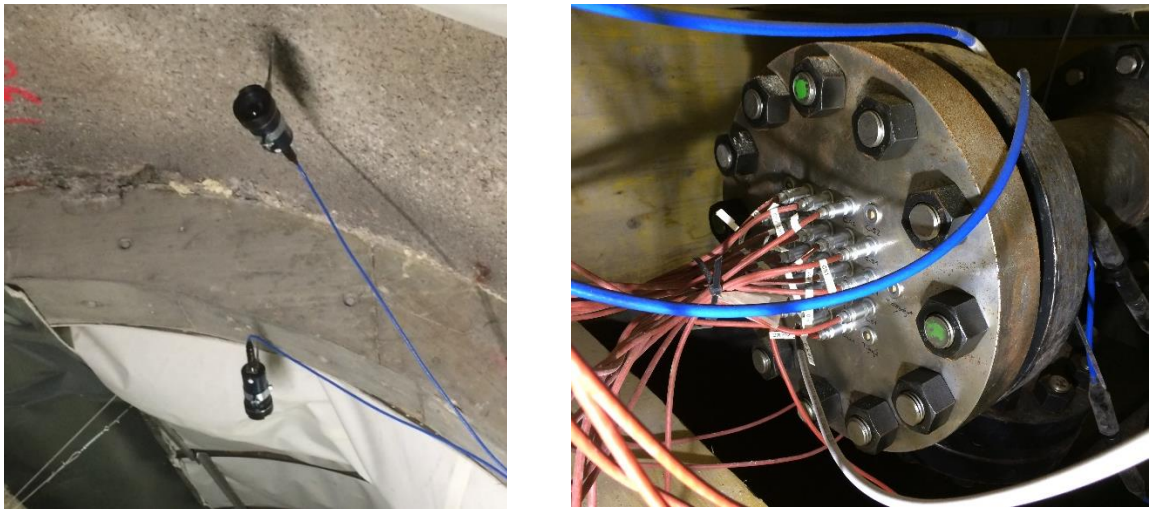

Fig. 5.22: Pressure-resistant cameras C1 and C2 according to the schematic in Fig. 5.21 (left) and one of the flanges equipped with pressure connectors taking the signals out of the pressure zone (right)

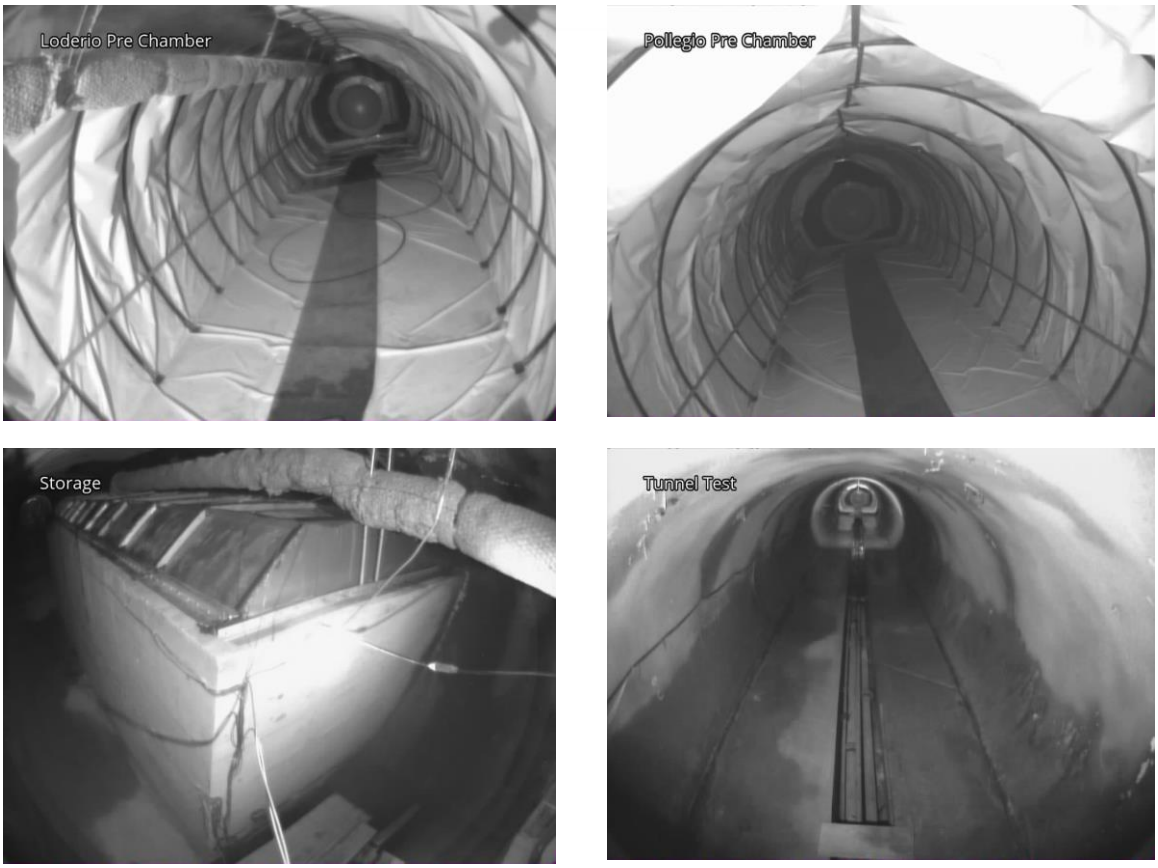

Fig. 5.23: Images captured by the high pressure cameras in the pressure zone. Clockwise from top left: the Loderio side plug, the membrane and insulated process air pipe; the Pollegio side plug and the membrane; the tunnel area, the thermal energy storage.

Thermal Energy Storage (TES)

The thermal energy storage (TES) is one of the key components of the plant as it allows the separation of heat from the compressed air and therefore safe storage of air in the cavern. The tank of the TES is 10 m long, 3 m high and about 2.8 m wide and will store the heat of the incoming air in a packed bed of rocks. The outer tank is made of CC 25/30 concrete enhanced with poly-propylene fiber. The fiber evaporates the first time the concrete walls are heated up and hence helps avoiding the creation of fissures in the concrete due to thermal stress. The inside of the concrete tank is lined with microporous thermal insulation and proprietary technology, high-performance concrete and filled with ~2 cm diameter sedimentary rocks. The temperature inside the TES, on the cover, at the inlet and outlet, as well as on the piping insulation is measured using custom-made Pt100 resistance temperature detectors.

The rocks that are filled in the TES will act as the heat storage medium, by cooling down the incoming air during charging and heating it up during discharging. They were delivered from the Rafzerfeld area in Zurich. Their thermo-physical properties such as thermal conductivity, heat capacity, and density

have been experimentally measured in a previous campaign at EMPA in Dübendorf. The rocks have a total volume of 43 m3 and have a mean diameter of approximately 2 cm.

Insulated pipes connect the feeding pipe to the storage entrance at its top. Axial compensators are placed in the piping in order to compensate the thermal expansion of the tubes.

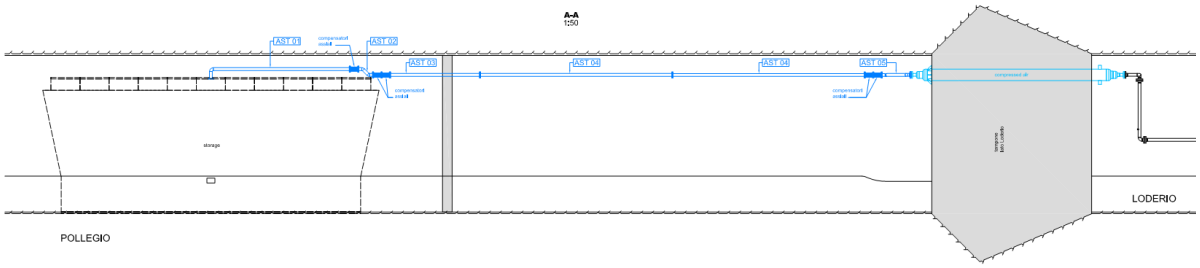

Fig. 5.24: Schematic of the Thermal Energy Storage (TES) placed in the plant.

Fig. 5.25: The thermal energy storage stores and releases the heat from the incoming process air and is a key component of the technology, allowing the exploitation of the produced heat during compressions.

5.6. Pollegio Pre-Chamber

A pre-chamber on the Pollegio side is constructed that allows the measurement of leakages from the Pollegio side main plug. For this, a small secondary plug was constructed 20 m after the Pollegio side main plug and an air-tight fire-resistant door is installed in it. A single tube leaves the pre-chamber which is used to measure the air leaking from the Pollegio plug (designated with AC13 and AC14 in Fig. 5.28). An anemometer was installed at the end of the tube that measures the air velocity and temperature. This data is then used to measure the mass flow rate of air. Unfortunately, due to the installations on the Loderio side, it was not possible to construct a similar air-tight pre-chamber there.

Also an additional discharging piping is installed on this side for faster discharging during normal operation or emergencies. Like on the Loderio side, a silencer diffuses the outflowing air at the end of the piping system. Pressure, temperature, and noise are measured at various positions.

A schematic of the installations is depicted in Fig. 5.26 while a picture is shown in Fig. 5.27. Like on Loderio side, the Pollegio side installations are monitored by a security camera. Fig. 5.30 shows an image captured by said camera.

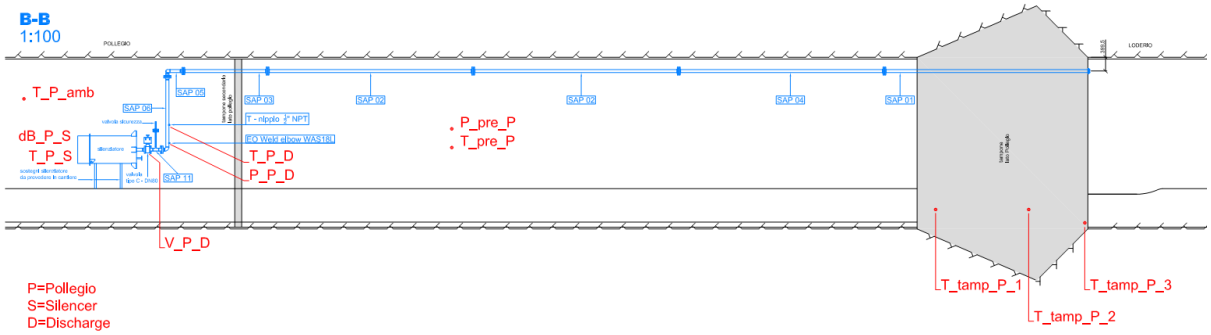

Fig. 5.26: Schematic of the Pollegio side installations and sensors.

Fig. 5.27: The Pollegio side installations corresponding to the schematic in Fig. 5.26.

The continuous water flow from the mountain needs to be guided out of the pressure cavern without releasing the pressurized air at the same time. In order to do so, a 5 m-long, 0.5 m-dia. water tank is installed with valves on both sides that allows the management of the water flow: the outlet valve is closed and the inlet is open until the tank is filled. A water-level sensor detects when the tank is full

which releases a command by the PLC to close first the inlet valve and consequently - after 10 seconds delay - open the outlet valve. Once the lower water-level detects that the tank is empty, the opposite is done until the tank is full again.

The water management system is depicted in Fig. 5.28 and a picture is shown in Fig. 5.29.

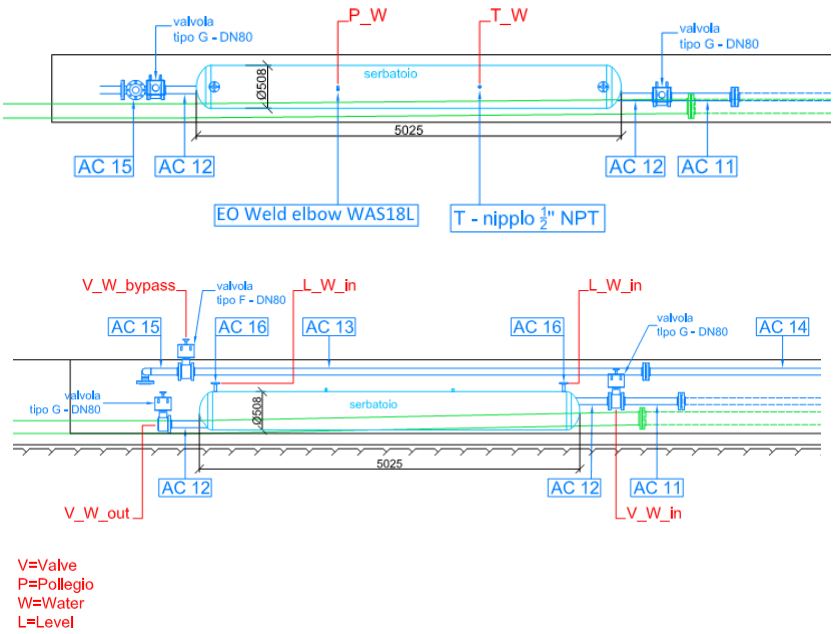

Fig. 5.28: Schematic of the Pollegio side water management system and sensors.

Fig. 5.29: The Pollegio side water management system and sensors.

Fig. 5.30: Image captured by the Pollegio side camera.

The sensors and instruments on the Pollegio side are managed by “Node 2”, depicted in Fig. 5.31.

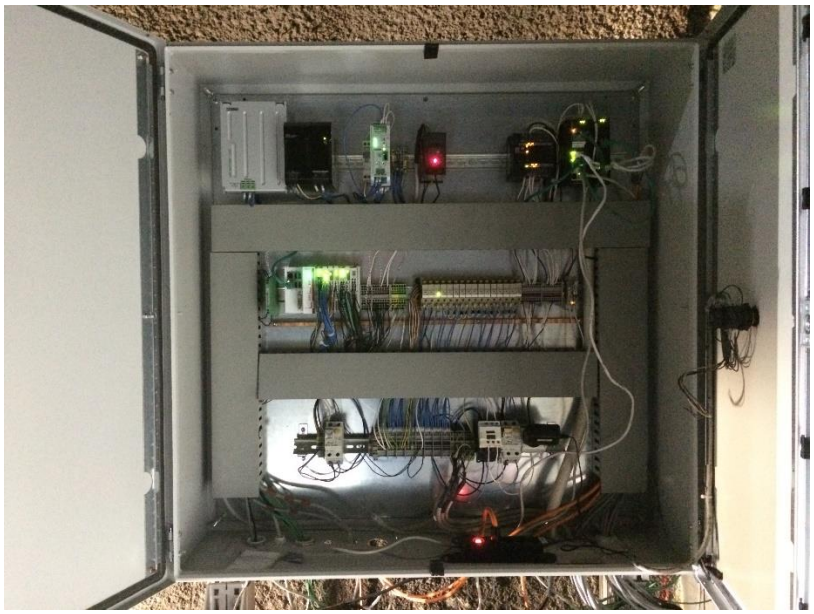

Fig. 5.31: Node 2 electric board and control panel that manages all the instruments and sensors on the Pollegio side, according to Fig. 5.3.

5.7. Geological Monitoring

The geological monitoring of the plant is executed by Amberg Technologies AG, an ALACAES shareholder. A schematic of the installed sensors is shown in Fig. 5.32.

Two 4-point extensometers are placed up to 20 m inside the rock behind each plug (red dots in Fig. 5.32). These extensometer measure the displacement of the rock caused by the acting pressure in the plant.

Two stress cells are placed between the two concreting phases of each plug. On the Loderio side, also two stress cells are placed at the interface of plug and mountain (turquoise dots in Fig. 5.32)

A geophone is installed on the pressure free side of the Loderio plug that measures vibrations caused by the plant operation (green dot in Fig. 5.32).

Fig. 5.33 depicts the Loderio side and Pollegio side Tachymeters that monitor the plug displacement using glass prisms installed on the plugs' surfaces (magenta dots on Fig. 5.32).

In three sections inside the pressure zone, surface extensometers are placed that measure the displacement of the cavern wall in 3 directions, as shown with the yellow dots in Fig. 5.32. Fig. 5.34 shows the surface extensometers in one of the sections as installed in the plant.

Further, strain gauges are fixed on the armoring of the plugs to measure deformations.

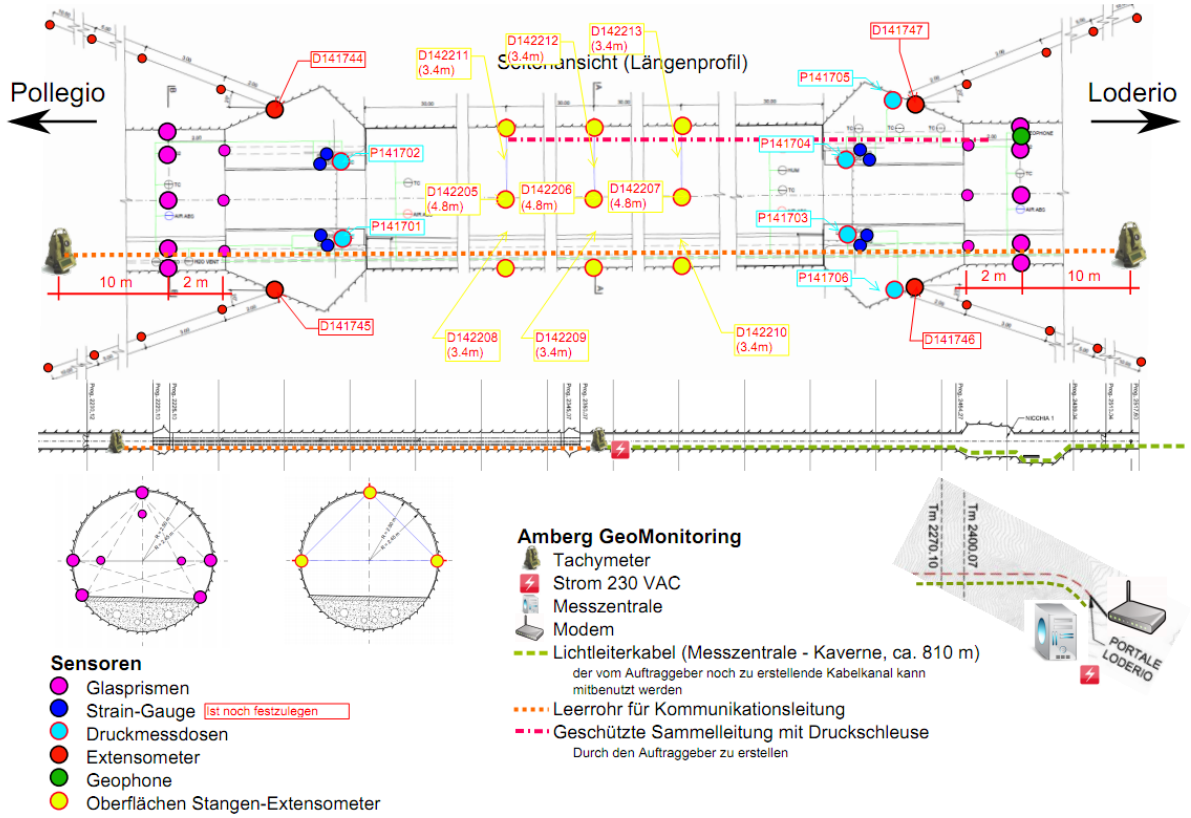

Fig. 5.32: Schematic of the geological monitoring concept of the plant.

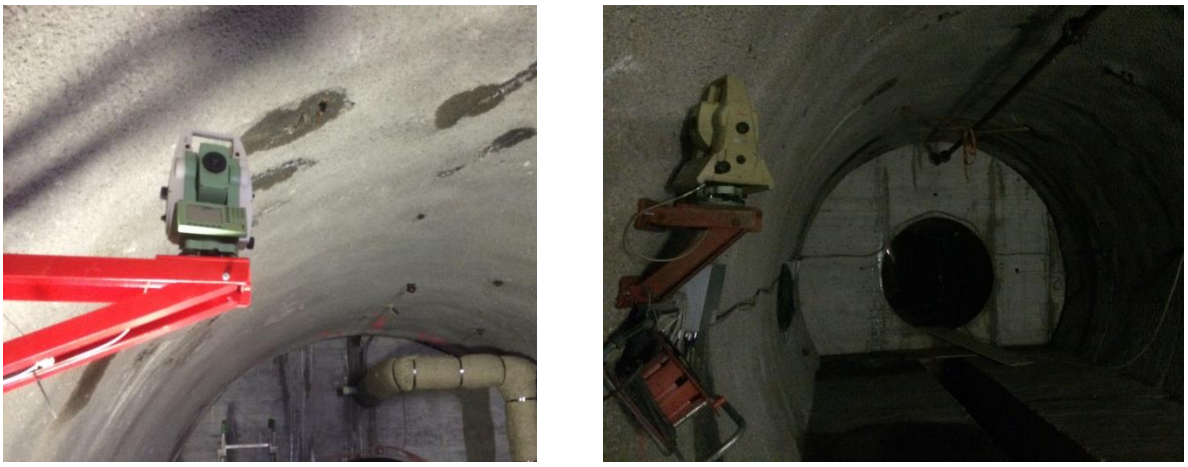

Fig. 5.33: The Loderio side (left) and Pollegio side (right) tachymeter that monitor the movement of the plugs.

Fig. 5.34: The surface extensometers measuring the cavern wall movement in three directions.

5.8. Data Acquisition, Command and Monitoring

As mentioned in Section 5.1, the plant is monitored and commanded using a SCADA system. All the programming was done by ALACAES in-house by Mr. Luciano Serio. The SCADA consists of different pages that each monitor and command a different section of the plant.

During plant operation, an email is generated automatically every hour with the most important plant parameters, images captured by the various cameras, as well as the historical evolution of each parameter in the last 24 hours, and sent to the plant supervisors. Although the plant is never unsupervised during operation, this allows a convenient and uncomplicated supervision and additional control of the plant performance 24/7.

The gathered data is backed up daily on two separate servers and a confirmation email is sent when the backup is completed.

Screenshots of the most important SCADA pages with a short description are provided in the following.

Home/Overview: Gives an overview of the most important parameters of the plant

Heater: Turn the heater on/off, set the temperature set point and monitor the electric consumption of the heater

Air Compressors: Overview of the compressor and booster with their most important parameters. Alarms turn on if a threshold is surpassed for any parameter. The pressure set point of the plant can be determined here. The compressors automatically turn off if the set point is reached

Geo Monitoring: Overview of the values of the geo-monitoring installations. This data is provided by Amberg Technologies SA that is in charge of the geological monitoring of the plant. The data is automatically transferred and elaborated by SCADA. Alarms appear if certain parameters exceed set thresholds or are not up-to-date. For each instrument, the historical data can be loaded in a separate page by clicking the “Historical Data” button.

Storage: Overview of the temperatures in and around the TES as well as the mass flow rate. Graphs depict the relevant temperature distributions in the TES. The historical data can be loaded in a separate page.

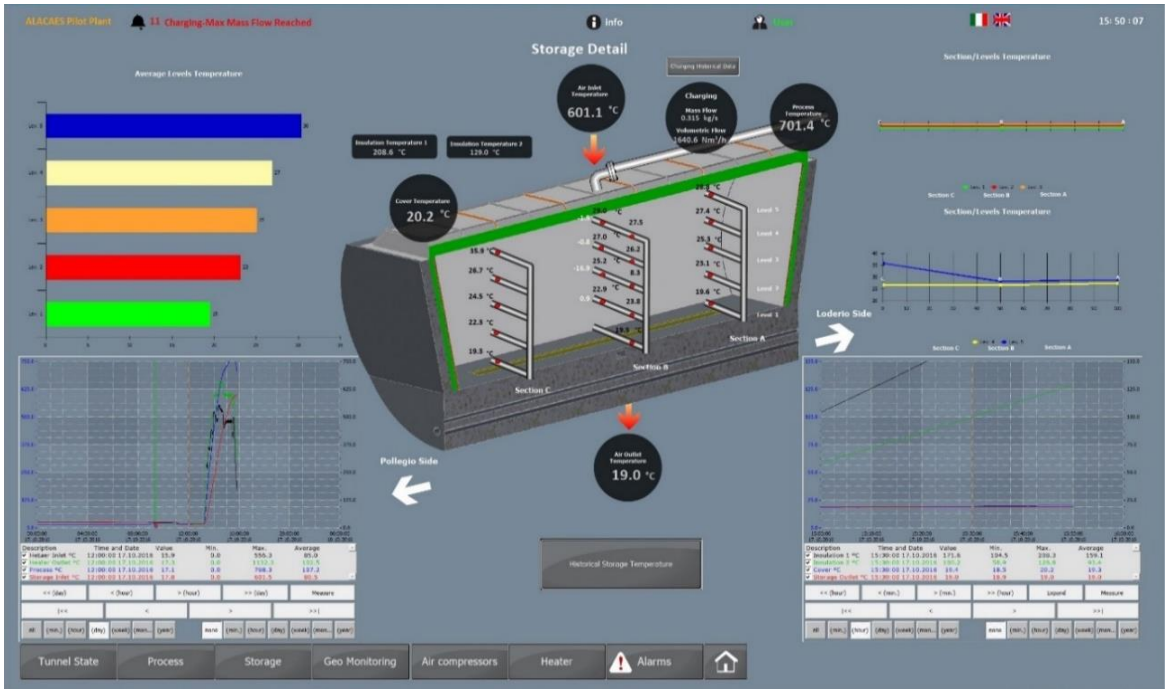

Process: Basically the main page of the SCADA. All of the valves can be operated from this screen, the compressors turned on/off, the heater turned on/off, the mass flow monitored, the water management system is monitored and managed, tunnel lights turned on/off, the ventilation system controlled and the pressure monitored at the same time.

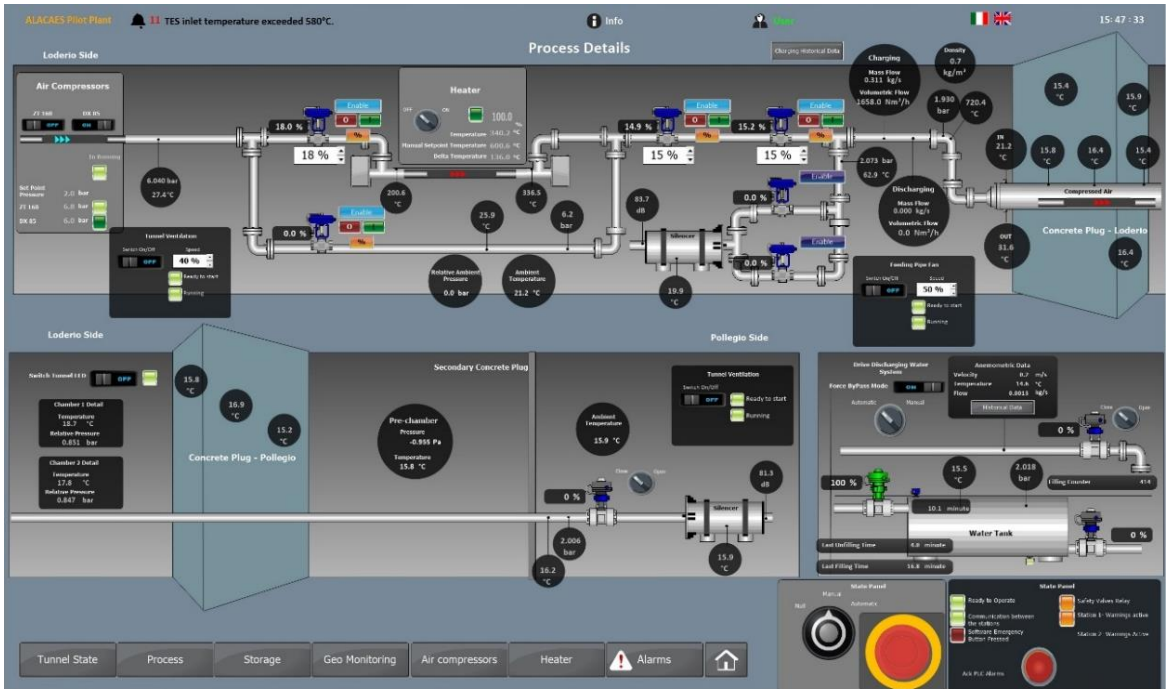

Tunnel State: Shows an overview of the pressure chamber including the TES and the plugs' temperatures. The pressure profile is compared to the theoretical pressure profile in real time in order to assess discrepancies caused by leakages.

Main Power Supply: Shows the overall electrical consumption of the plant and the power data such as frequency, voltage and current.

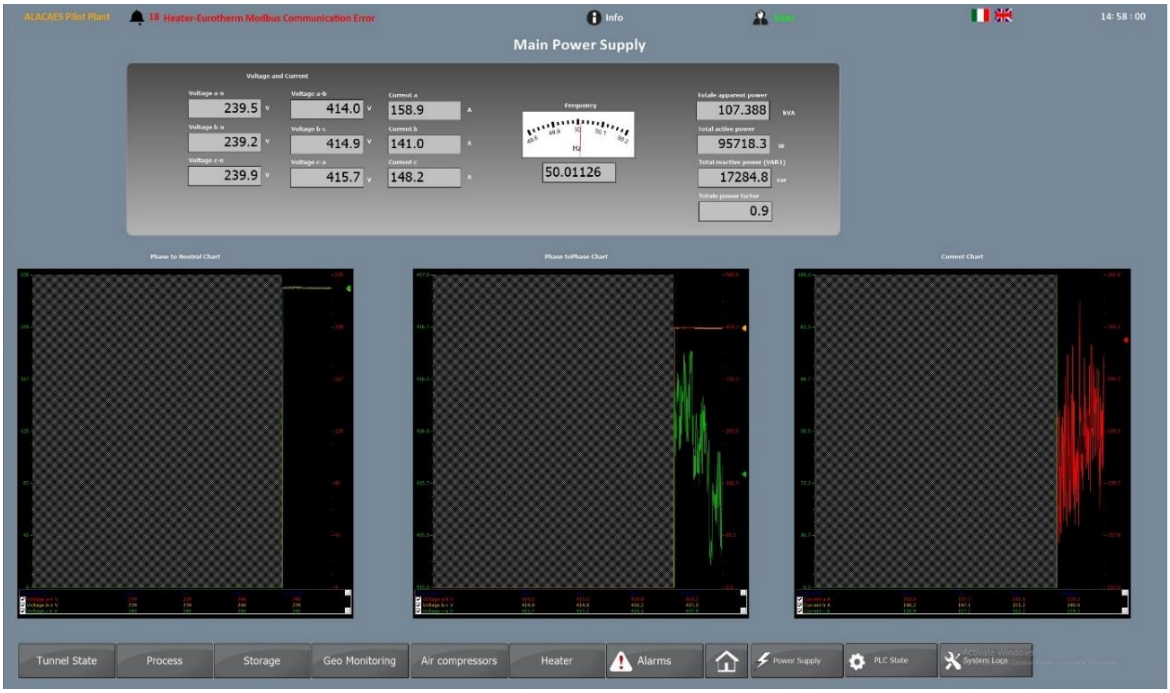

PLC Status: Shows the status of the PLCs. Details and origin of any alarm can be found and back-tracked using this page.

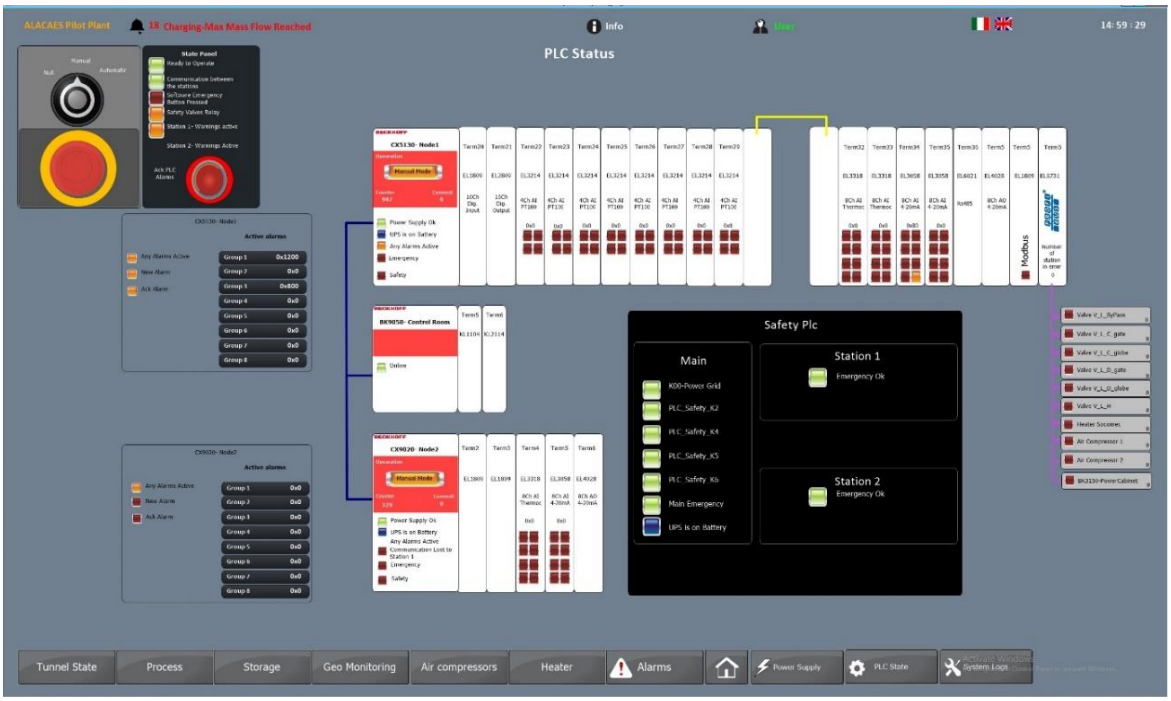

6. Methodology

A series of tests have been executed to assess the technology's feasibility. The most important points to prove are the following:

- Can an unlined cavern be used for cyclic loads? Is the rock displacement and air leakage from the rock acceptable and in line with theoretical calculations?
- Can the concrete plugs effectively seal the pressure zone and does their deformation correspond to the simulated values using finite analysis?
- How does the TES perform in a pressurized environment and how does it compare to ambient pressure applications?
- Can the TES effectively cool down the hot pressurized process air and avoid temperature increase in the cavern while also having an acceptable round-trip efficiency?
- How do the critical plant components perform in the pressurized zone (pipelines, flanges and connectors, instruments)?

Upon completion of the plant construction, the commissioning and testing of the plant was started. The following procedure was followed:

- Commissioning of the "hot components": The goal was to check the correct functioning of all the components that undergo a temperature increase, hence everything from the heater until the TES. For this, tests were conducted using only the heater with open access doors (therefore no pressure increase in cavern). The temperature of the piping was increased up to 650 °C to ensure that no problems will occur. The tubing on the ambient pressure side of the Loderio plug is placed on rolling cylinders to allow free movement of the components. On the pressurized side, axial compensators were placed between the tubes to compensate the thermal expansion. These tests were concluded successfully and without any problems.
- "Cold" pressure tests: With closed access doors and shut off heater, these tests were done to assess the air-tightness of the cavern, the rock behavior when the cavern is pressurized, and the adequacy of unlined rock caverns for compressed air energy storage. The charging and discharging paths are depicted in Fig. 6.1. The results of these tests are reported in Section 7.1.
- "Hot" pressure tests: The main tests to assess the ability of caverns for compressed air energy storage with thermal energy recuperation. In these tests, the air is compressed and subsequently heated in the heater to simulate an adiabatic compressor. Hence, the pressure is increased in the cavern while simultaneously the TES is being charged. The plant is subsequently discharged in order to measure the efficiency of the plant. The charging and discharging paths are depicted in Fig. 6.1. The results of these tests are reported in Section 7.2.

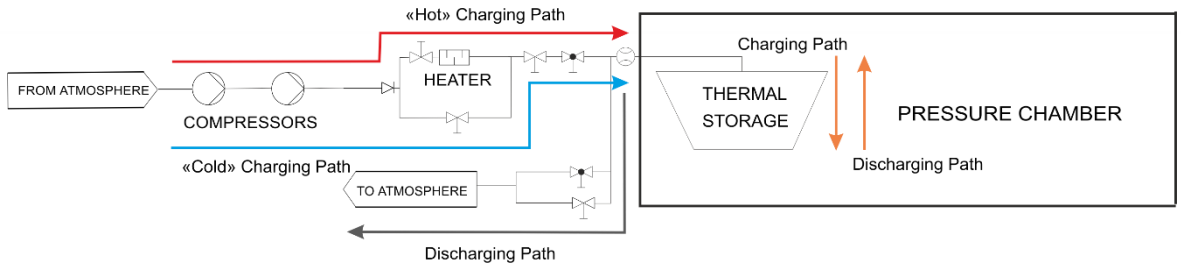

Fig. 6.1: Simplified Flow Diagram of the plant showing the different paths for operating the plant.

7. Results

The results of the “Cold” and “Hot” pressure tests as described in Section 6 are presented in the following.

7.1. “Cold” Pressure Tests

After the initial tests with the compressors, leakages were observed from different parts of the plant. Therefore, before continuing with the pressure tests, these problems needed to be solved.

Air Leakage and Losses

The leakages were observed from three areas: the steel access doors, the area around the feeding pipe through the Loderio plug, and the concrete/rock interface as well as any other not lined spot of the concrete plugs.

Steel access doors: It was quickly noticed that the camprofile sealing is not adequate for use with air and repeated opening/closing of the doors. These sealing gaskets consist of a metal core, rectangular in cross section, covered with another material, in our case graphite. The metal core would bend under the pressure of the door and not stay in its seat anymore upon opening and re-closing of the doors. The graphite coating would fall off in pieces after opening the doors and therefore the sealing would not guarantee air-tightness anymore. Even upon placement of a new sealing gasket, significant losses were observed. After initial struggling, rubber sealing was found to effectively seal the doors. Once the rubber sealing was added, no more leakage was observed from this area (See Fig. 7.1). By applying the rubber sealing, the losses from the plant were reduced by approximately 30%.

Fig. 7.1: Damaged graphite layer on the original camprofile sealing (left) and rubber sealing placed on the door seat that eliminated the leakages from the doors (right).

Feeding pipe: Further losses were observed from the volume around the feeding pipe on the Loderio plug. It seems that air managed to get behind the steel lining on the internal side of the plug and escape through the placement tube, although said tube was welded to the steel lining. In order to overcome these losses, the first 40 cm of the volume from the pressure-free side were filled with an epoxy resin (See Fig. 7.2). This showed to effectively eliminate the losses from this area, and therefore, the losses from the plant were reduced by another 37%.

Fig. 7.2: The empty volume around the inlet tube on the Loderio plug where significant losses were observed (left) and the same zone after filling the first 40 cm of the volume with an epoxy resin (right).

Main Plugs: The most significant losses of the plant occur from the main plugs; e.g. from the rock/concrete interface, the outer concrete surface itself, and any surface in the access cylinder that is not covered with steel lining (See Fig. 7.3). These losses, are - according to experts - very costly to overcome without any guarantee to be eliminated. Therefore, it was decided to accept these losses and execute the tests with the highest achievable pressure. At a later stage and in collaboration with international experts, ALACAES is planning to try to reduce these leakages in order to be able to operate the plant at the design point of 33 bar (See Outlook).

Fig. 7.3: Leakages observed from the main plugs. Top left: through cracks on the surface of the concrete on the pressure-less side. Top and bottom right: the exposed concrete in the access cylinder between the steel cylinder and the steel door seat. Bottom left: through the concrete/rock interface, were the most important losses occur.

The losses from the plant were quantified by building pressure in the plant and subsequently closing the valves. The decrease in pressure over time was then used to calculate the mass flow of air leaking from the plant. The following graph shows the air leakage rate as a function of pressure for all “cold” pressure tests.

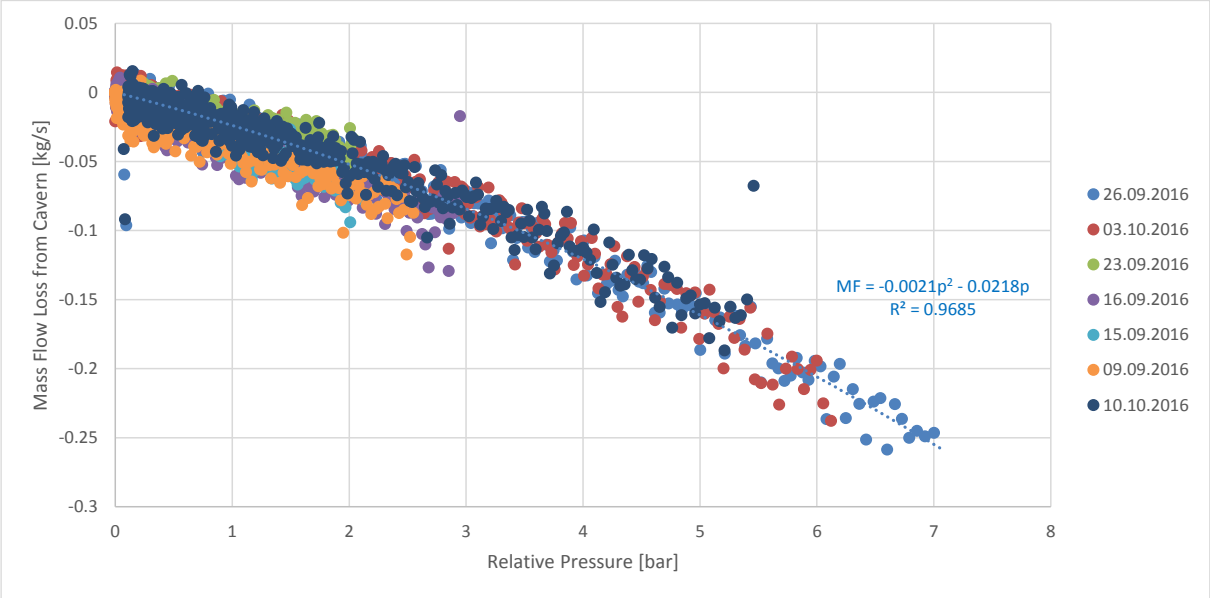

Fig. 7.4: The air leakage rate from the plant as a function of pressure for all “cold” pressure tests. At 7 bar the leakage rate approaches 0.3 kg/s, impeding a further increase of plant pressure (maximum mass flow supplied by the compressors is 0.36 kg/s).

The losses from the Pollegio plug could be separately quantified using the pre-chamber described in Section 5.6. The following graph shows these losses for all “cold” pressure tests.

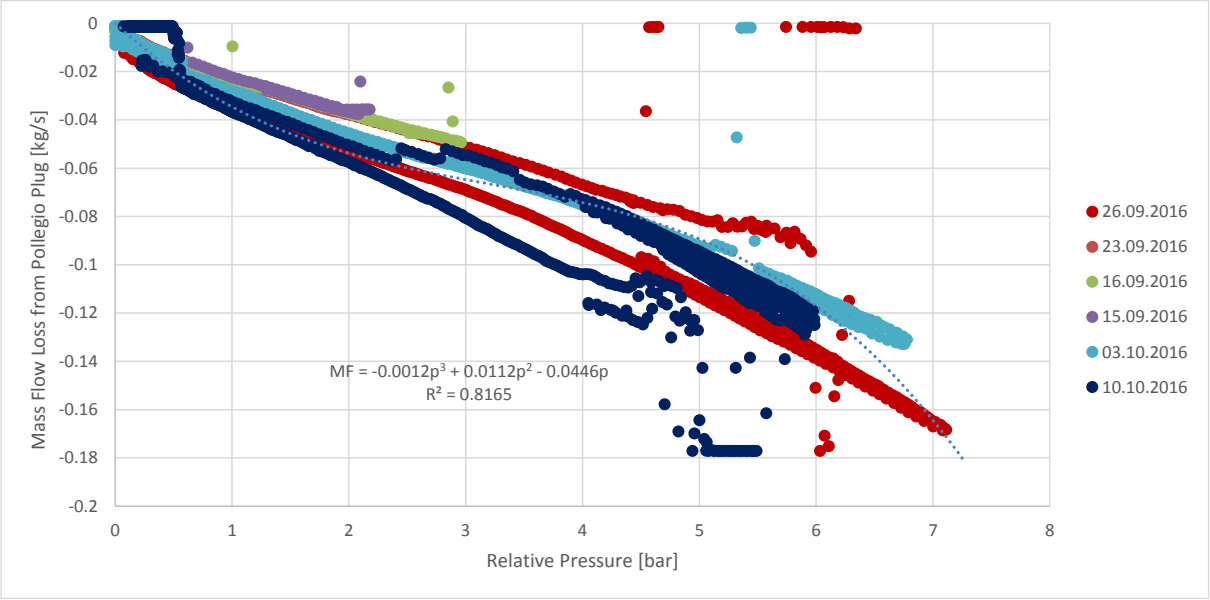

Fig. 7.5: The air leakage rate through the Pollegio plug as a function of pressure for all tests.

While the losses vary slightly from test to test - which is ascribed to changes in the fissures in the concrete and the water content around the plug with each test – it can be seen that a significant amount of the losses are due to the Pollegio plug. Comparing the losses from the Pollegio side and the total plant losses, by using the fitted polynomials on Fig. 7.4 and Fig. 7.5, the leakage from the Pollegio plug is calculated to be 55-70% of the total plant losses.

As mentioned in Section 5.6, it was not possible to construct a similar pre-chamber on the Loderio side. Hence, the losses from the Loderio plug could not be quantified separately. However, visible and phonic examination of the two plugs show losses in the same range for both plugs, but slightly higher at the Pollegio plug. For instance, at pressures below 2 bar, there are almost no detectable losses from the Loderio plug, while such losses can be heard on the Pollegio side already. With increasing pressure, losses from the Loderio plug increase but remain always smaller in magnitude compared to the Pollegio losses.

While due the lack of a pre-chamber on the Loderio side, the losses from the Loderio plug cannot be quantified, the qualitative comparison above concludes that losses from the rock itself are either not existent or not significant, otherwise the Pollegio side losses would have been a much smaller fraction of the overall losses.

Further, if a rock fracture would have led to escape of air from the pressure zone, the Pollegio side losses would not have coincided with the overall plant losses at low pressure (See Fig. 7.6 and Fig. 7.21), but there would be a significant difference between Pollegio losses and total plant losses also at low pressure.

Therefore, it can be concluded that the losses from the mountain itself are not significant and that the significant losses occur from the plugs.

The other components of the plant, such as the process air piping and water, cable and signals pipelines do not show any leakage.

Test Results

Despite the efforts to overcome the losses, the ones from the main plugs increase with pressure and do not allow the pressure of the plant to exceed 6-7 bar. At this threshold, the losses due to the leakages approach the maximum mass flow supplied by the compressors. Hence, the tests had to be done with 6 bar as maximum pressure. The goal of these tests was to assess the adequacy of the tunnel for use as pressure vessel and the rock behavior under cyclic operation.

The following tests are executed:

- Two charging runs up to 6-7 bar with subsequent idle state to assess rock behavior and plant leakage.
- Charging the plant up to 6 bar followed by 4 cycles between 4-6 bar to assess plant and rock performance under cyclic operation.

In the mass flow/pressure charts that follow, the legend entries are defined as:

- Total Mass Flow out of Cavern: is the mass flow leaking out of the cavern when the valves are closed. It is calculated using the pressure variation over time to calculate the mass of air leaving the pressure zone.

- Losses from Pollegio Plug: is the mass flow measured using the anemometer installed at the outlet of the Pollegio pre-chamber as explained in Section 5.6.
- Charging Mass Flow: is the charging mass flow measured by the Pitot tube installed on the process air piping on the Loderio side.
- Discharging Mass Flow: is the discharging mass flow measured by the Pitot tube installed on the process air piping on the Loderio side.
- Chamber Pressure: is the average of the measured chamber pressure by the two pressure sensors installed in the pressure zone.

26.09.2016 - Charging to 7 bar (1): The test was started on 26.09.2016 and finished on 03.10.2016. The plant is charged to 7 bar, discharged to about 4.5 bar and charged again to 7 bar before being left in idle state with the valves closed. The plant is then discharged through the leakages to ambient pressure (i.e. 0 bar relative pressure). The following graph shows the mass flows and pressure curves as a function of time for this test. As explained in the previous section, it can be seen that a significant portion of the losses occurs from the Pollegio plug (> 60% of total losses). At a pressure of around 2 bar, basically all of the losses occur from the Pollegio plug. The anemometer measuring the Pollegio side losses failed for some time around 27.09.2016. Hence, its curve is interrupted.

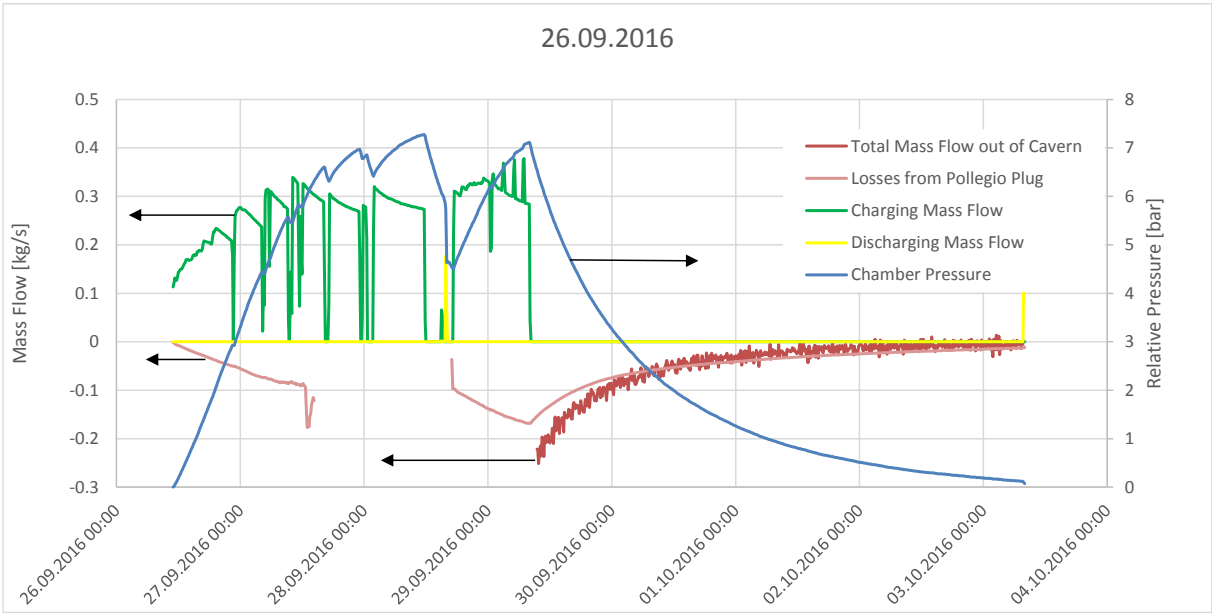

Fig. 7.6: The mass flow and pressure curves for the first “cold” test up to 7 bar.

The ground response to the pressure tests is monitored using the instruments installed by Amberg Technologies and explained in Section 5.7. The following graphs show the measured data. As it can be seen, most of the instruments did not measure any relevant ground response, demonstrating its adequacy for pressurized air storage up to the operated pressure values. For this test, all measured data is shown for completeness. For the subsequent tests, only the data that showed a relevant change in its value will be presented.

Tachymeters

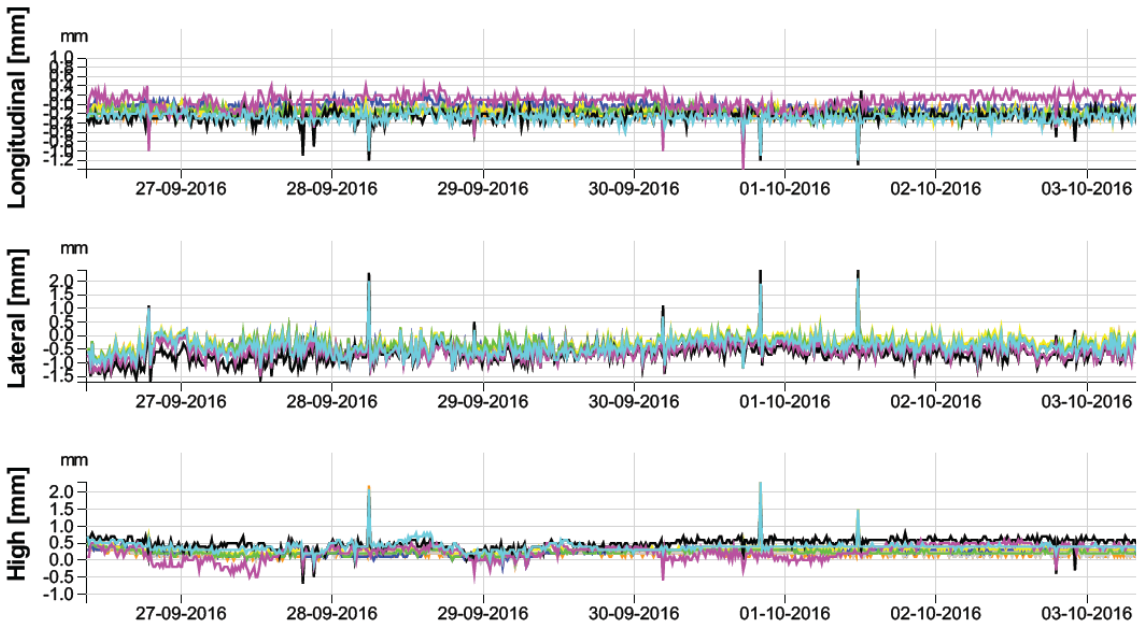

Fig. 7.7: Loderio side tachymeter data: No relevant displacement of the plug was observed during the test. The peaks seen in several points are outliers that are not directly related to the pressure in the cavern.

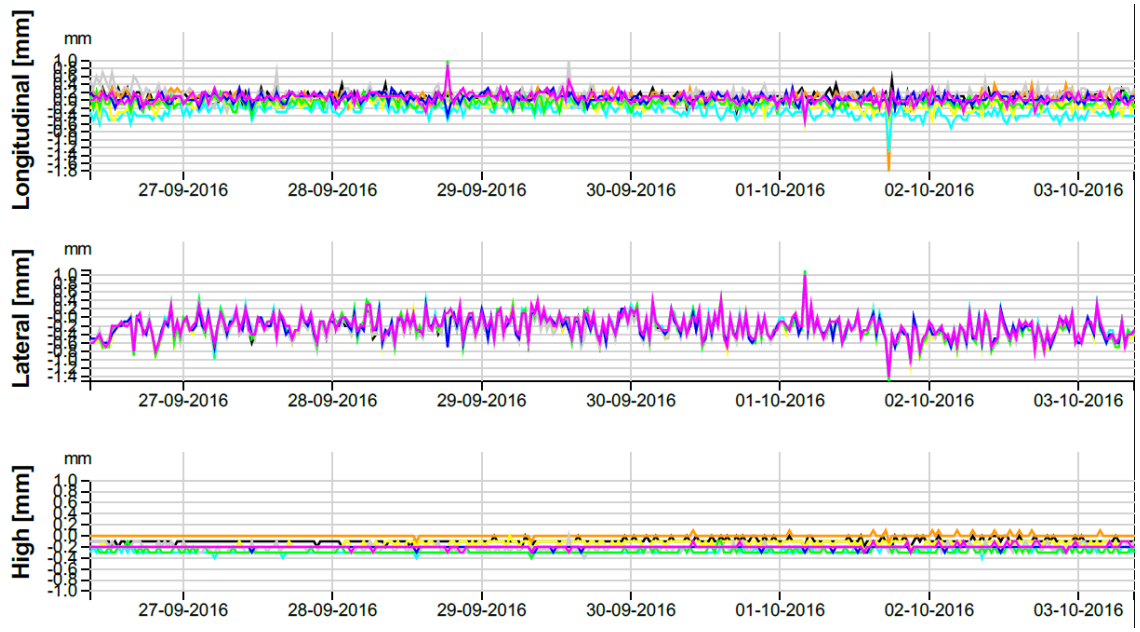

Fig. 7.8: Pollegio side tachymeter data: No relevant displacement of the plug was observed during the test.

Surface extensometers

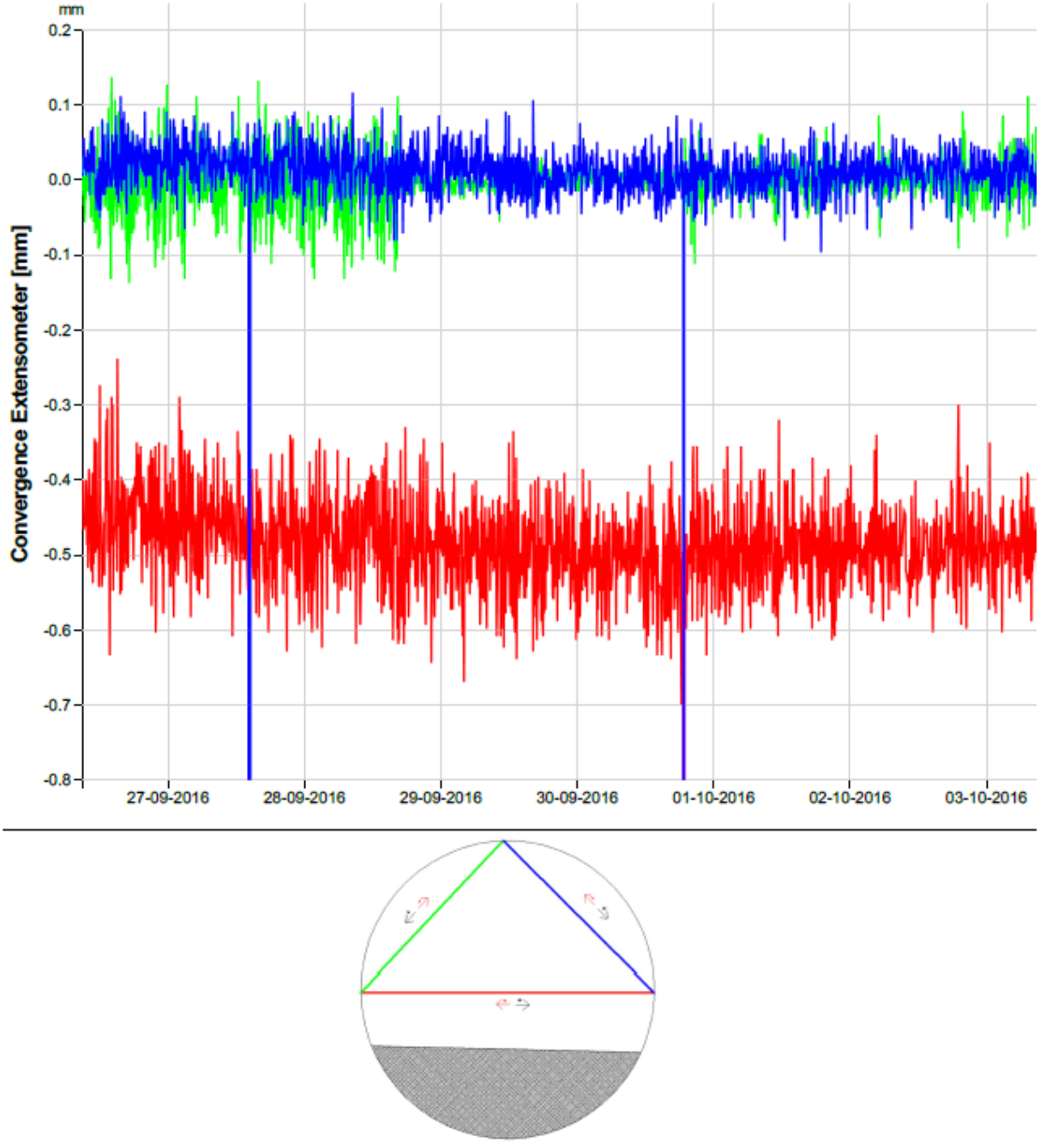

Fig. 7.9: 1st section: Also the surface extensometers did not show any relevant movement with the pressure increase in the chamber. The peaks of the blue line are outliers due to temporary sensor failure.

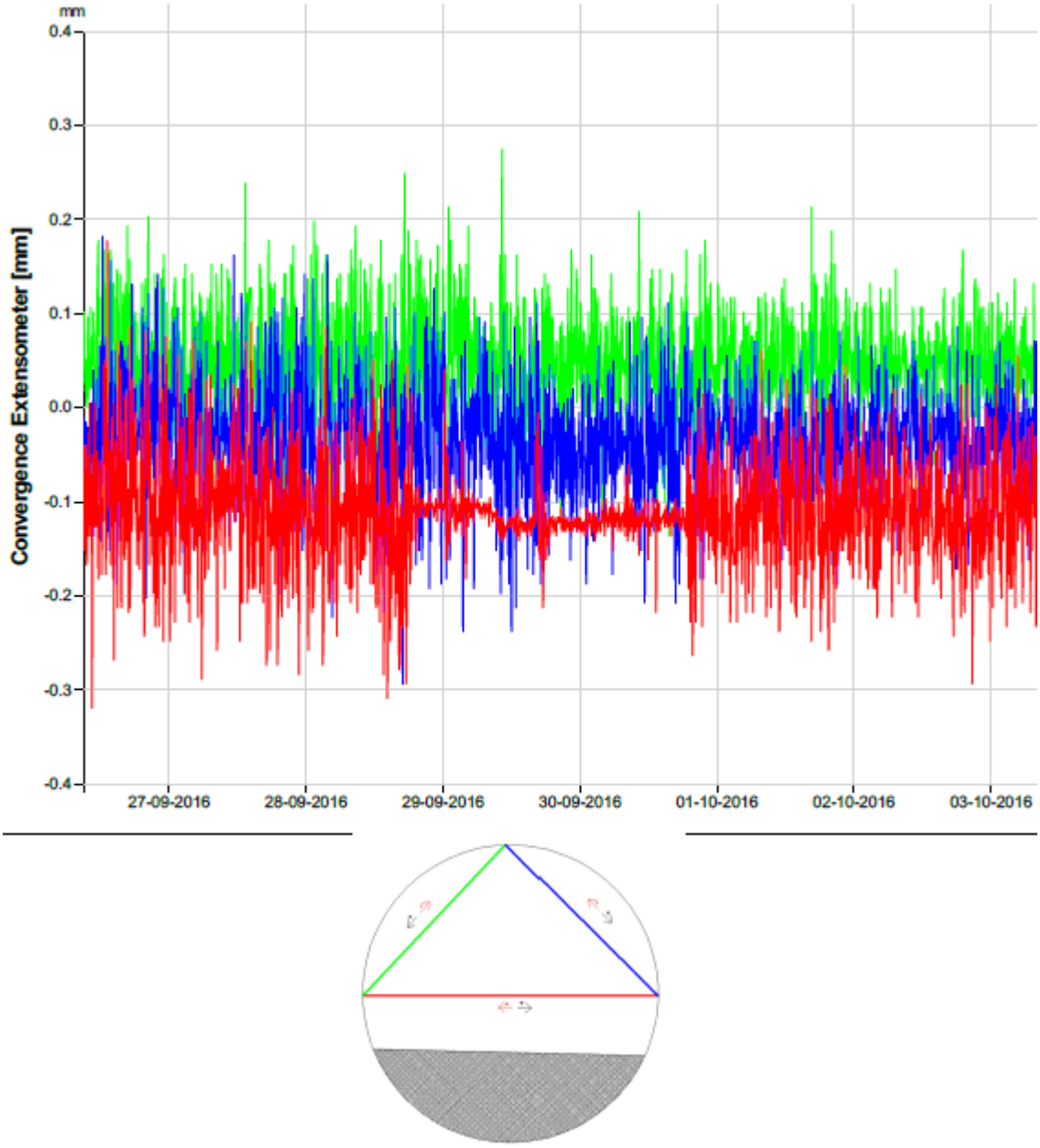

Fig. 7.10: 2nd section: The surface extensometers did not show any deviation with the pressure increase in the chamber. The decrease in oscillation of the red rod does not seem to have any relation to the pressure curve.

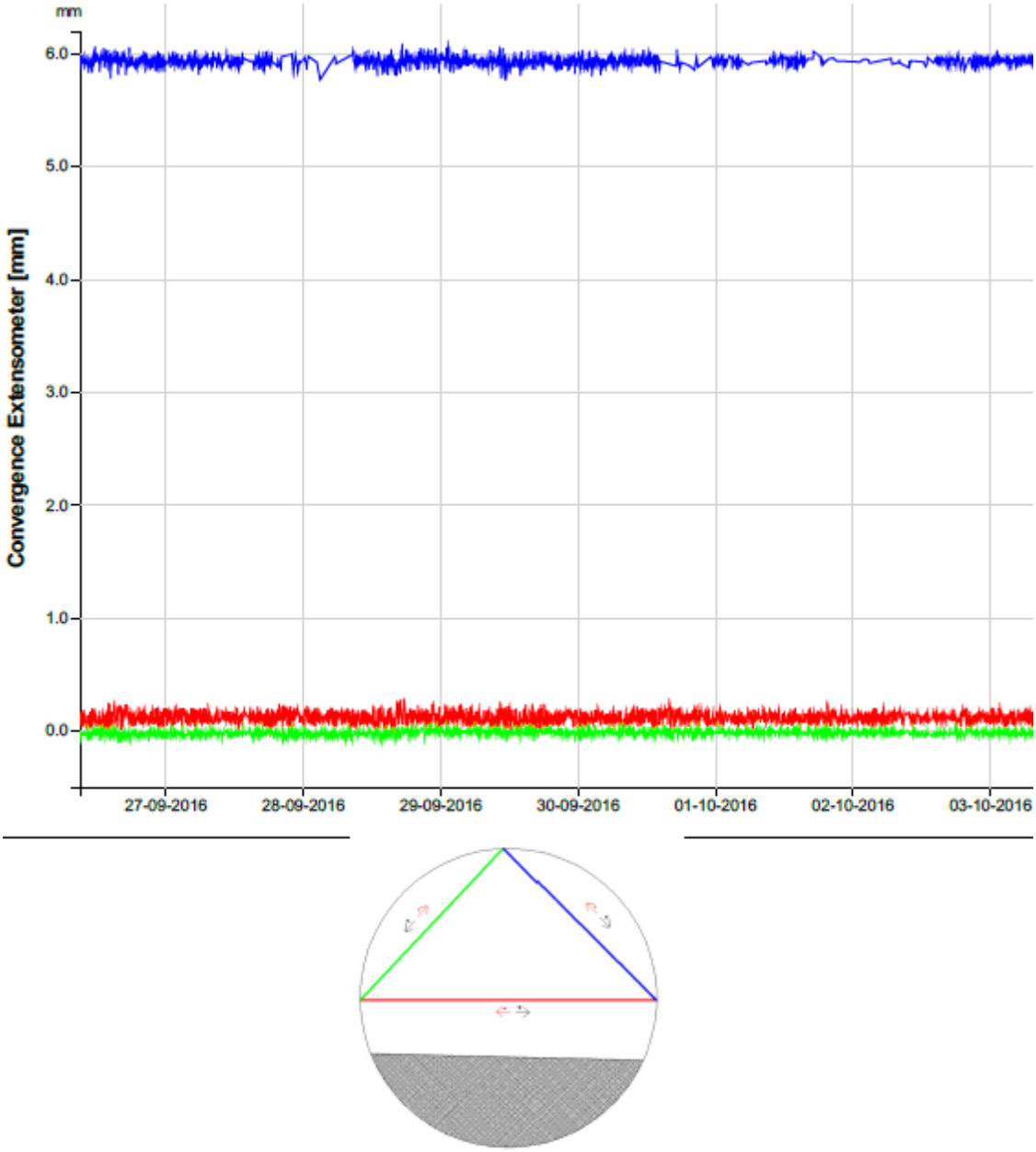

Fig. 7.11: 3rd section: The surface extensometers did not show any deviation with the pressure increase in the chamber. The blue rod had an initial offset and its increased value is not a consequence of the pressure increase in the cavern.

Rock extensometers

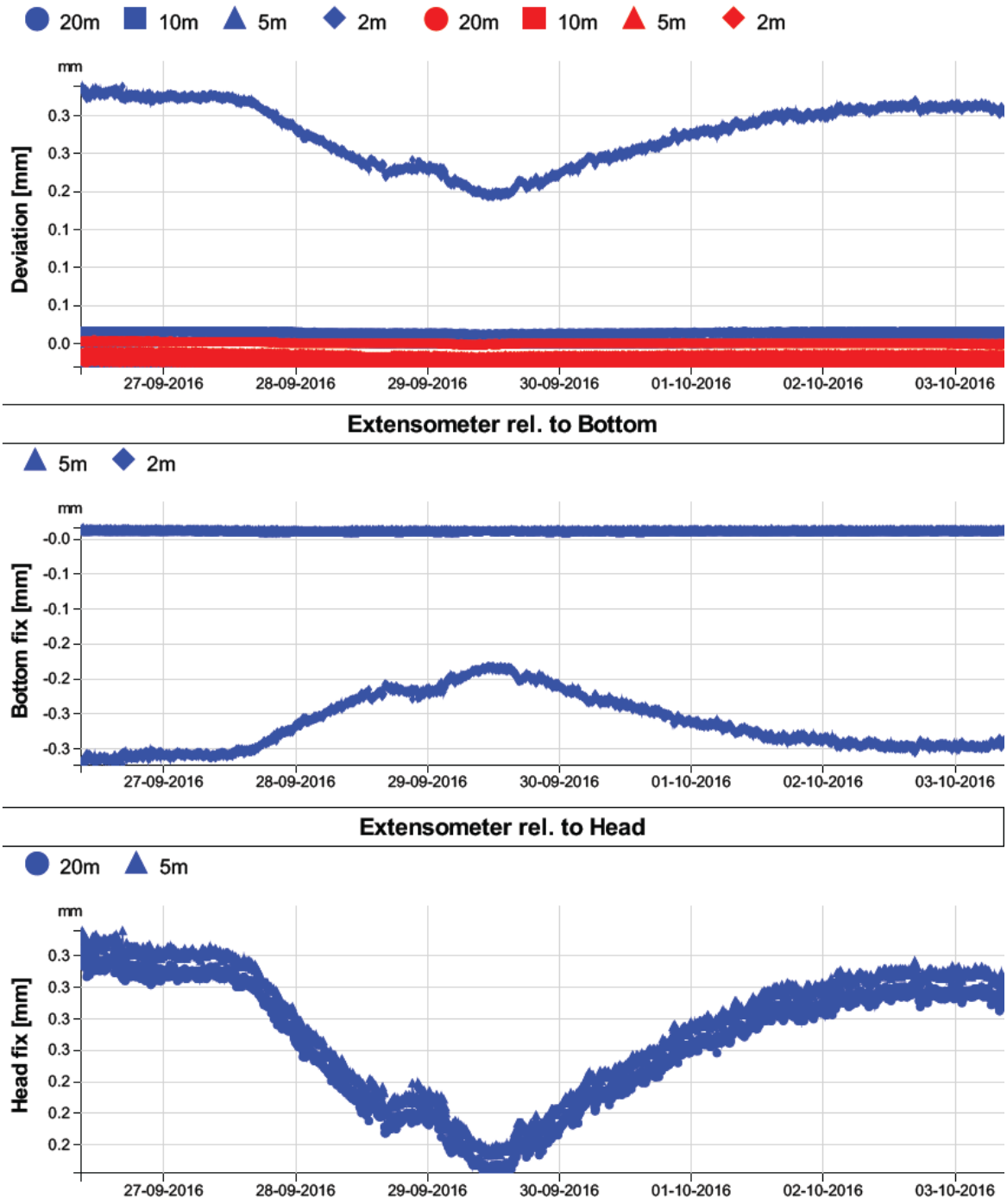

Fig. 7.12: Loderio rock extensometers: The blue markers represent the bottom extensometer (D141746) and the red markers the top extensometers (D141747, see Fig. 5.32). While the top extensometer did not show any variation, the bottom extensometer moved by about 0.1 mm due to the increased pressure. It returned to its initial state at the end of the discharging. The variation is considered negligible for the plant's performance.

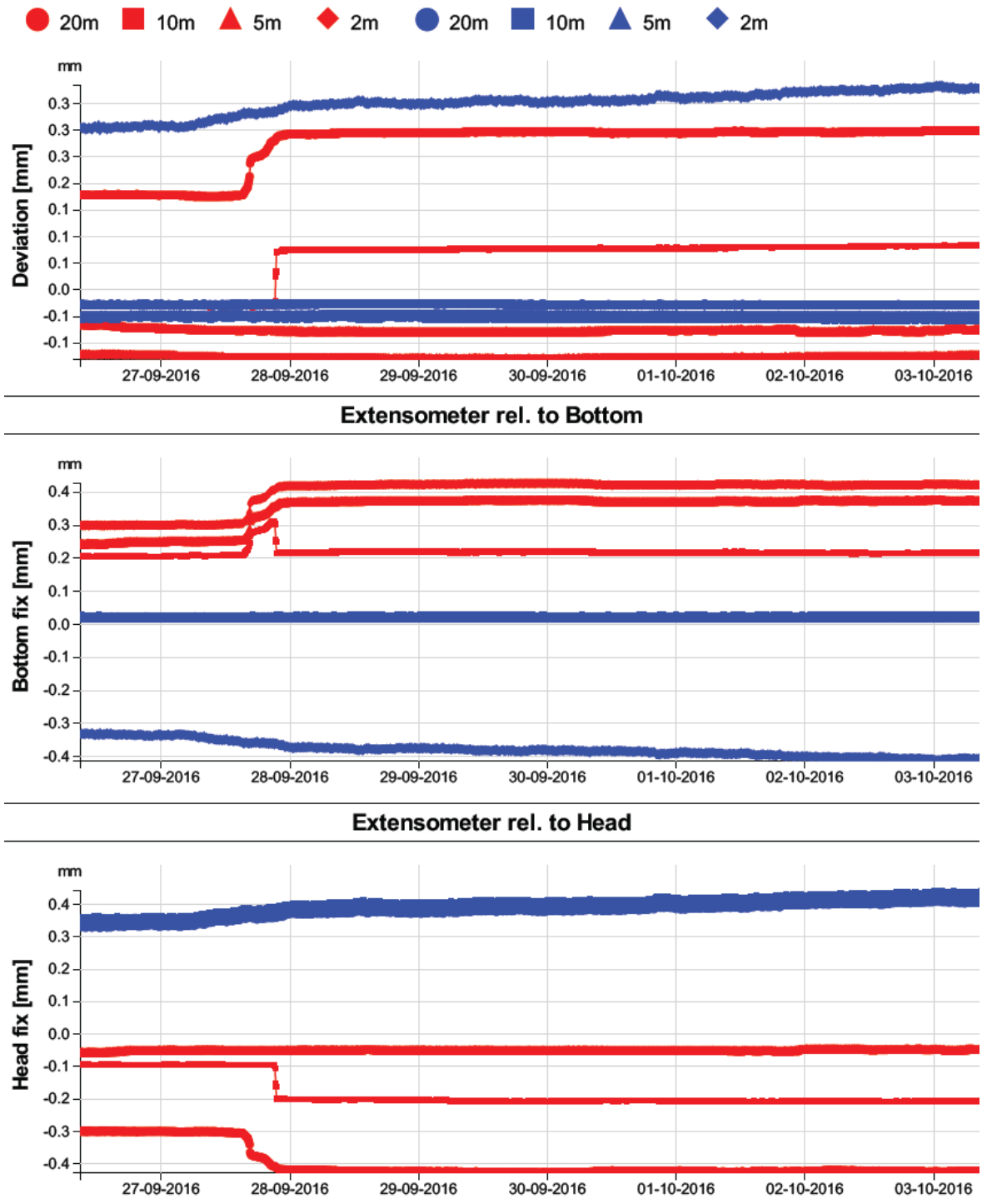

Fig. 7.13: Pollegio rock extensometers: The blue markers represent the bottom extensometer (D141745) and the red markers the top extensometers (D141744, see Fig. 5.32). The top extensometer had a jump of about 0.1 mm the first time the plant reached 7 bar and did not return to its initial state. However, this jump of 0.1 mm is considered negligible for the plant's performance. The bottom extensometer showed a gradual, irreversible move during the test.

Stress cells

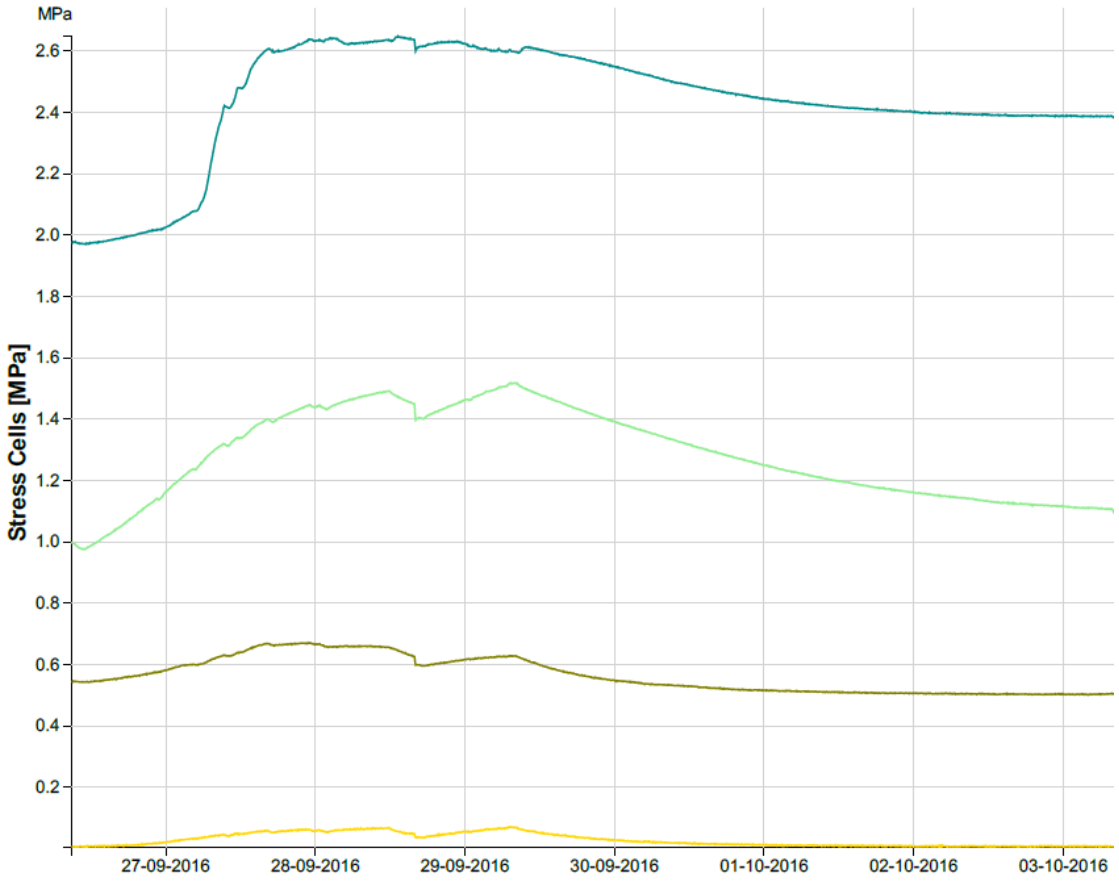

Fig. 7.14: Loderio stress cells: The values measured by the stress cells varied linearly with the pressure. The green and blue lines represent the cells placed between the plug and the rock. Their values did not return to the initial state. The brown and yellow lines, represent the cells placed between the two concreting phases of the plug and showed a reversible behavior.

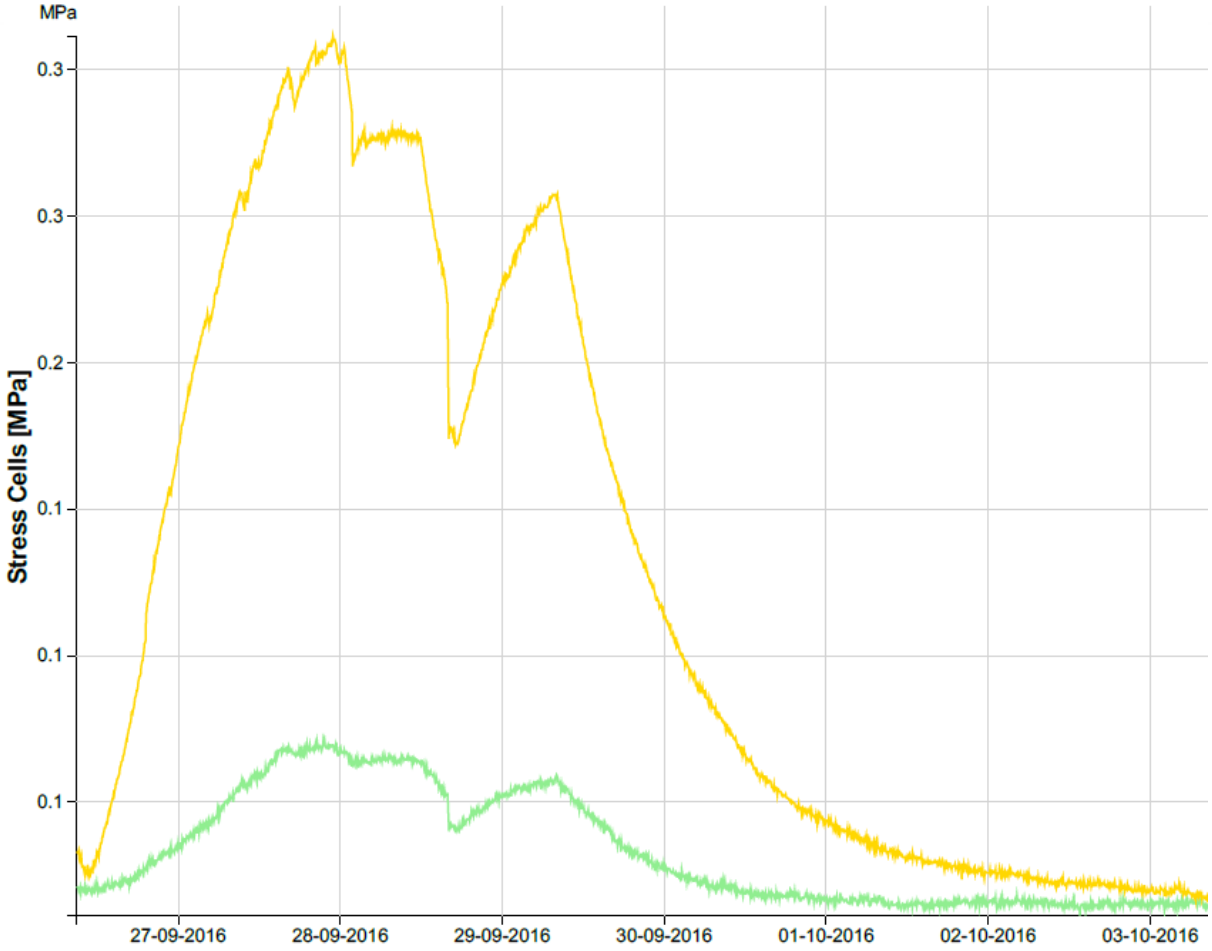

Fig. 7.15: Pollegio Stress cells: The values measured by the stress cells varied linearly with the pressure. Both cells are placed between the two concreting phases of the plug. Their values varied similar to the Loderio side stress cells that are placed between the concreting phases, and showed a reversible behavior.

Geophone

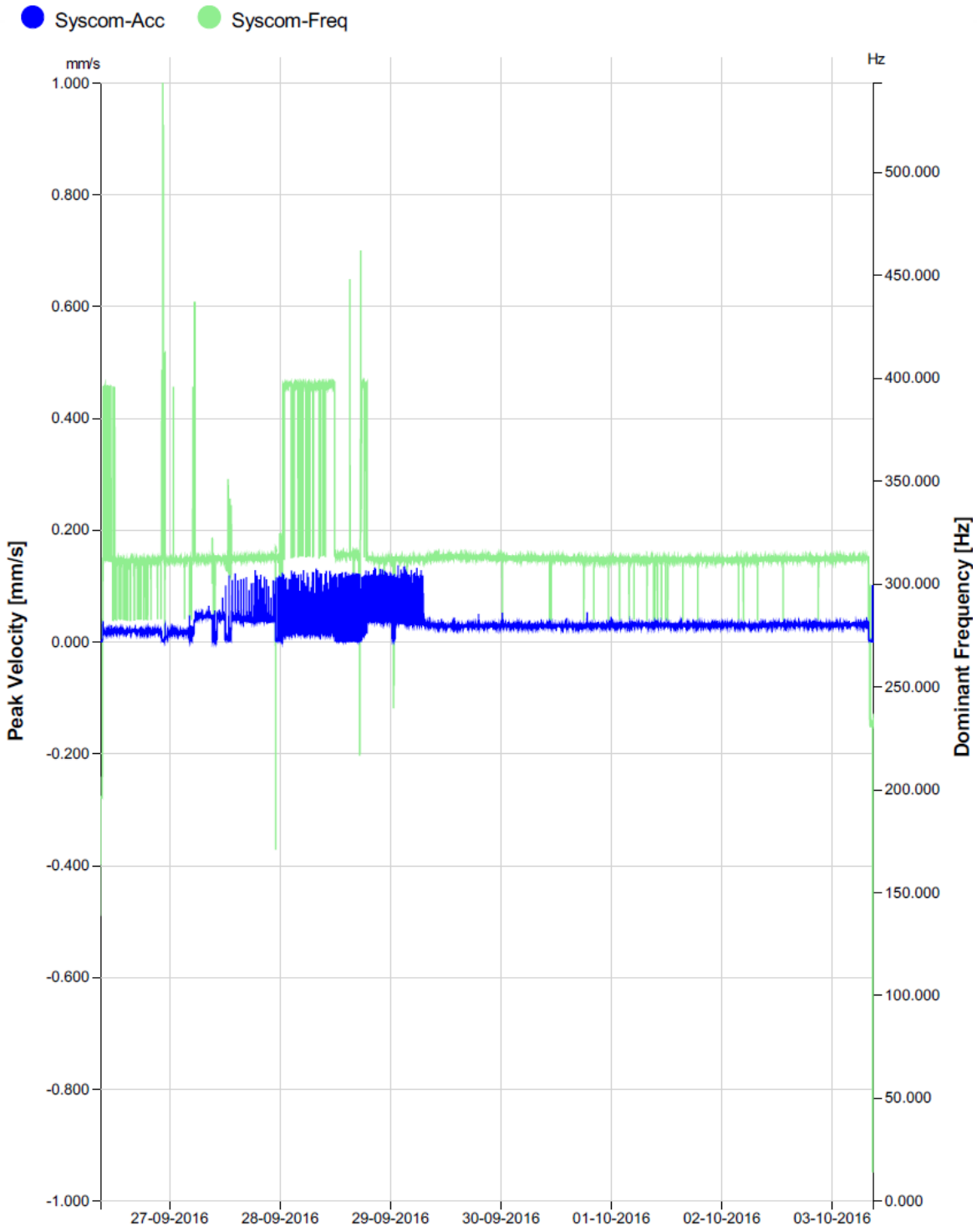

Fig. 7.16: Geophone: the velocities and frequencies measured by the geophone during the test. None of the values exceed acceptable threshold values and hence no events* were registered.

*an event is when the velocity or frequency exceed values that are acceptable according to general standards.

03.10.2016 - Charging to 6 bar (2): The test was started on 03.10.2016 and finished on 10.10.2016. The plant is charged to 6.8 bar, left idle until the pressure drops to 6 bar, charged again to 6.3 bar and then left in idle state with the valves closed. The plant is then discharged through the leakages to ambient pressure. The following graph shows the mass flows and pressure curves as a function of time for this test. The mass flow and leakage behavior is similar to the previous test.

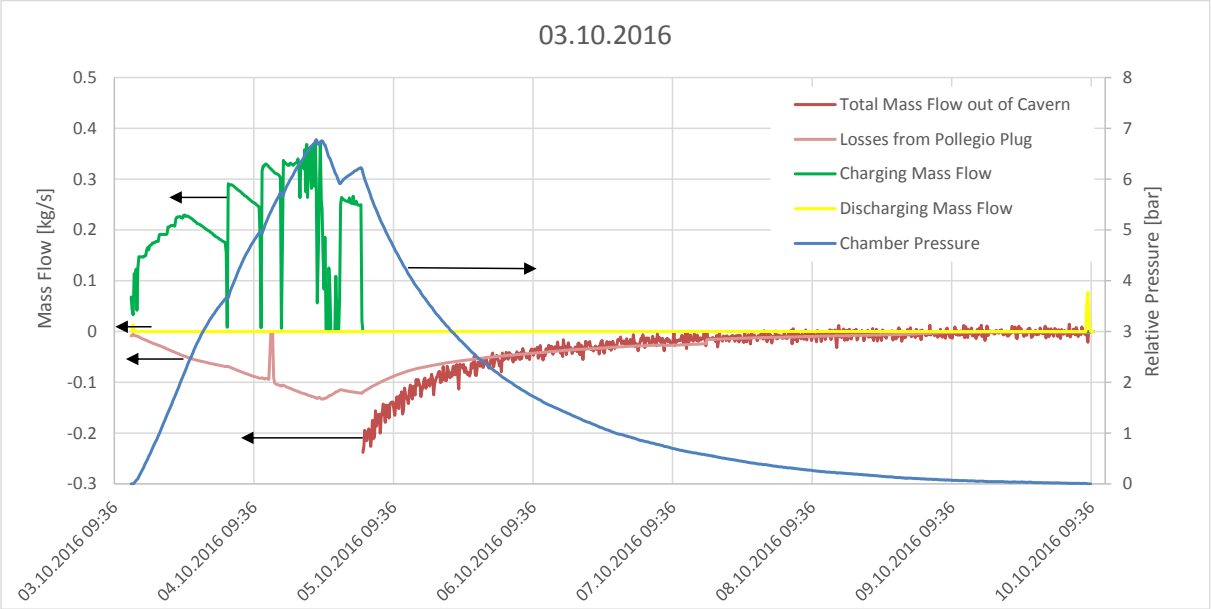

Fig. 7.17: The mass flow and pressure curves for the second “cold” test.

Also for this test, the geotechnical monitoring instruments did not register any noticeable changes in the ground response. Below you can find the data that showed a variation:

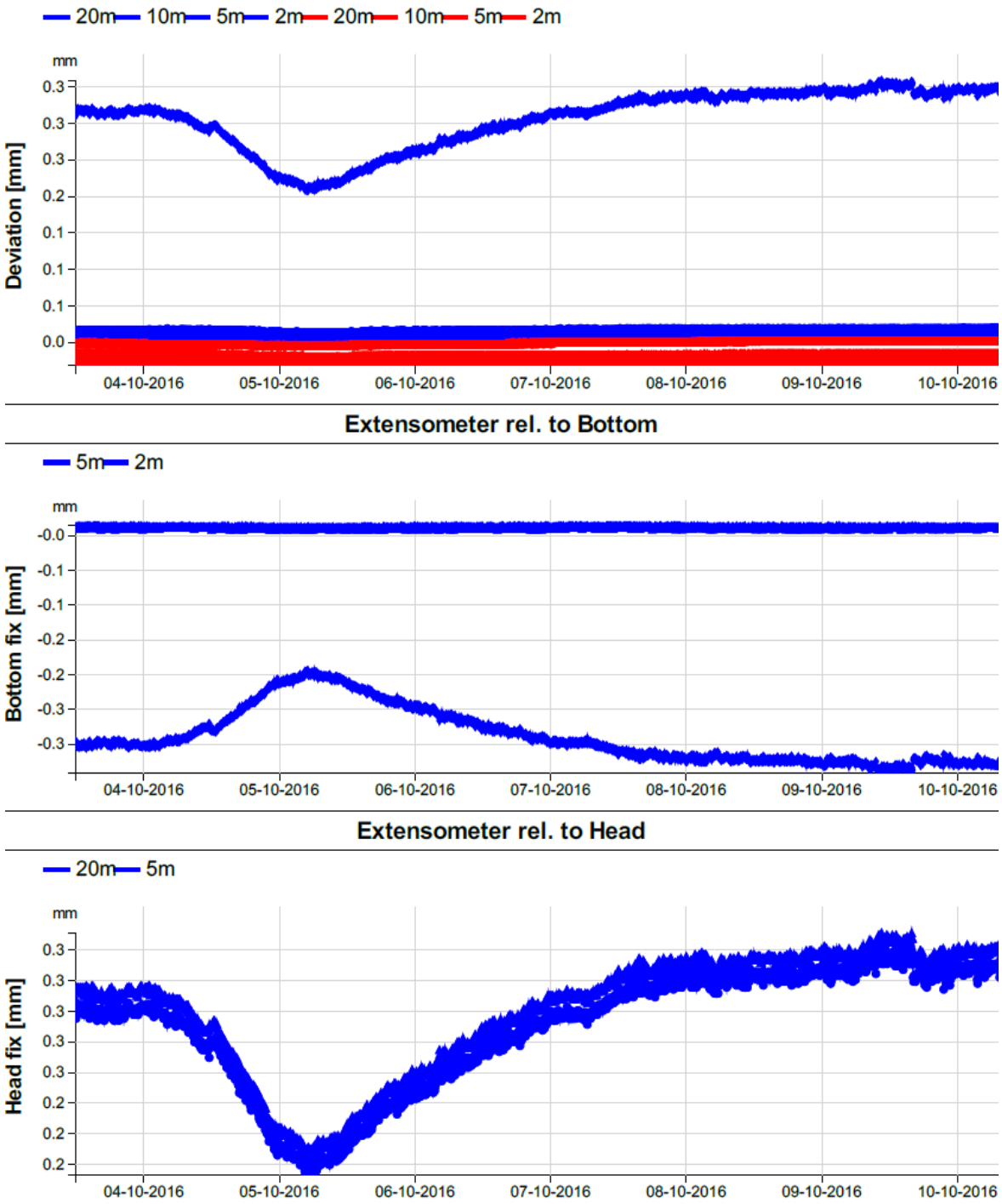

Fig. 7.18: Loderio rock extensometers: The blue markers represent the bottom extensometer and the red markers the top extensometers (see Fig. 5.32). Like for the first test, the bottom extensometer moved by about 0.1 mm due to the increased pressure. It returned to its initial state at the end of the discharging. The variation is considered negligible for the plant's performance.

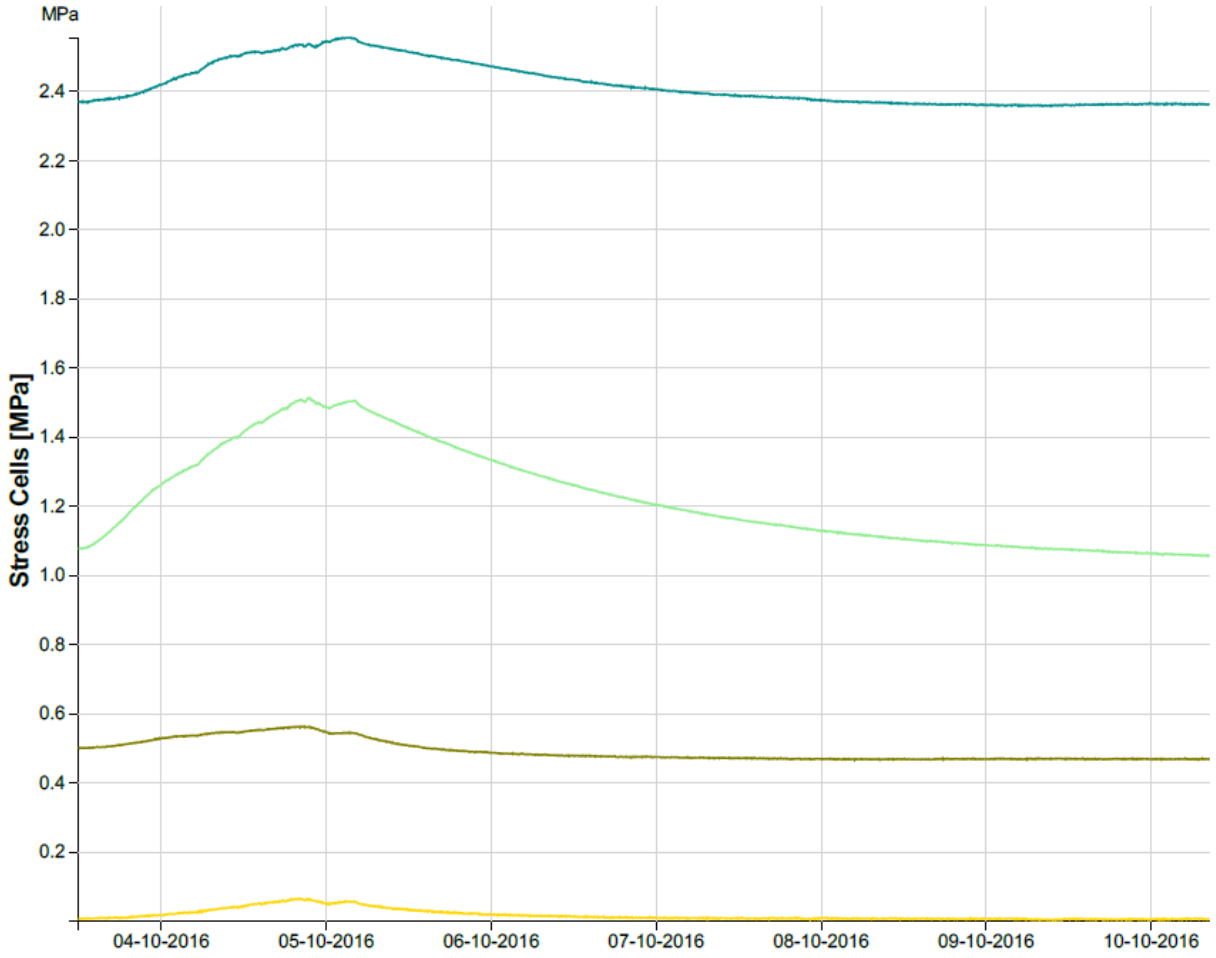

Fig. 7.19: Loderio stress cells: The values measured by the stress cells varied linearly with the pressure. The green and blue lines represent the cells placed between the plug and the rock. Their values returned to the initial state in contrast to the first test. The brown and yellow lines, represent the cells placed between the two concreting phases of the plug and showed a similar behavior to the first test.

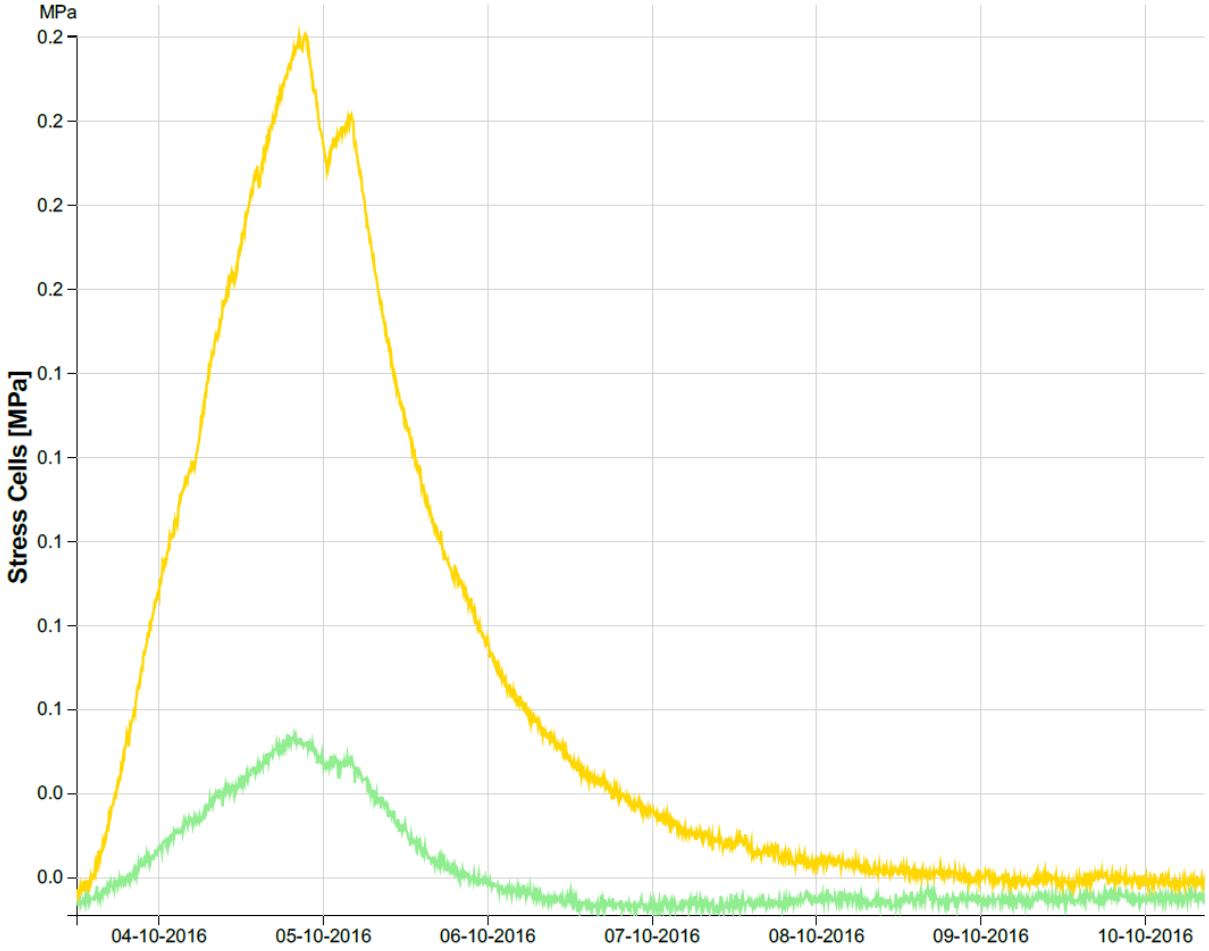

Fig. 7.20: Pollegio stress cells: The values measured by the stress cells varied linearly with the pressure. Both cells are placed between the two concreting phases of the plug. Their values varied similar to the Loderio side stress cells and similar to the previous test.

10.10.2016 - Cycling 4-6 bar: This test was started on 10.10.2016 and finished on 17.10.2016. The plant is initially charged to 6 bar. Subsequently, 4 cycles between 4 and 6 bar are carried out. Finally, the plant is left in idle state at 5.5 bar with the valves closed. The plant is then discharged through the leakages to ambient pressure. The following graph shows the mass flows and pressure curves as a function of time for this test. The mass flow and leakage behavior is similar to the previous tests.

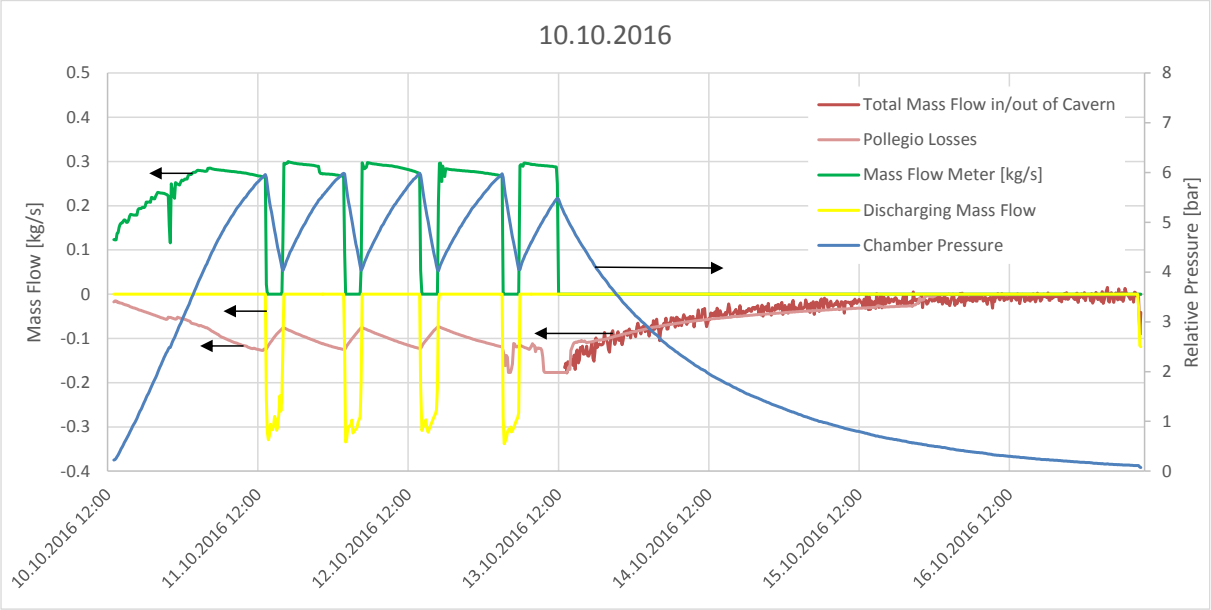

Fig. 7.21: The mass flow and pressure curves for the third “cold” test.

Also for the third “cold” test, the geotechnical monitoring instruments did not register any noticeable changes in the ground response. Below you can find the data that showed a variation:

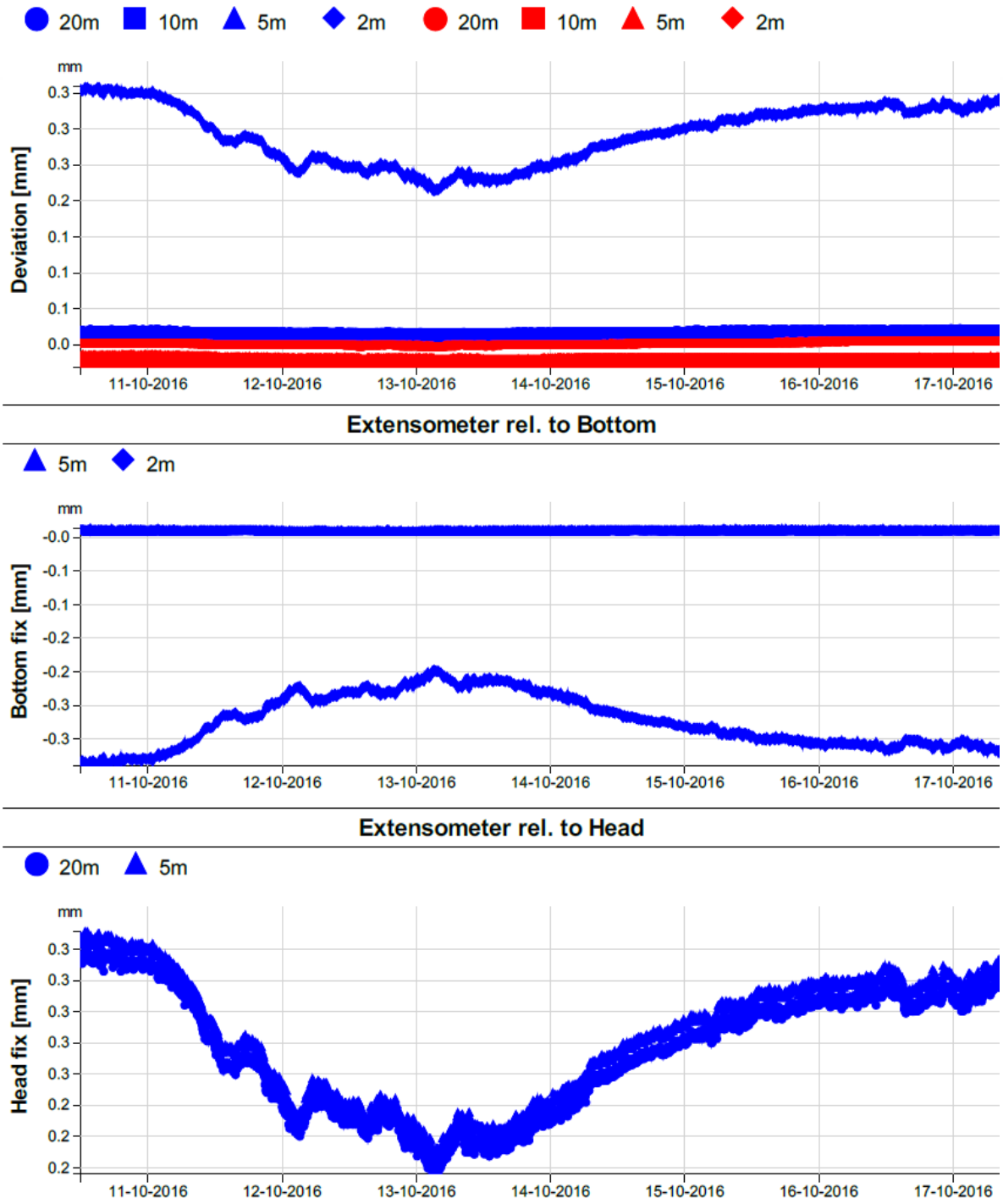

Fig. 7.22: Loderio rock extensometers: The blue markers represent the bottom extensometer and the red markers the top extensometers (see Fig. 5.32). Like for the previous tests, the bottom extensometer moved by about 0.1 mm due to the increased pressure. It returned to its initial state at the end of the discharging. The variation is considered negligible for the plant's performance.

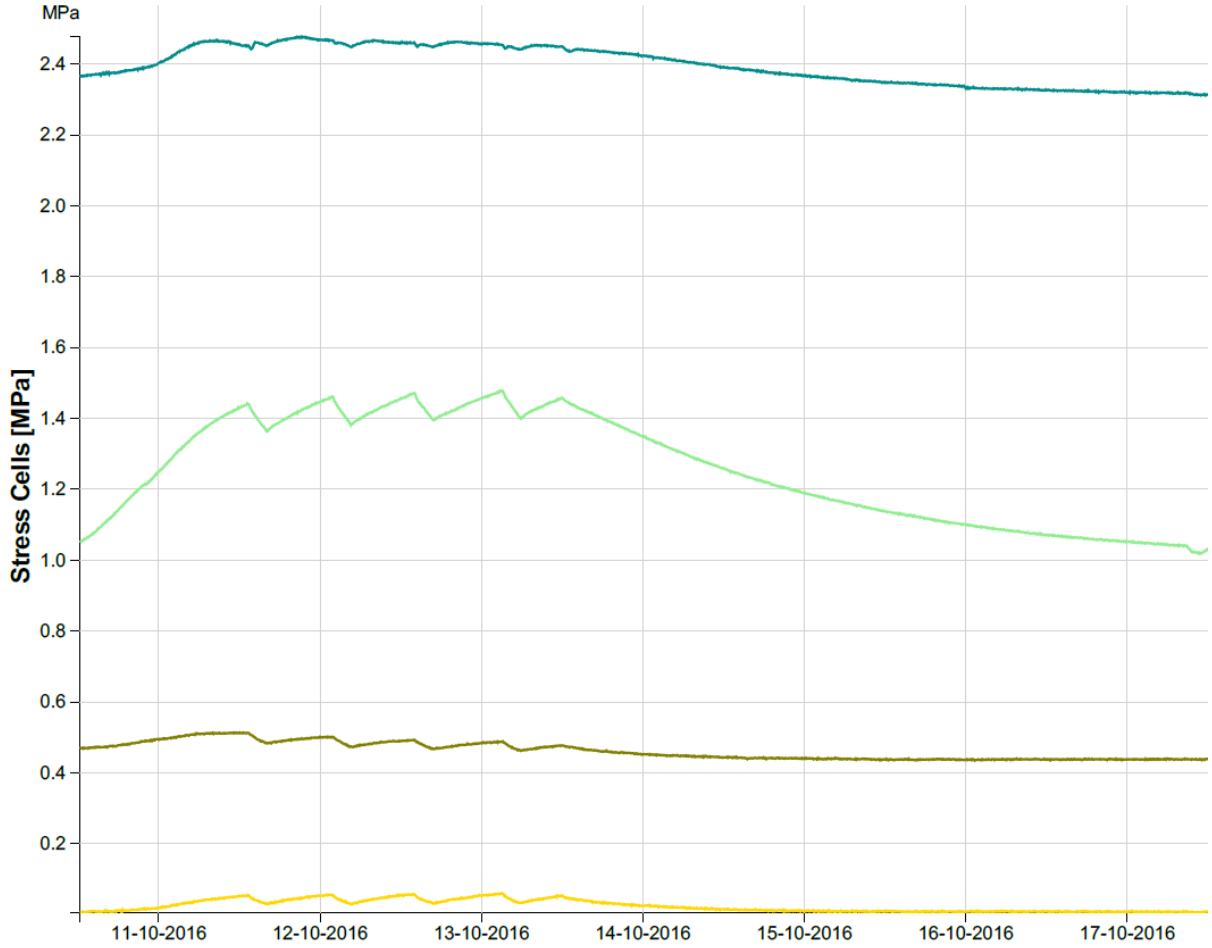

Fig. 7.23: Loderio stress cells: The values measured by the stress cells varied linearly with the pressure. The cycling can be clearly seen also on the values registered by the stress cells. The green and blue lines represent the cells placed between the plug and the rock. The brown and yellow lines, represent the cells placed between the two concreting phases of the plug. All values showed similar behavior to the previous tests.

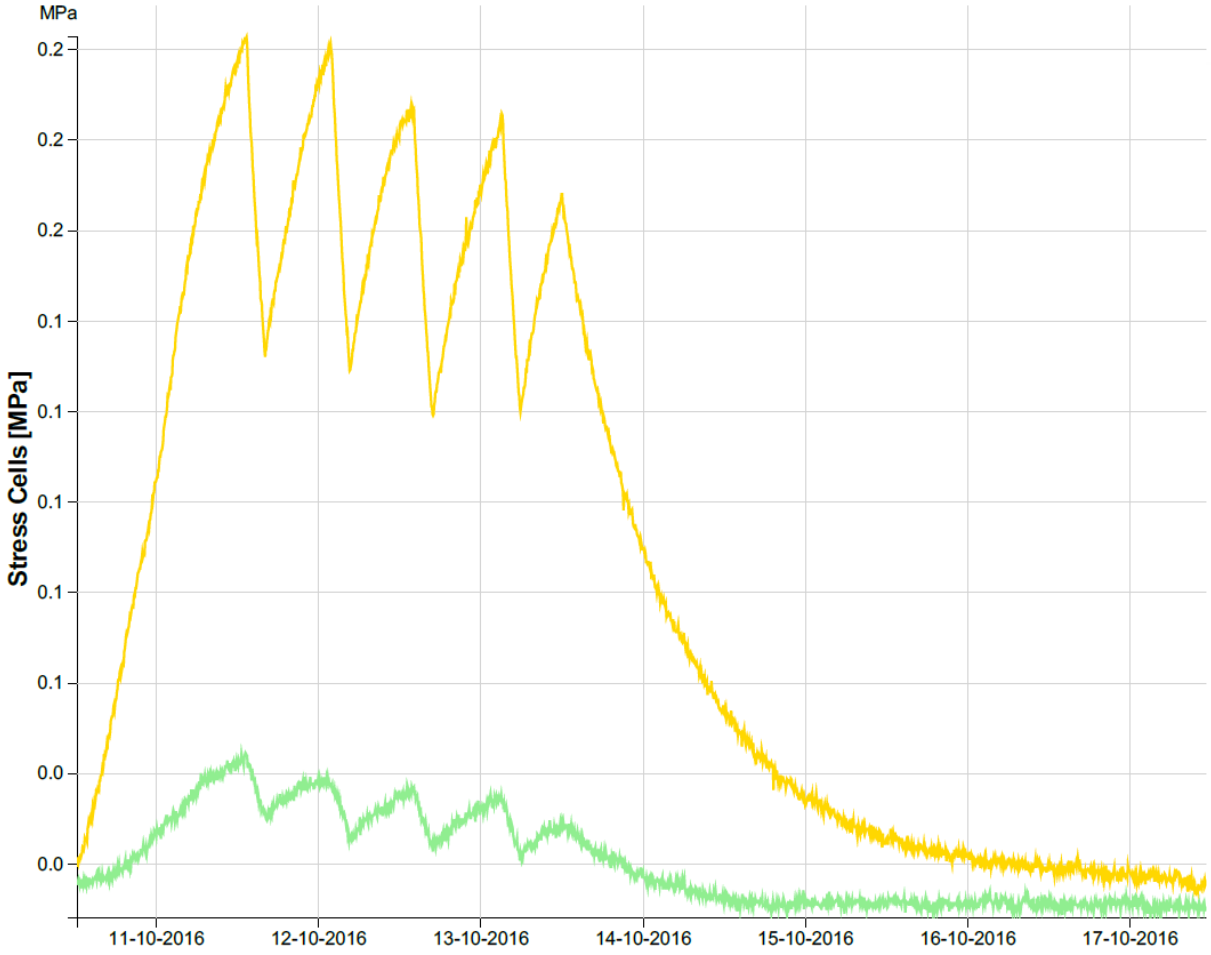

Fig. 7.24: Pollegio stress cells: The values measured by the stress cells varied linearly with the pressure. Both cells are placed between the two concreting phases of the plug. Despite similar peak pressure values in the plant during the cycling, the peak pressure registered by the stress cells reduced with cycling.

7.2. “Hot” Pressure Tests

For the “Hot” pressure tests, the compressors are operated simultaneously with the heater in order to simulate an adiabatic compressor. As explained in Section 4, conventional CAES plants use isothermal compressors, where the naturally generated heat during compression is removed. These compressors typically have multiple compression steps and after each step the air is cooled down before being further compressed. The main reason for the isothermal compression is the temperature limit of the material used in the compressors. With advancement of technology, however, nowadays compressors exist that can compress air to high pressures while also keeping the heat generated during compression. These kind of compressors are called adiabatic compressors and are the machines that shall be used in an adiabatic CAES plant. However, due to the relatively small size of the ALACAES pilot plant, it does not make commercial or technical sense to use adiabatic compressors. Therefore, an adiabatic compressor is simulated using an isothermal compressor combined with a heater. This is justified because the aim of this project is to “demonstrate the ability of caverns for compressed air

storage with thermal energy recuperation” and not to assess the accompanying turbo-machinery. The compressors are already existent (e.g. compressor part of the Alstom/Ansaldo GT26 gas turbine), and the turbines are also readily available.

The “Hot” pressure tests have been designed and configured in close collaboration with the Professorship of Renewable Energy Carriers at ETH Zurich. Using their in-house mathematical model, the optimum operating conditions were simulated and used as benchmark for the tests. The test results are then used to validate the numerical model, which is then used to simulate a scale-up AA-CAES plant. Using this approach, it can be reassured that the model that is used for the design of commercial plants is valid and has been verified with real-world experiments (See Outlook).

The Thermal Energy Storage (TES)

As mentioned in Section 4 and introduced in Section 5.5 a proprietary Thermal Energy Storage (TES) is used to capture and separate the heat from the compressed air (See Fig. 7.25). After the hot compressed air enters the TES from the top through the inlet pipe, it flows through the packed bed of rocks. Due to the large active surface area of the packed bed, an efficient heat transfer takes place between the air and the storage medium (i.e. rocks), resulting in an effective cool down of the air before it leaves the TES again at the bottom. This is the charging path. During discharging, the direction is reversed. As the discharging valves outside of the pressure chamber are opened, due to the overpressure in the chamber, air is sucked in through the bottom of the TES, heats up as it flows through the packed bed and leaves at the top, where it flows through the insulated pipes until it reaches the silencer (See Fig. 5.9 and Fig. 5.24).

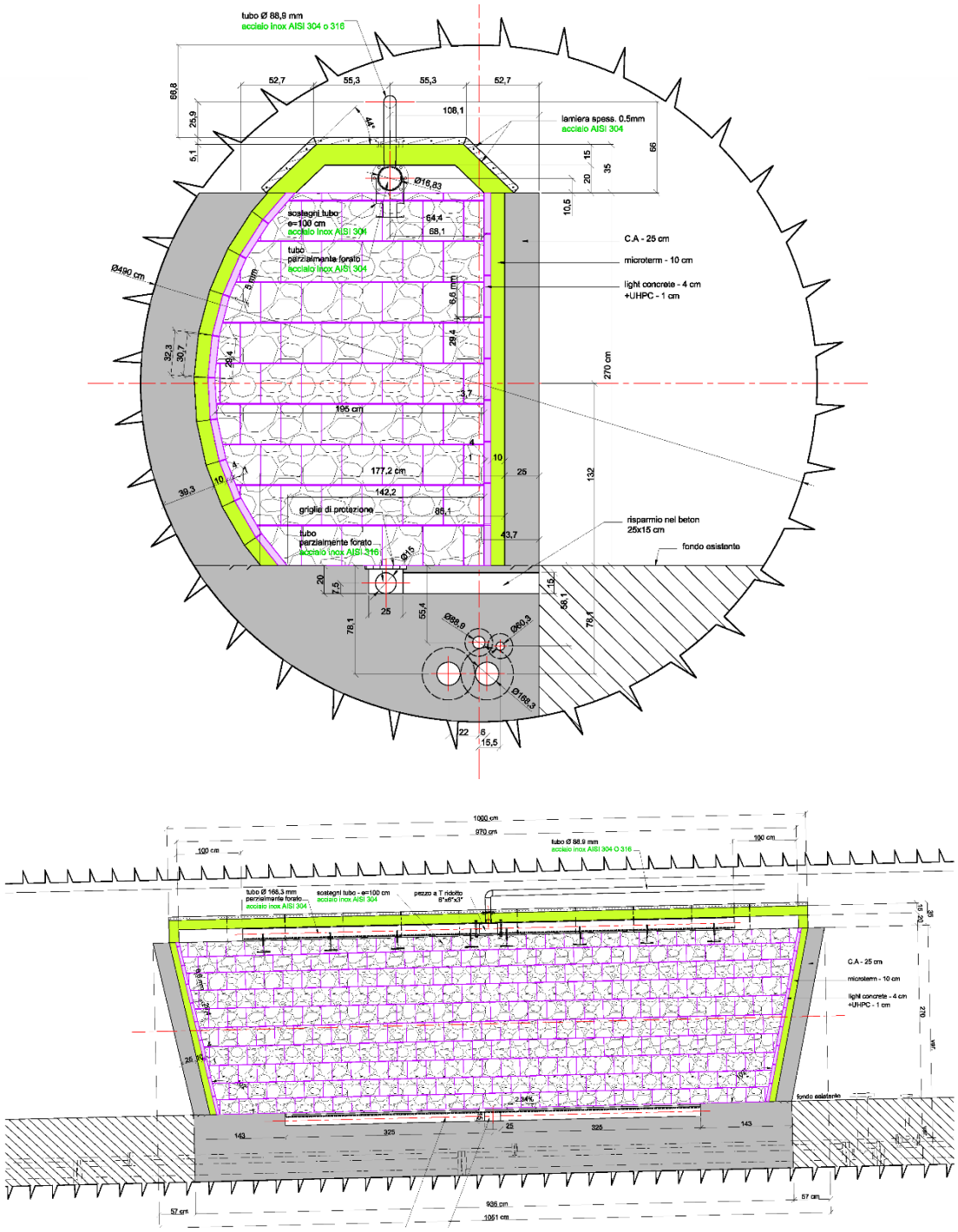

Fig. 7.25: Technical Drawings of the TES.

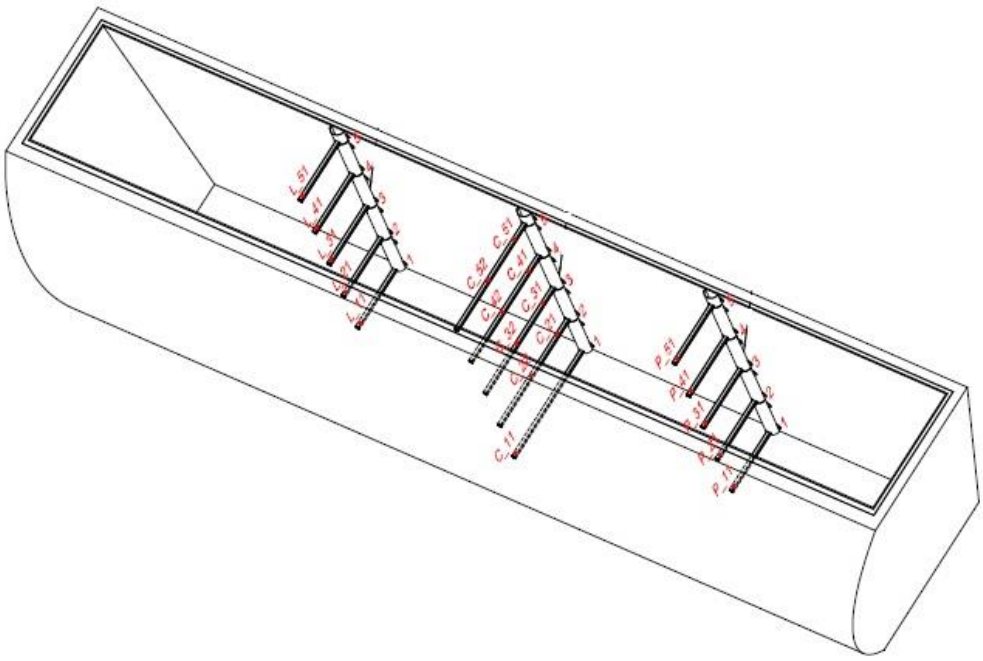

Fig. 7.26: Sketch of the Thermal Energy Storage (TES) with the position of the temperature sensors and level numbering.

Pre-Charging

The concept of pre-charging is explained in detail in literature[11] [12]. A thermocline TES, such as the one in the ALACAES pilot plant, needs to undergo 20-30 regular cycles before it reaches its optimum, steady-state performance. During these initial cycles, the TES has a low performance that in a commercial plant cannot be used for production of electricity or in the downstream application. In order to overcome this limitation, the TES can be pre-charged for a certain duration. This means that the TES is fed with the maximum plant temperature for several hours or days (depending on the TES design) before the cycling is started. In this way, it is possible to obtain the optimum, steady-state performance already after the first cycles. This approach is also used in the tests on the pilot plant. The pre-charging ramp and duration has been optimized using simulations carried out by ETH's PREC lab.

Test Results

Two sets of tests are executed:

- In the first test, the chamber is pressurized to 5.7 bar while the TES is simultaneously pre-charged with 520 ° air. Once at 5.7 bar, 3 consecutive cycles of 2:45 h charging/discharging

[11] Giw Zanganeh, High-Temperature Thermal Energy Storage for Concentrated Solar Power with Air as Heat Transfer Fluid, ETH Dissertation 21802, 2014
[12] Zanganeh G., et. al., 2014, Design of Packed Bed Thermal Energy Storage Systems for High-Temperature Industrial Process Heat, Applied Energy, Vo. 137, pp 812-822

are carried out, followed by 3 consecutive cycles of 0.5 bar pressure variation. The inlet temperature during all charging runs was 550 °C.

- For the second test, the chamber is pressurized to 5.75 bar while the TES is simultaneously charged. Once at 5.75 bar, 2 consecutive cycles of 2:45 h are carried out, followed by 2 consecutive cycles of 1:22 h and 3 consecutive cycles of 4.07 h. The charging temperature during all charging runs was again 550 °C.

These tests are explained in detail and their results are shown below.

The energy flows and the corresponding efficiencies are calculated for all cycles. For a clear overview of the energy flows, the thermal energy in the hot air and the mechanical energy in the compressed air are calculated separately.

The thermal energy carried by the incoming or outgoing air is calculated as

$$E_{th} = \dot{m}(c_p T_{TES,top} - c_p T_{TES,bottom})\Delta t$$

with $\dot{m}$ the mass flow rate measured by the installed mass flow meter, c_p the heat capacity of air at the given temperature, and Δt the time interval. $T_{TES,top}$ and $T_{TES,bottom}$ are the top (inlet during charging and outlet during discharging) and bottom (vice versa) temperatures of the TES. E_{th} is therefore the net energy entering the TES. For these calculations the temperature at the TES top is taken as the reference temperature leaving the plant, and not the temperature measured at the mass flow meter, which is about 25 m away from the TES. The reason for this is that the temperature variation between these two points is highly dependent on the plant design which will be subject to optimization in a commercial plant.

The thermal efficiency of the plant is therefore

$$\eta_{th} = \frac{E_{th,discharging}}{E_{th,charging}}$$

$T_{TES,top}$ is designated as “TES inlet temperature” and $T_{TES,bottom}$ as “TES out” in the following graphs.

The mechanical energy of compressed air entering the cavern is calculated using the equation for compressor work[13]:

$$E_{mech,ch} = CW = \frac{\dot{m} c_{p,in} T_{in}}{\eta_c}\left[\left(\frac{p_{out}}{p_{in}}\right)^{\frac{\gamma-1}{\gamma}} - 1\right]$$

with $\gamma = 1.4$ the specific heat ratio of air and $\eta_c = 0.85$ a representative compressor efficiency. The index *“in”* refers to the inlet conditions to the compressor, therefore ambient conditions in our case, and the index *“out”* to the compressor outlet conditions which is in our case equal to the cavern inlet conditions (after compressor and heater).

The mechanical energy of the compressed air leaving the cavern is calculated using the equation for turbine work:

[13] US National Aeronautics and Space Administration (NASA), Glenn Research Center Database

$$E_{mech,out} = TW = \dot{m}\eta_t c_{p,in} T_{in} \left[1 - \left(\frac{p_{out}}{p_{in}}\right)^{\frac{\gamma-1}{\gamma}}\right]$$

with $\eta_t = 0.9$ a representative turbine efficiency. The index *"in"* refers to the inlet conditions to the turbine, therefore the cavern outlet conditions. However, since we want to separate the thermal energy from the mechanical energy $c_{p,in}$ and T_{in} are taken as ambient conditions. Their energy has been considered in E_{th} above. The index *"out"* refers to the turbine outlet conditions, therefore ambient conditions in our case.

The mechanical efficiency is therefore calculated as

$$\eta_{mech} = \frac{E_{mech,out}}{E_{mech,in}}$$

And the overall plant efficiency is obtained by

$$\eta_{tot} = \frac{E_{mech,out} + E_{th,discharing}}{E_{mech,in} + E_{th,charging}}$$

It is important to note that the efficiency calculations done in the report do not consider the total outlet energy vs. the total inlet energy of the plant. Instead, the pressure chamber interface is taken as the reference point for efficiency calculations (i.e. the top of the TES), neglecting all other plant components such as heater and isothermal compressor efficiency. This is justified because the aim of the project was to assess the performance of the pressure zone and the TES and not the turbo-machinery installed upstream, which in this case is not representative for an AA-CAES plant.

31.10.2016 – Pre-charging to 5.7 bar and two cycling approaches

Pre-Charging

The plant is charged to 5.7 bar. When the cavern reached 1.5 bar, the heater is turned on and the TES is charged with 520 °C air. The results are shown in the following:

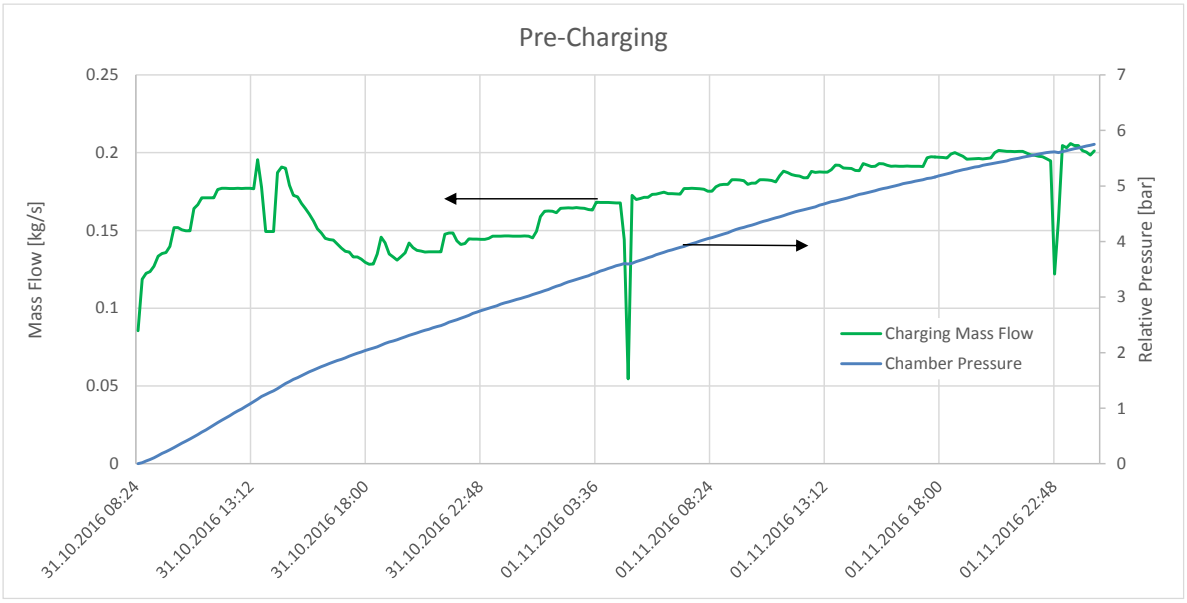

Fig. 7.27: The charging mass flow rate and pressure evolution during pre-charging.

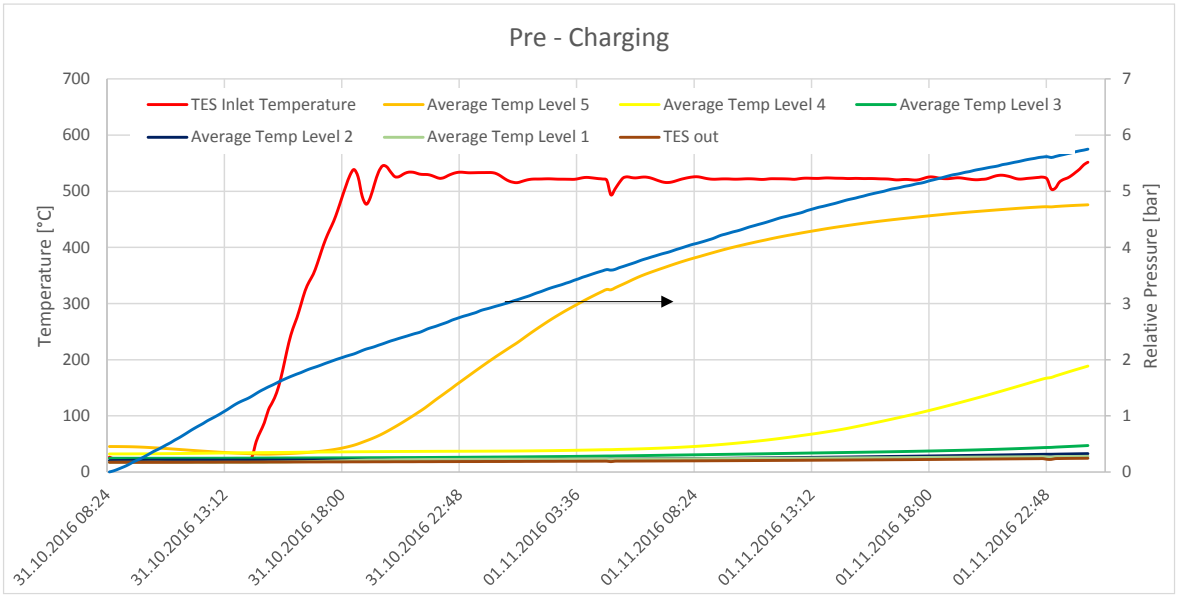

Fig. 7.28: The inlet temperature, temperature evolution in the TES and pressure evolution in the chamber during pre-charging.

Cycling

After the pre-charging, 2 cycling approaches were carried out that are presented in the following. Fig. 7.29 and Fig. 7.30 show the pressure, mass flow and temperature evolution during the cycling.

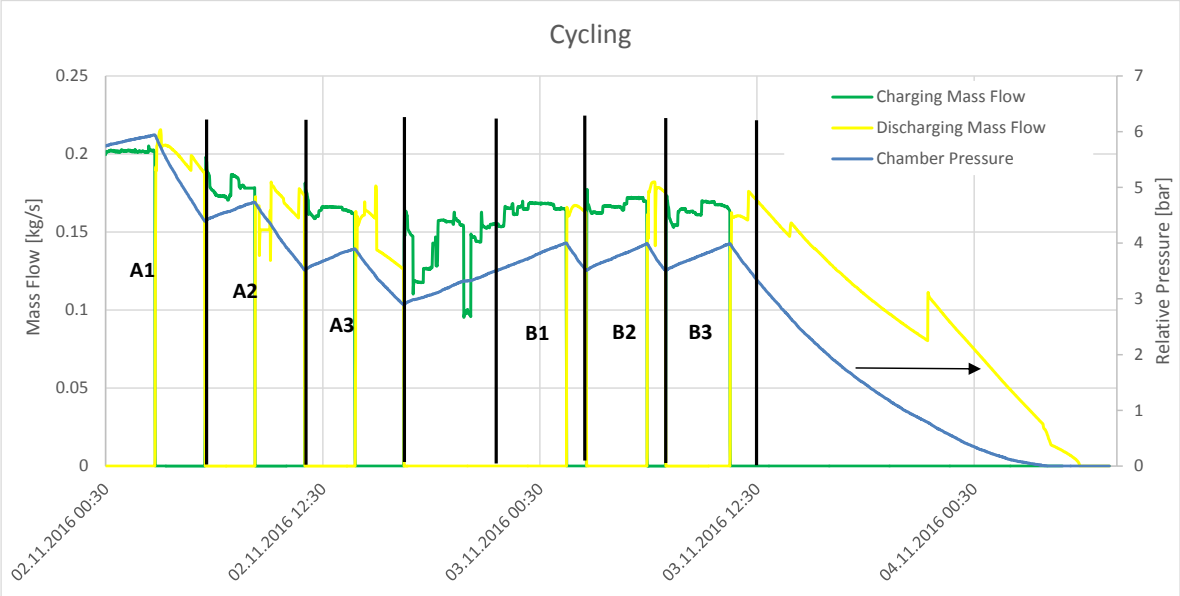

Fig. 7.29: The charging and discharging mass flow rates and pressure evolution in the plant for the two cycling approaches.

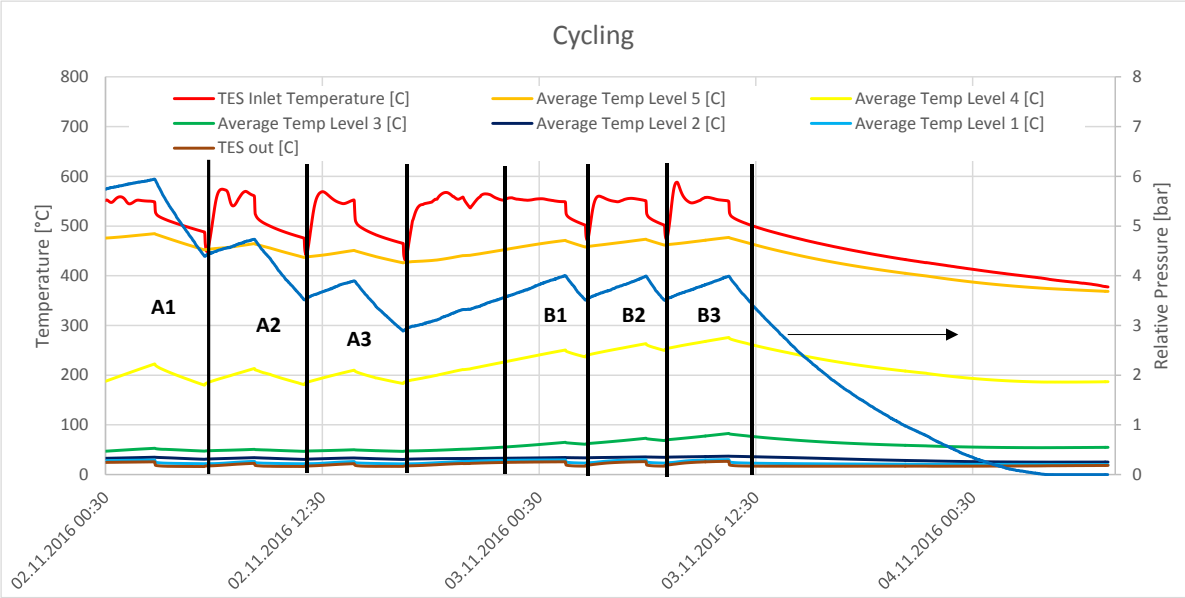

Fig. 7.30: The temperature profiles in the TES and the pressure evolution in the chamber for the two cycling approaches.

Cycling Approach A

Once at 5.7 bar, 3 consecutive cycles were carried out with each charging/discharging lasting 2:45 h. The charging was carried out with 550 °C inlet temperature. The test details are shown in Table 7.1 and the results depicted in Fig. 7.29 and Fig. 7.30. Since the charging and discharging duration was

the same, due to the leakages mentioned in Section 7.1, despite similar charging and discharging mass flow rates, the pressure at the end of the discharging is much lower than at the beginning of the charging. For instance, for the first cycle, the pressure at the beginning of the charging was 5.7 bar. At the end of the first cycle, this pressure dropped to 4.4 bar, therefore a drop of 1.3 bar with respect to the initial condition. For the 2nd and 3rd cycles, this pressure drop is reduced due to smaller leakage rates at lower pressures.

Cycle		Start Time	Start Pressure	End Time	End Pressure
A1	Charging	00:30	5.7	03:15	5.94
	Discharging	03:15	5.94	06:00	4.4
A2	Charging	06:00	4.4	08:45	4.73
	Discharging	08:45	4.73	11:30	3.52
A3	Charging	11:30	3.52	14:15	3.9
	Discharging	14:15	3.9	17:00	2.8

Table 7.1: Test details of approach A. Start date 2.11.2016

Fig. 7.31 shows the TES top temperature and pressure evolution for the three cycles of approach A. Due to the leakages, the pressure level drops with cycle number. The temperature evolution is relatively stable with cycling and shows a small drop with each cycle. This is attributed to two facts. First, the thermal inertia of the piping between the heater and the TES, combined with the relatively small mass flows used in the pilot plant, causes a ramping time of approx. 45 minutes before the TES charging temperature is back to 550 °C, therefore reducing the inlet energy during charging. Second, the pre-charging of the TES was not sufficient and would need to be optimized.

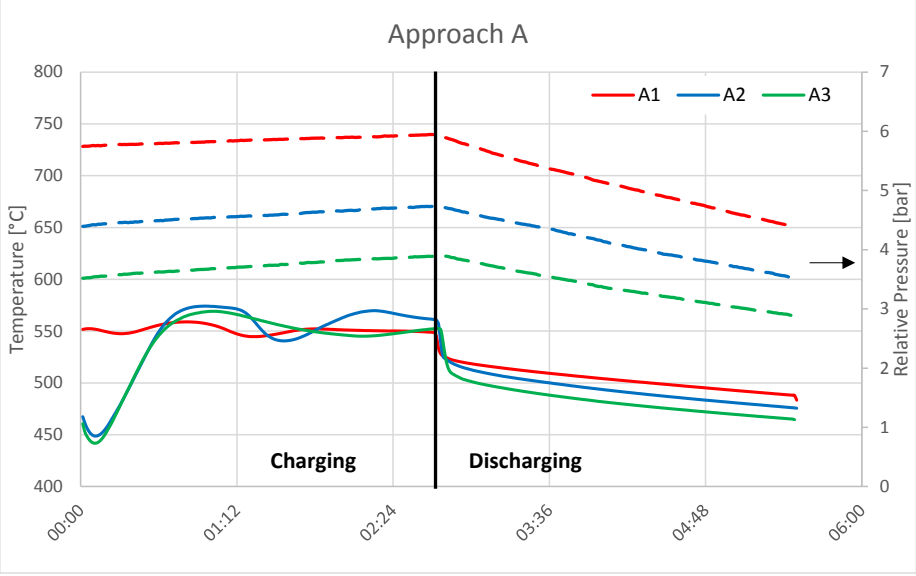

Fig. 7.31: The TES top temperature (inlet during charging and outlet during discharging) and pressure evolution for the three cycles of approach A. Solid lines represent temperature and dashed line pressure.

Table 7.2 summarizes the energy flows and efficiency calculations for these tests. The thermal efficiency is about 75-82%, the mechanical efficiency around 26-42%, and the overall plant efficiency about 66-72%.

Cycle		E_{th} [KWh]	E_{mech} [KWh]	η_{th}	η_{mech}	η_{tot}
A1	Charging	391.45	157.54	**76.64%**	**35.92%**	**65.96%**
	Discharging	300.03	56.58			
A2	Charging	293.37	102.24	**82.57%**	**42%**	**72.08%**
	Discharging	242.23	42.94			
A3	Charging	269.35	83.32	**75.03%**	**40.64%**	**66.91%**
	Discharging	202.10	33.86			

Table 7.2: Energy flow and efficiency calculations for tests A.

Cycling Approach B

After the cycling approach A that followed similar charging/discharging durations, the cycling approach B was executed that followed a similar pressure variation of 0.5 bar between 3.5 and 4 bar. After the end of the tests of approach A, the pressure in the plant was at 2.8 bar. Therefore, the pressure was first increased to 3.5 bar before the cycling started. The test details are summarized in Table 7.3. Due to the leakages the charging takes much longer than the discharging (3:30 h charging vs. 1:00 h discharging).

Cycle		Start Time	Start Pressure	End Time	End Pressure
B1	Charging	22:00	3.5	1:58	4
	Discharging	01:58	4	03:00	3.5
B2	Charging	03:00	3.5	06:25	4
	Discharging	06:25	4	07:29	3.5
B3	Charging	07:29	3.5	11:00	4
	Discharging	11:00	4	12:05	3.5

Table 7.3: Test details of approach B. Start date 2.11.2016

Fig. 7.32 shows the TES top temperature and pressure evolution for the three cycles of approach B. The approach here was to keep the same pressure range for charging and discharging, which, due to the leakages, resulted in much longer charging time than discharging time. Therefore, the cycle efficiency is very poor and not representative for the plant performance.

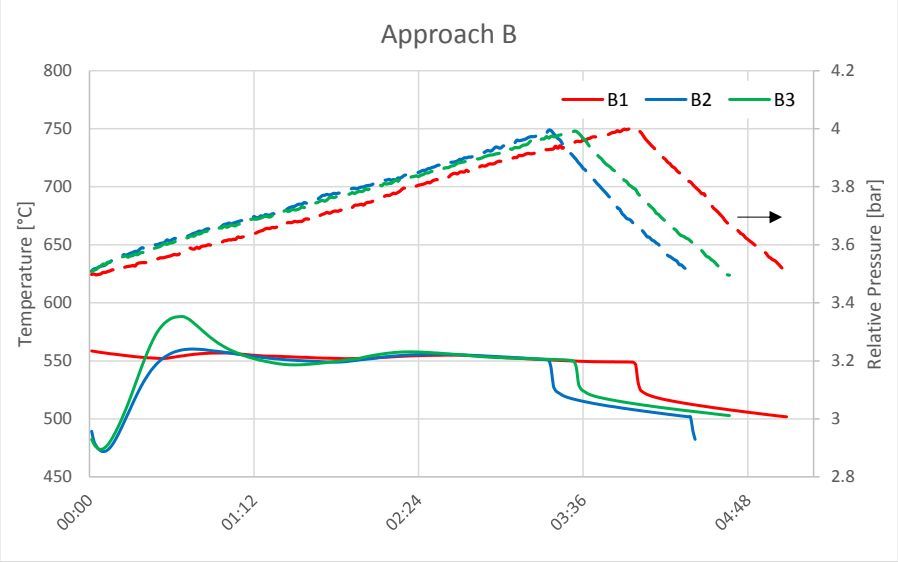

Fig. 7.32: The TES top temperature (inlet during charging and outlet during discharging) and pressure evolution for the three cycles of approach B. Solid lines represent temperature and dashed line pressure.

Table 7.4 summarizes the energy flows and efficiency calculations for tests B. As mentioned above, due the much longer charging time than discharging time, the efficiencies are rather low and not representative.

Cycle		E_{th} [KWh]	E_{mech} [KWh]	η_{th}	η_{mech}	η_{tot}
B1	Charging	395.52	120.54	**25.31%**	**13.68%**	**22.59%**
	Discharging	100.11	16.49			
B2	Charging	334.27	103.24	**29.48%**	**15.71%**	**26.23%**
	Discharging	98.53	16.22			
B3	Charging	350.68	107.50	**27.20%**	**14.57%**	**24.24%**
	Discharging	95.38	15.67			

Table 7.4: Energy flow and efficiency calculations for tests B.

Idle Time

Once the plant was at ambient pressure, the TES was left in “idle”, meaning that no air is circulated through the TES in charging or discharging direction. This helps to determine the thermal degradation of the TES with time when the plant is not operational. Fig. 7.33 shows the temperature evolution and energy stored in the TES during the idle time. In the first 24 h, the TES lost 3.24% of the stored energy and in the second 24 h 3.28%, therefore showing a stable loss rate. Again, this relatively high loss rate is attributed to the small size of the TES compared to a commercial size plant (See Outlook for losses of a scale-up plant).

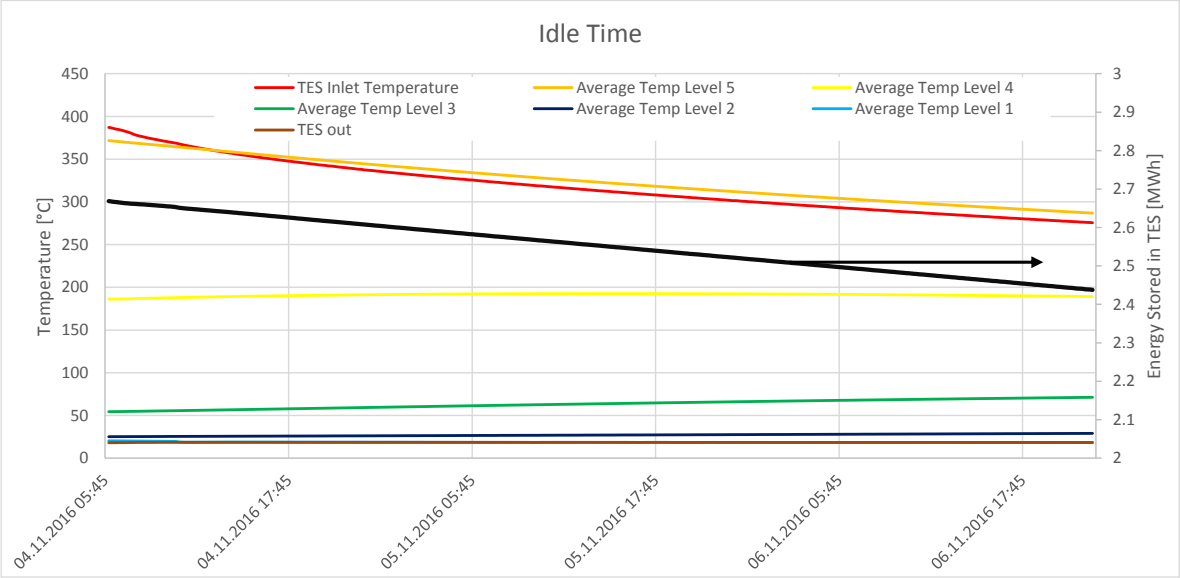

Fig. 7.33: The temperature evolution and energy stored in the TES during idle time; i.e. no mass flow through the TES.

14.11.2016 – Pre-charging to 5.75 bar and three cycling approaches

Pre-Charging

For the second test, the chamber is pressurized initially to 5.75 bar while the TES inlet temperature is continuously increased to 550 °C. The pressure evolution as well as the mass flow rate and the inlet and storage temperatures are shown in the following graphs.

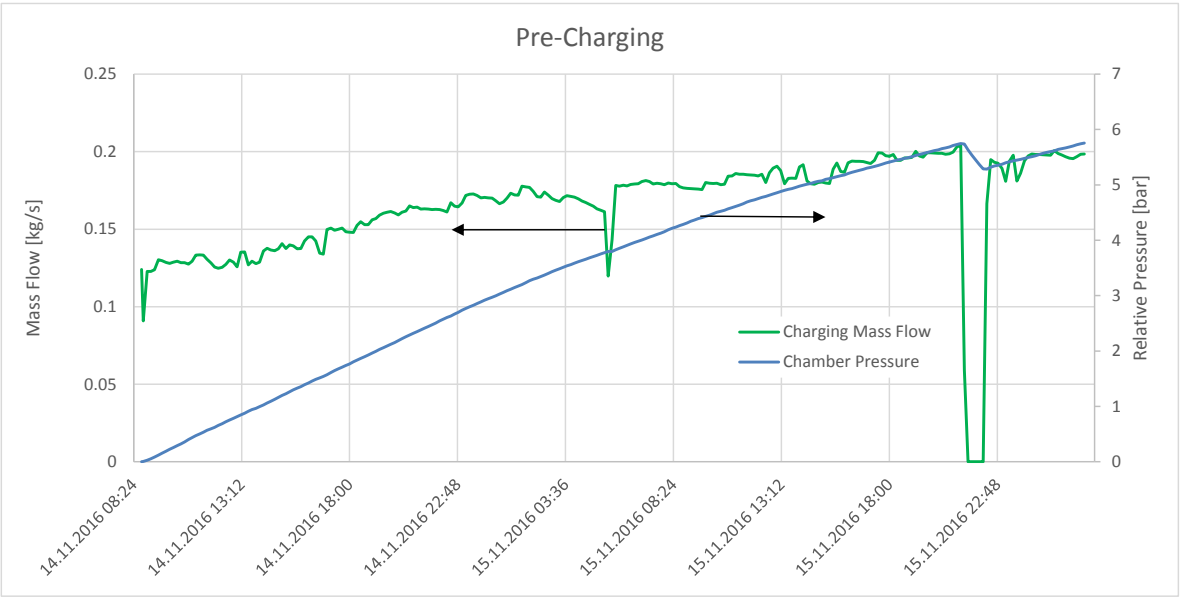

Fig. 7.34: The charging mass flow rate and pressure evolution during pre-charging. When the pressure arrived at 5.7 bar, the plant was discharged by mistake for approx. 40 minutes.

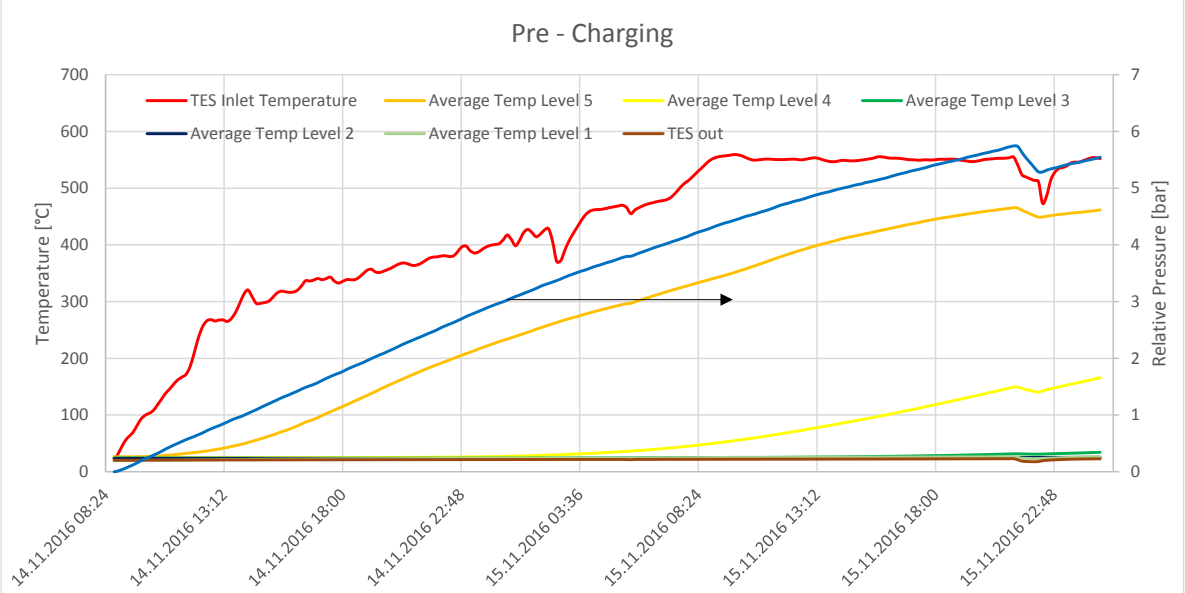

Fig. 7.35: The inlet temperature, temperature evolution in the TES and pressure evolution in the chamber during pre-charging. When the pressure arrived at 5.7 bar, the plant was discharged by mistake for approx. 40 minutes.

Cycling

After the pre-charging, 3 cycling approaches were carried out that are presented in the following. Fig. 7.36 and Fig. 7.37 show the pressure, mass flow and temperature evolution during the cycling.

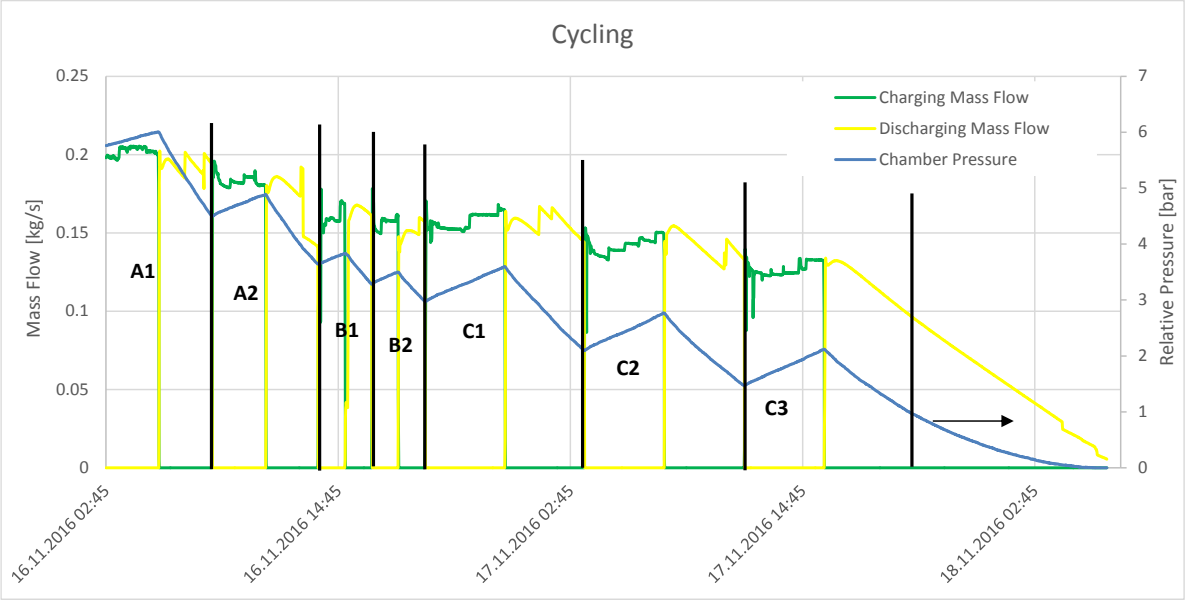

Fig. 7.36: The charging and discharging mass flow rates and pressure evolution in the plant for the three cycling approaches.

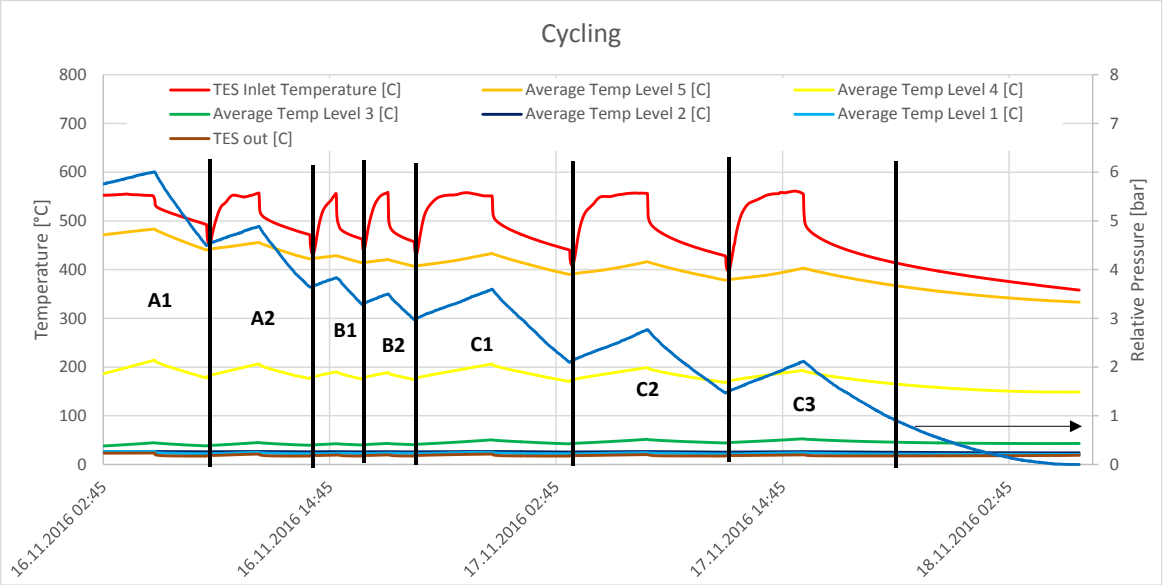

Fig. 7.37: The temperature profiles in the TES and the pressure evolution in the chamber for the three cycling approaches.

Cycling Approach A

Once the plant achieved 5.75 bar, 2 consecutive cycles of 2:45 h charging/discharging were carried out. The test details are shown in Table 7.5

Cycle		Start Time	Start Pressure	End Time	End Pressure
A1	Charging	02:45	5.75	05:30	6.00
	Discharging	05:30	6.00	08:15	4.5
A2	Charging	08:15	4.5	11:00	4.87
	Discharging	11:00	4.87	13:45	3.65

Table 7.5: Test details of approach A. Started on 16.11.2016

Fig. 7.38 shows the TES top temperature and pressure evolution for the three cycles of approach A. Cycle A1 had a more stable inlet temperature during charging as it followed directly the pre-charging phase. The performance of Cycle A2 is slightly worse than A1 due to the lower inlet temperature during charging and non-optimized pre-charging.

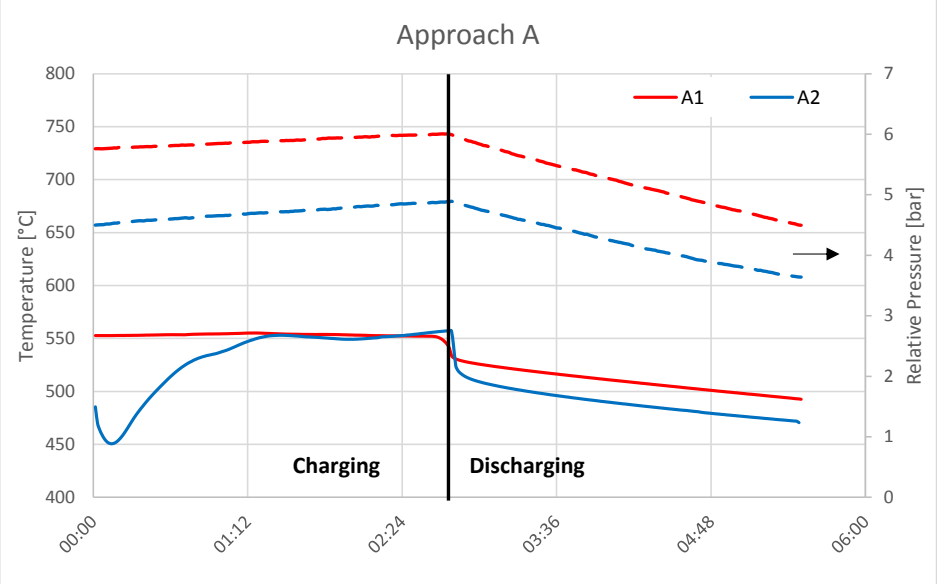

Fig. 7.38: The TES top temperature (inlet during charging and outlet during discharging) and pressure evolution for the three cycles of approach A. Solid lines represent temperature and dashed line pressure.

The energy flows and efficiency calculations are shown in Table 7.6. The thermal efficiency is 82-87%, the mechanical efficiency around 40% and the overall plant efficiency around 71-74%.

Cycle		E_{th} [KWh]	E_{mech} [KWh]	η_{th}	η_{mech}	η_{tot}
A1	Charging	336.83	134.92	**87.51%**	**40.99%**	**74.21%**
	Discharging	294.76	55.30			
A2	Charging	296.07	107.79	**82.18%**	**40.93%**	**71.17%**
	Discharging	243.31	44.11			

Table 7.6: Energy flow and efficiency calculations for tests A.

Cycling Approach B

Immediately after concluding the first approach, approach B was carried out that consists of 2 consecutive cycles of 1:22 h charging/discharging. The test details are shown in Table 7.7.

Cycle		Start Time	Start Pressure	End Time	End Pressure
B1	Charging	13:45	3.65	15:07	3.84
	Discharging	15:07	3.84	16:30	3.28
B2	Charging	16:30	3.28	17:52	3.5
	Discharging	17:52	3.5	19:15	2.9

Table 7.7: Test details of approach B.

Fig. 7.39 shows the TES top temperature and pressure evolution for the three cycles of approach B. Both cycles show a similar performance due to the similar charging conditions.

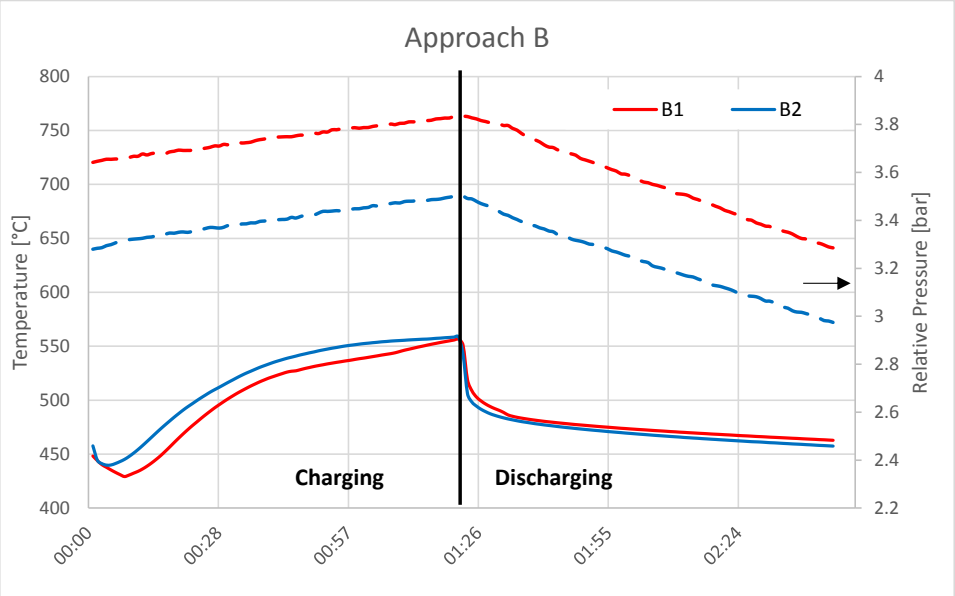

Fig. 7.39: The TES top temperature (inlet during charging and outlet during discharging) and pressure evolution for the three cycles of approach B. Solid lines represent temperature and dashed line pressure.

The energy flows and efficiency calculations for the tests of approach B are shown in Table 7.8. The TES thermal efficiency is about 87-89%, the mechanical efficiency of the compressed air about 48% and the overall plant efficiency 78%. The mechanical efficiency increased with respect to Approach A due to the lower leakage rates at lower operating pressures.

Cycle		E_{th} [KWh]	E_{mech} [KWh]	η_{th}	η_{mech}	η_{tot}
B1	Charging	118.62	39.34	**89.21%**	**47.25%**	**78.76%**
	Discharging	105.81	18.59			
B2	Charging	121.38	36.91	**86.82%**	**48.45%**	**77.88%**
	Discharging	105.38	17.89			

Table 7.8: Energy flow and efficiency calculations for tests B.

Cycling Approach C

The last tests followed immediately the tests of approach B and consisted of 3 consecutive cycles of 4:07 h charging/discharging. The test results are summarized in Table 7.9.

Cycle		Start Time	Start Pressure	End Time	End Pressure
C1	Charging	19:15	2.9	23:22	3.6
	Discharging	23:22	3.6	03:30 (17.11.2016)	2.1
C2	Charging	03:30	2.1	07:37	2.75
	Discharging	07:37	2.75	11:45	1.49
C3	Charging	11:45	1.49	15:52	2.1
	Discharging	15:52	2.1	20:00	1.05

Table 7.9: Test details of approach C.

Fig. 7.40 shows the TES top temperature and pressure evolution for the three cycles of approach C. The long discharging time causes the TES to be discharged beyond its optimum design point (2:45 h), causing in a worsening performance with increased cycling.

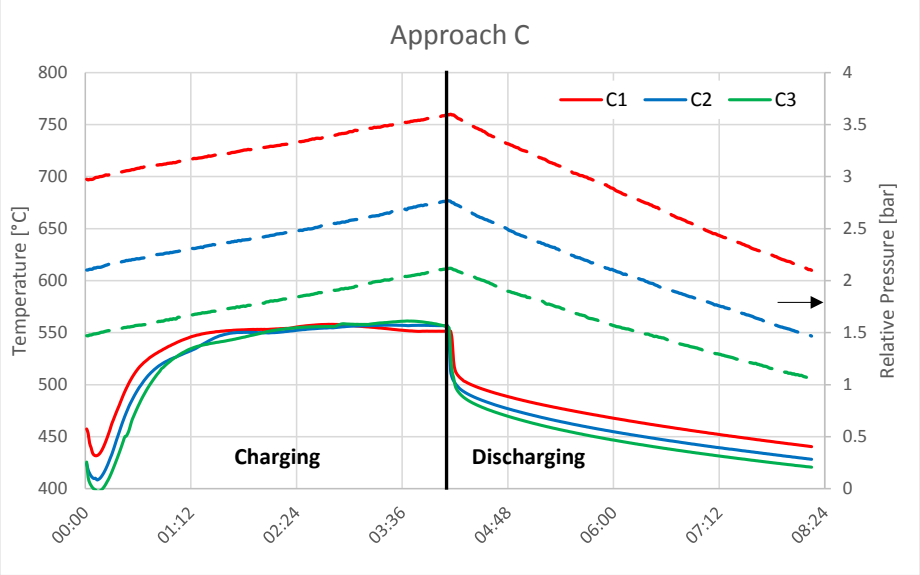

Fig. 7.40: The TES top temperature (inlet during charging and outlet during discharging) and pressure evolution for the three cycles of approach C. Solid lines represent temperature and dashed line pressure.

The energy flows and efficiency calculations are shown in Table 7.10. The TES thermal efficiency is 78-84%, the mechanical efficiency of the compressed air about 47-50% and the overall plant efficiency 74-78%. The mechanical efficiency increased with respect to Approach B further due to the lower leakage rates at lower operating pressures.

Cycle		E_{th} [KWh]	E_{mech} [KWh]	η_{th}	η_{mech}	η_{tot}
C1	Charging	382.83	109.51	**84.11%**	**46.95%**	**78.54%**
	Discharging	321.98	51.41			
C2	Charging	340.84	80.64	**84.17%**	**50.16%**	**77.66%**
	Discharging	286.88	40.45			
C3	Charging	302.77	57.89	**78.02%**	**50.05%**	**73.53%**
	Discharging	236.21	28.97			

Table 7.10: Energy flow and efficiency calculations for tests C.

Idle

After the pressure in the plant was completely discharged, the storage was left in idle mode (no flow through the TES) in order to measure the thermal losses during idle time. The temperature evolution and the energy stored in the TES is shown in Fig. 7.41. The losses in the first 24 h were 3.89% and in the second 24 h 3.55%, and therefore similar to the first set of tests.

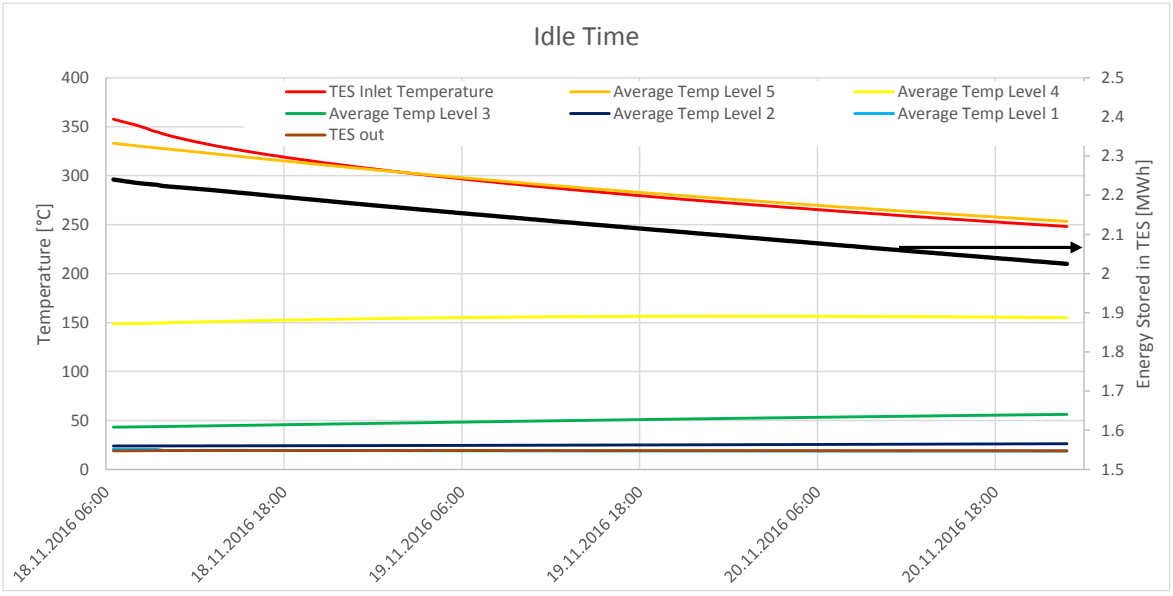

Fig. 7.41: The temperature evolution in the TES during idle time; i.e. no mass flow through the TES.

Plant Assessment

The ALACAES pilot and proof of concept plant had multiple purposes. One of the main purposes was to understand and verify potential problems that could arise during the operation of an AA-CAES plant caused by the elevated temperatures of the incoming process air.

In this segment, these challenges are addressed and evaluated based on the experimental data of the tests of 31.10.2016. The results for the second “Hot” test of 14.11.2016 were similar and are therefore not reproduced here.

Chamber, Rock, and Piping Temperature

Fig. 7.42 shows the pressure evolution as well as the rock, chamber and piping temperature during the tests of 31.10.2016. Each temperature curve is the average of the two measurement points in the plant, as shown in Fig. 5.21. The piping temperature refers to the pipelines in the central canal carrying water and cables and not the process air piping leading to the TES. The rock temperature is measured at a depth of 10 cm from the tunnel wall surface and the chamber temperature sensors are loose in the air.

The chamber temperature rises to around 20 °C during charging and drops to around 17 °C during discharging. The chamber temperature variations are caused by the compression or expansion of air in the tunnel, caused by physical principles similar to the ones underlying the concept of AA-CAES (See Section 4). However, since the chamber is not adiabatic (i.e. there is heat exchange with the mountain), the temperature in the chamber stabilizes around a fixed value during charging and discharging. This is important because too high or too low temperatures in the cavern could cause problems to the sensors as well as creating additional stress on the mountain due to thermal expansion of the rock and shotcrete.

The rock temperature, measured at a depth of 10 cm from the tunnel wall surface, is even more stable and varies by around 1-2 °C during the tests.

The piping temperature varies accordingly by around 3-4 °C. This is crucial because the pipelines in the canal are fixed from both sides in the main plugs without the possibility of thermal expansion, as explained in Section 5. Therefore, big temperature variations in the pipe temperature would cause thermal expansion of the pipes that could lead to breaking of the pipes or opening of the joints, and therefore cause a catastrophic failure of the plant.

These results also show that the TES can effectively cool down the air and keep the cavern temperature at safe and acceptable values, which is one of the most important characteristics of the ALACAES technology.

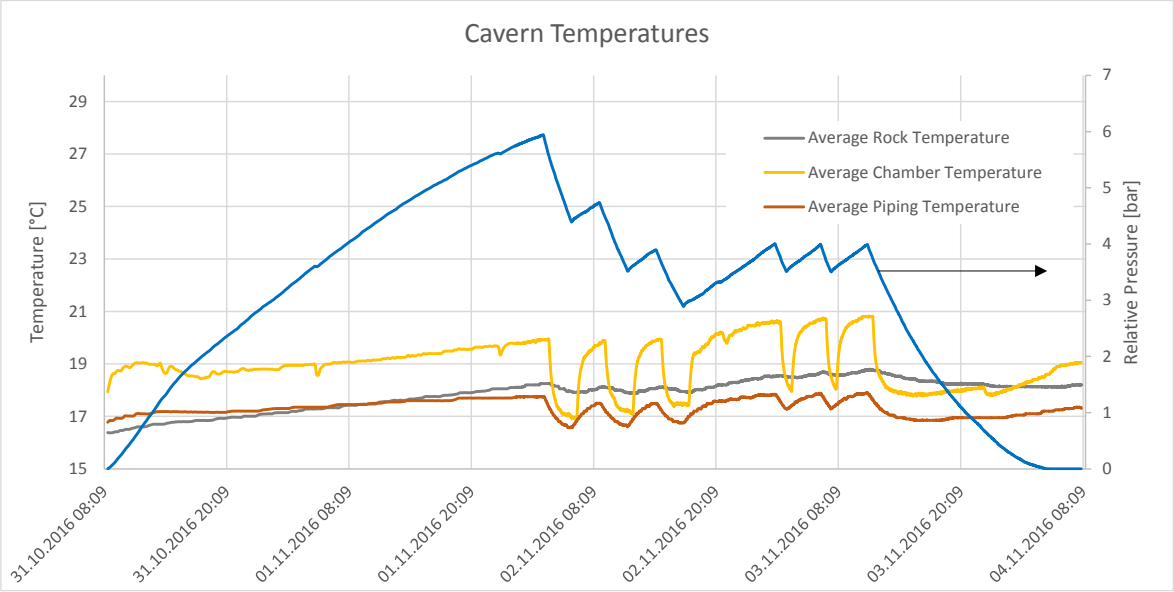

Fig. 7.42: The pressure evolution and the average rock, chamber and piping temperature in the plant for the tests of 31.10.2016.

Piping Insulation and TES Cover Temperature

Fig. 7.43 shows the TES inlet temperature as well as the insulation on the piping leading to the TES and the TES cover temperature evolution for the tests of 31.10.2016. The location of the temperature measurements is shown in Fig. 5.21. The TES cover temperature measurement is fixed to the outer surface of the lid.

With a TES inlet temperature of around 550°C, the piping insulation temperature does not exceed 120 °C, which is well below the burning point of the silicon/glass fiber membrane of 300 °C that is placed in the first 15 m after the plug where the pipeline passes through (See Fig. 5.23). This is important for safety reasons in order to eliminate the risk of fire in the plant.

The TES cover temperature achieves a maximum temperature of 40 °C while being charged with 550 °C. This proves the effective insulation used in the storage to keep the losses to a minimum and reduce the risks caused by having high temperatures in the pressure chamber. Also, this is important in order to avoid damage to the lid caused by thermal expansion.

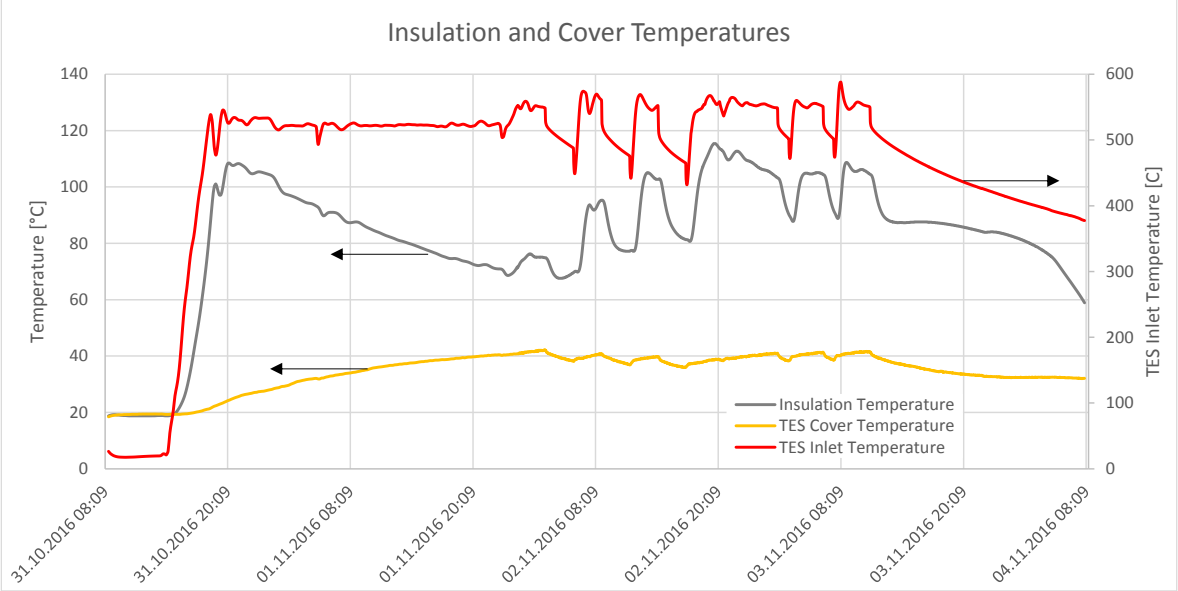

Fig. 7.43: The piping insulation and the TES cover and inlet temperature evolution during the tests of 31.10.2016.

Feeding Pipe Temperatures

Feeding pipe refers to the 5 m long pipe crossing through the Loderio Plug (see Section 5.4 for details). Fig. 7.44 depicts the TES inlet temperature as well as the feeding pipe temperatures with the position of the sensors depicted in Fig. 5.9.

The cooling air outlet temperature stays below 40 °C throughout the tests and the pipe outer surface temperature increases to a maximum of 23 °C.

It was important that the feeding pipe outer surface temperatures (FP1, 2, 3) do not increase significantly as this could cause cracking of the concrete structure and therefore worsen the plug performance.

Further, after filling the area around the feeding pipe with an epoxy resin in order to eliminate leakages from this area as explained in Section 7.1, it was important to keep the feeding pipe outlet temperature as low as possible in order to avoid cracking of the resin due to thermal expansion.

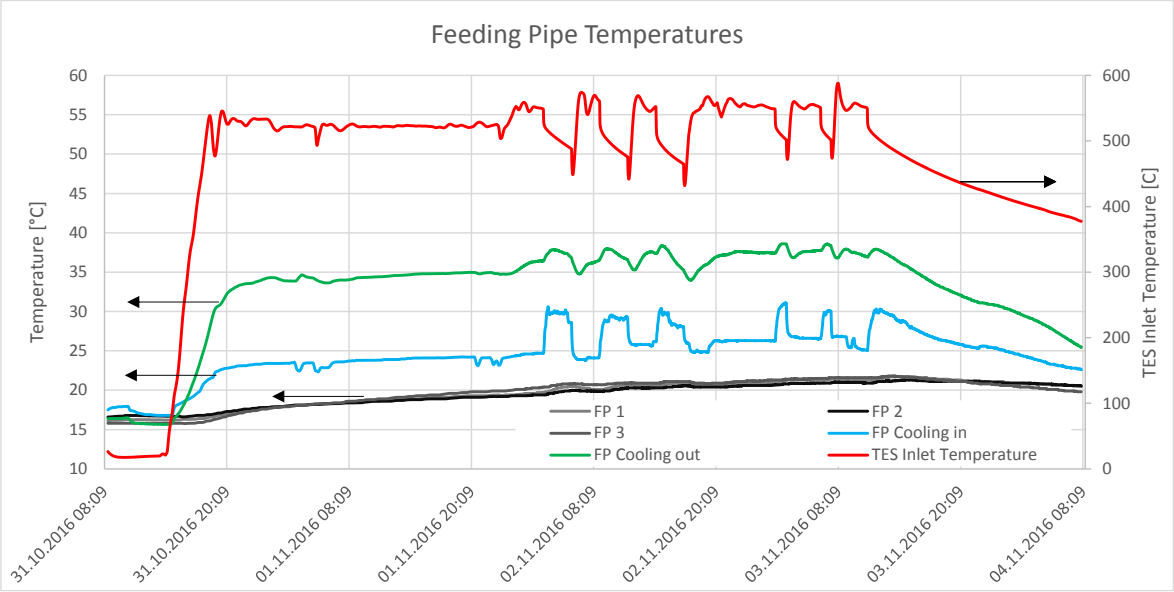

Fig. 7.44: TES inlet temperature and the feeding pipe inlet, outlet as well as tube surface temperatures during the tests of 31.10.2016.

TES inlet vs. Process Air Temperature

Fig. 7.45 depicts the TES inlet temperature and the process air temperature evolution during the tests of 31.10.2016. The position of the process air temperature measurement is depicted in Fig. 5.9 as “T_MF”.

As it can be seen in the graph, there is a 50 °C temperature drop between the heater and the TES inlet. While for this pilot plant these losses are not relevant, it is of utmost importance that these losses are minimized for a commercial plant by using better insulation material or minimizing the distance between compressor and TES. However, it should be noted that a higher mass flow rate of the process air – which will be the case for a scale-up plant - will reduce significantly the temperature drop along the pipeline.

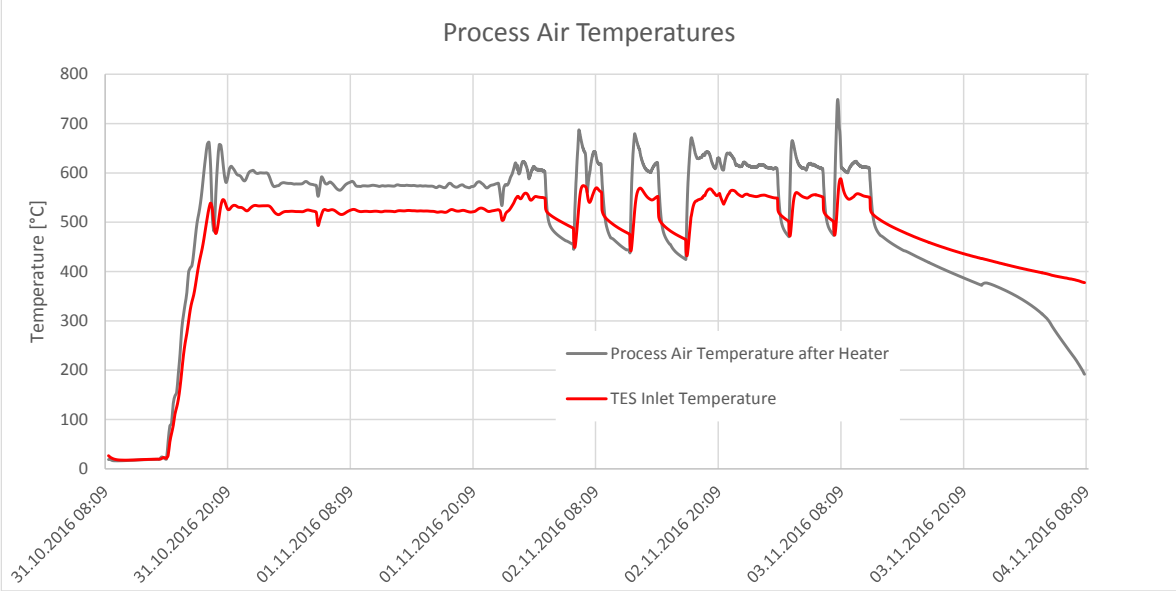

Fig. 7.45: Process air and TES inlet temperature evolution during the tests of 31.10.2016.

7.3. Water Drainage

Using the water management system introduced in Section 5.6, it was possible to register changes in the amount of incoming water into the cavern as a function of pressure. It was observed that the filling time of the tank increases significantly when the pressure inside the cavern is increased, proving that the increased pressure in the chamber impedes the water from entering to the pressure zone. This phenomenon was anticipated. The plant has a minimum rock coverage of 400 m above the plant, which, due to continuous and constant flow of water into the tunnel, is most probably saturated with water. Therefore, water should theoretically continue entering into the pressure zone up to a pressure of 40 bar, which corresponds to the hydrostatic pressure of the water acting on the plant. The following graph shows the water tank filling time and cavern pressure as a function of time for one of the tests. The relation between the filling time and the pressure was similar for all tests, therefore, only one case is shown here.

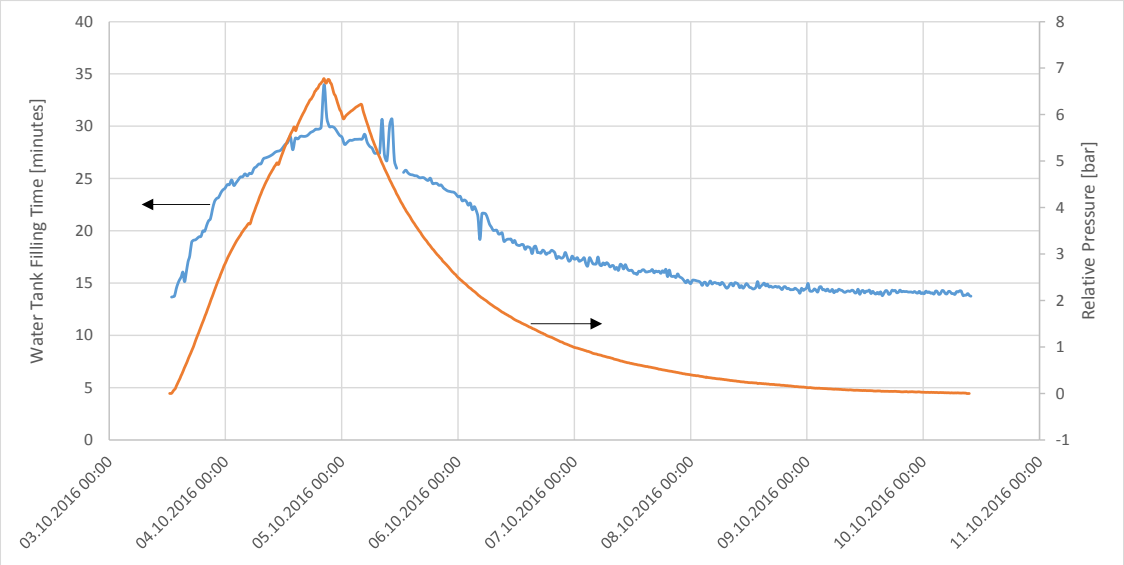

Fig. 7.46: Water tank filling time and cavern pressure as a function of time for one of the tests. The filling time increases with increasing pressure, since the pressure in the cavern impedes the flow of water into the pressure zone.

The water evacuation time, on the other hand, shortens drastically with increased pressure due to the high pressure in the water tank that pushes out the water forcefully during unloading. The following graph shows the water tank unloading time and cavern pressure as a function of time for one of the tests. The relation between the unloading time and the pressure was similar for all tests. Therefore, only one case is shown here.

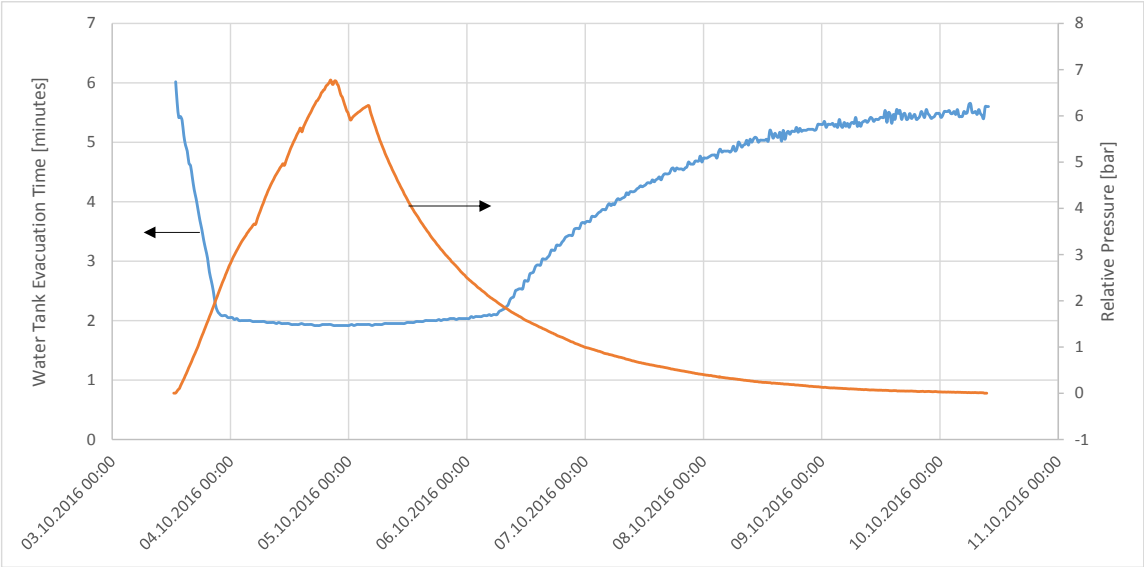

Fig. 7.47: Water tank evacuation time and cavern pressure as a function of time for one of the tests. The evacuation time decreases with increasing pressure due to the forceful ejection of water from the tank caused by the elevated pressure present in the tank. A minimum evacuation time of 2 minutes is achieved at around 1.5 bar.

7.4. Image Processing

The images taken with the high pressure camera were analyzed with the structural similarity method using Lab View's Vision module by National Instruments. Fig. 7.48 to Fig. 7.51 show the image distortion and cavern pressure for each camera as a function of time, and the captured images at 0 and 6 bar for one of the tests. For the cameras pointing on the membranes at the two ends, the change in the image is correlated to the movement of the membrane, which at elevated pressure adheres to the cavern wall, demonstrating its effectiveness in sealing the area next to the plug. For the Storage and Tunnel cameras, the change in the image is due to the reduced humidity with increasing pressure, as explained in Section 7.3. The reduced water flow into the cavern causes the humidity to decrease. The image distortion behavior is similar for all tests. Therefore, only one set of data is presented here.

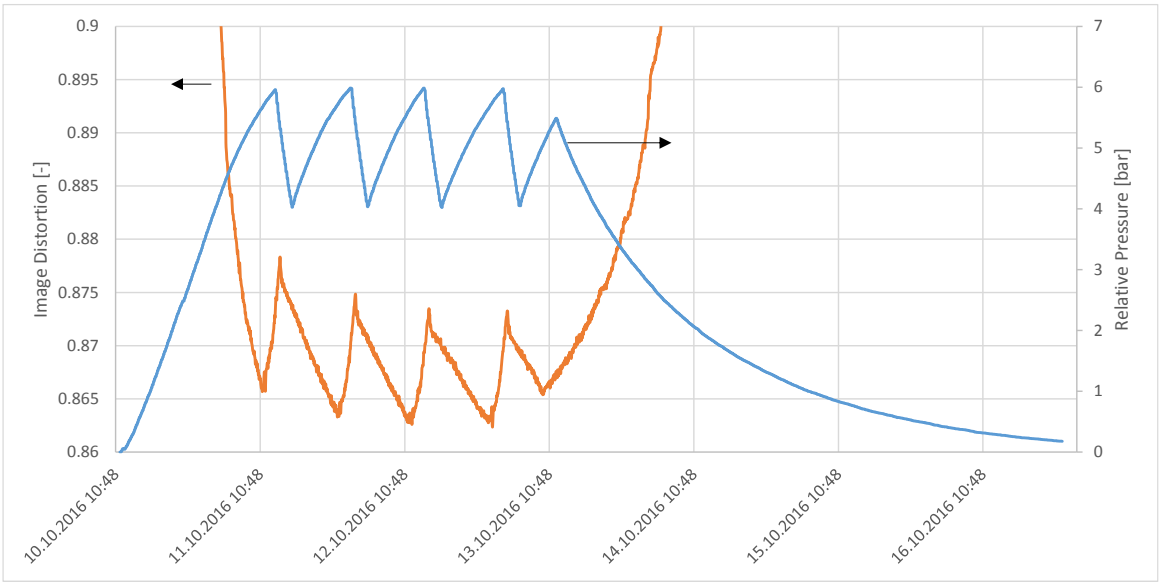

Fig. 7.48: Top: Image distortion and cavern pressure as a function of time for the camera looking at the Loderio side membrane for one of the tests. It can be seen that the image distortion follows the pressure change in the cavern, caused by movement of the membrane. Bottom left: Image captured by the Loderio camera with cavern relative pressure at 0 bar. It can be seen that the membrane is

loose. Bottom right: Image captured by the same camera with cavern relative pressure at 6 bar. The membrane sticks to the wall to create an impermeable zone in the vicinity of the Plug.

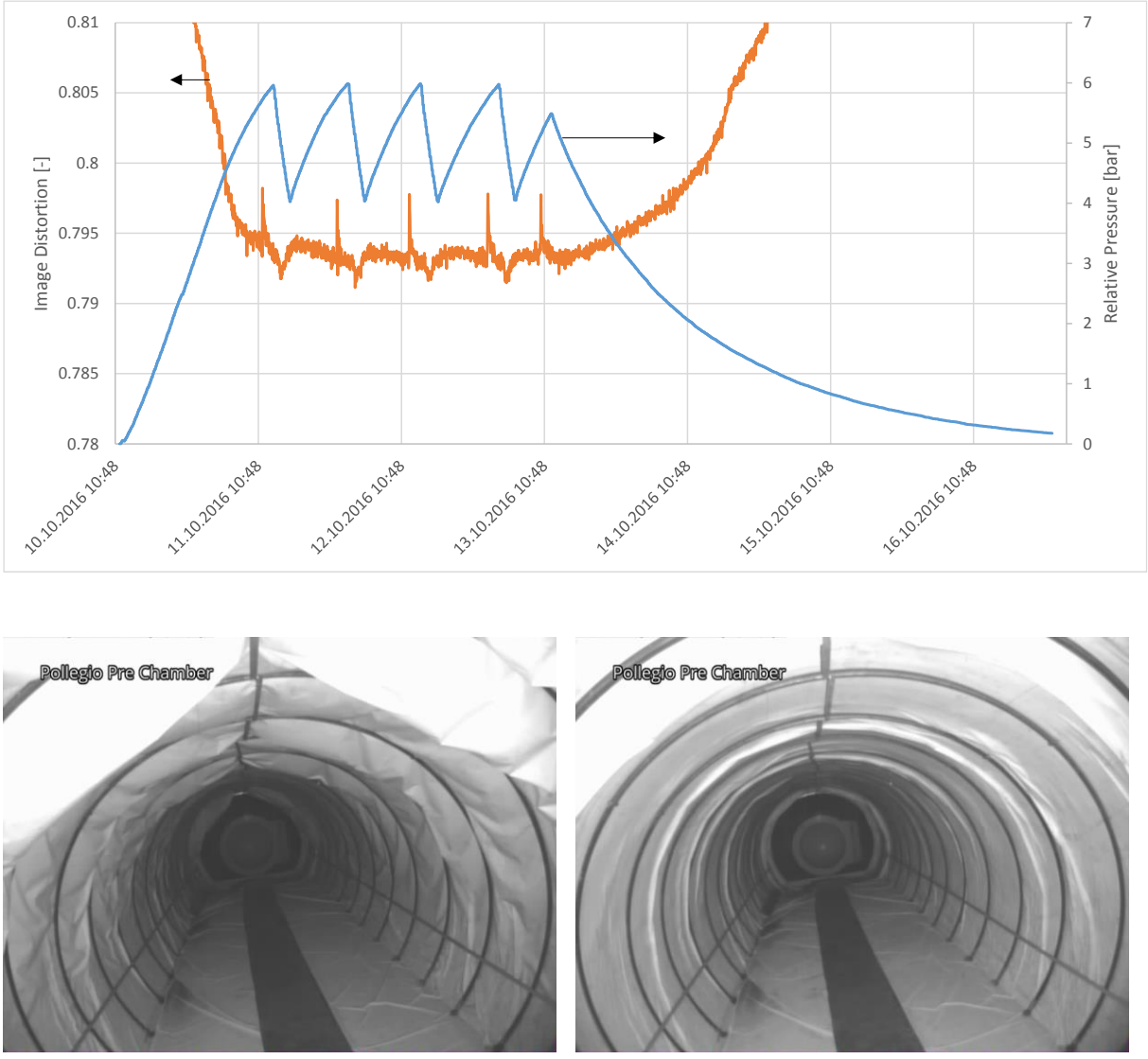

Fig. 7.49: Top: Image distortion and cavern pressure as a function of time for the camera looking at the Pollegio side membrane for one of the tests. It can be seen that the image distortion follows the pressure change in the cavern, caused by movement of the membrane. Bottom left: Image captured by the Pollegio camera with cavern relative pressure at 0 bar. It can be seen that the membrane is loose. Bottom right: Image captured by the same camera with cavern relative pressure at 6 bar. The membrane sticks to the wall to create an impermeable zone in the vicinity of the Plug.

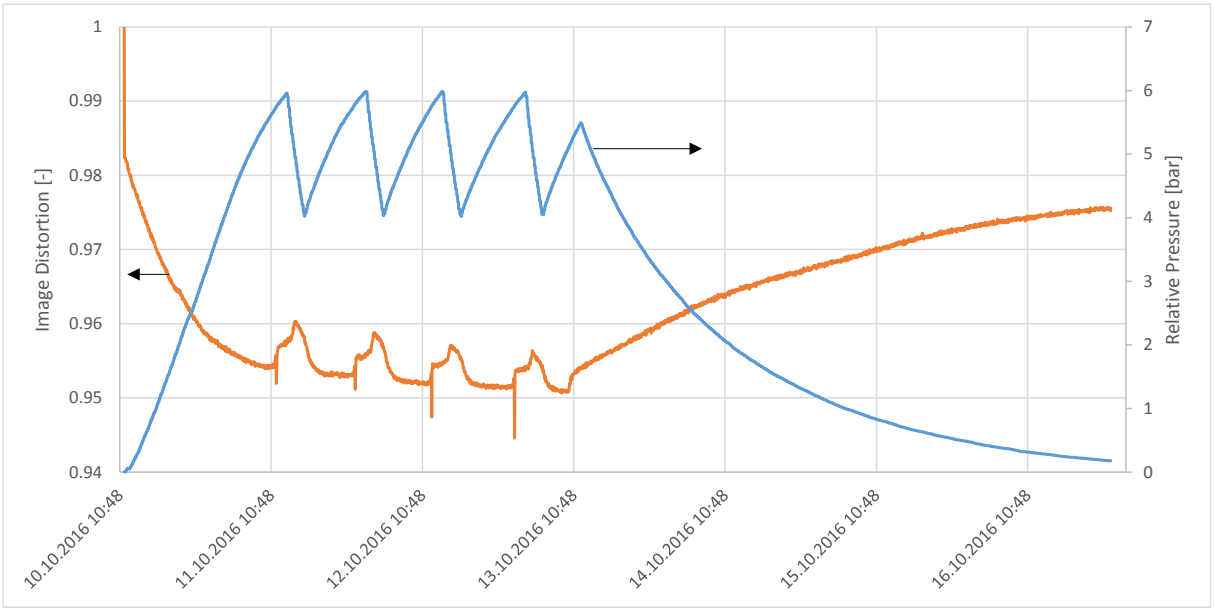

Fig. 7.50: Top: Image distortion and cavern pressure as a function of time for the camera looking at the TES for one of the tests. It can be seen that the image distortion follows the pressure change in the cavern, caused by change of humidity in the cavern. Bottom left: Image captured by the TES camera with cavern relative pressure at 0 bar. It can be seen that the pavement (bottom left) is wet. Bottom right: Image captured by the same camera with cavern relative pressure at 6 bar. The increased pressure impedes water in the mountain rock from entering in the pressure zone, causing the humidity to decrease and the pavement to partially dry.

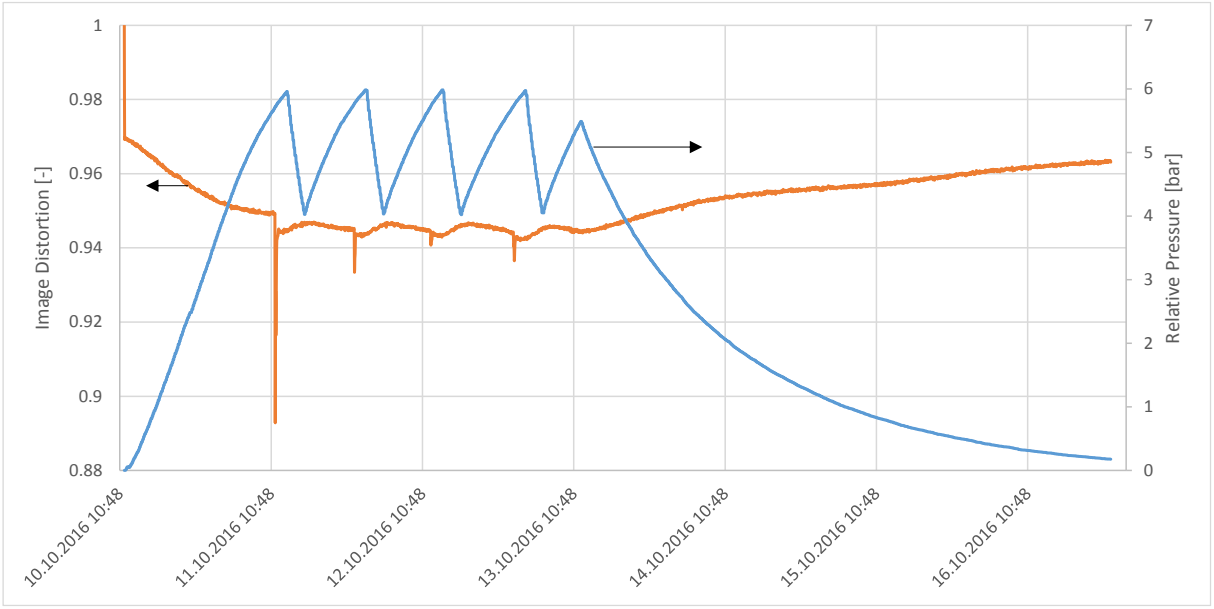

Fig. 7.51: Top: Image distortion and cavern pressure as a function of time for the camera looking at the pressure zone. It can be seen that the image distortion follows the pressure change in the cavern, caused by change of humidity in the cavern. Bottom left: Image captured by the Tunnel camera with cavern relative pressure at 0 bar. It can be seen that the pavement is quite wet. Bottom right: Image captured by the same camera with cavern relative pressure at 6 bar. The increased pressure impedes water in the mountain rock from entering in the pressure zone, causing the humidity to decrease and the pavement to partially dry.

8. Outcome & Discussion

The world's first pilot plant of an adiabatic compressed air energy storage technology was built and tested. The focus of the pilot plant was to assess the ability of caverns for compressed air storage with thermal energy recuperation. The turbo-machinery and other auxiliary parts were not the focus of the plant since those components are readily available in the market.

The plant was designed to store air at up to 33 bar and 550 °C using an unlined rock cavern in the Swiss Alps for which an unused tunnel in canton Ticino was transformed into the pilot plant. 120 m of the tunnel was closed with two 5-m thick concrete plugs. A proprietary thermal energy storage (TES) system was installed inside the pressure zone to store the heat during charging and release it during discharging. Temperatures, pressures and the geology was closely monitored to assess the performance of the plant.

With exception of the main plugs, all components worked as expected: The rock deformation was negligible and no significant losses were measured from the rock itself. The TES performed effectively and cooled down the incoming compressed hot air from 550 °C to ambient temperatures at its outlet, therefore, keeping the temperature in the pressure zone low and stable throughout the tests. No problems were observed with respect to rock integrity, rock deformation, or other issues with the electromechanical installations.

However, the main plugs, constructed at the two ends of the plant in order to contain the pressure, showed significant leakages, preventing the plant to achieve the design pressure. Therefore, the tests had to be done with a maximum pressure of 7 bar.

In addition to many smaller tests done during the commissioning, three 5 day long tests were conducted with pressure only (i.e. no heat) and two 5-day long tests were conducted with pressure and heat combined.

The plant efficiency, measured at the interface to the pressure zone, was in the range of 65-79% and the TES had a thermal efficiency of 75-89%.

The general conclusion of the project is highly favorable for ALACAES' proprietary technologies, i.e. the thermal energy storage and its performance when placed in the pressure zone, as well as regarding the ability of unlined rock caverns for compressed air energy storage. The main problem with the plant, i.e. the losses through the main plugs, was of civil engineering nature and not a patented or proprietary technology. ALACAES is currently investigating further steps to solve this problem (see Outlook below).

9. Conclusion

The questions raised in Section 6 can now be answered using the insight gained from the tests:

Q: Can an unlined cavern be used for cyclic loads? Is the rock displacement and air leakage from the rock acceptable and in line with theoretical calculations?

A: The unlined cavern showed to work without any problems for the storage of compressed air. The rock displacement was negligible and it could be concluded that no significant leakage occurs from the unlined rock. However, the significant losses from the main plugs did not allow to assess these assertions at the design point of 33 bar, and only a maximum pressure of 7 bar could be achieved in the cavern. The rock performance and suitability for air storage is generally dependent on whether the rock undergoes plastic deformation during cycling or if it stays in its elastic range. When cycling within the elastic limit, the deteriorating effect on the rock is expected to be very slow and hence the influence on air tightness as well. In contrast, if plastic behaviour occurs in every cycle, damages to the structure of the initially airtight bulk are to be expected in the long term. Applying basic principles of fracture mechanics, damages are most likely to occur eventually and they then tend to widen by amassing at interfaces (existing fissures / cracks in the bulk, interfaces between bulk and materials with different mechanical properties: grout zone, concrete, weakness zones). In order to assess the geological adequacy of a scale-up plant, simulations of the rock deformation need to be done in order to ensure that they stay in the elastic limit of the rocks. Also during operation of the plant, the deformations need to be monitored to ensure no plastic deformation of the rock.

Q: Can the concrete plugs effectively seal the pressure zone and does their deformation correspond to the simulated values using finite analysis?

A: While they did not show any relevant deformation during operation, it was observed that the concrete plugs were not able to effectively seal the pressure zone, and the increasing losses with increasing pressure prevented the pressure in the chamber to exceed 7 bar. While the investigation to the cause of this is still ongoing, preliminary analysis and expert opinion suggests that the problem is with the conceptual design of the plugs and not their construction. Geostock, a world-leading company in underground storage of pressurized hydrocarbons, suggest that in addition to the concrete plug and consolidation grouting, a “hydrodynamic containment” around the cavern is necessary to guarantee air-tightness. Hydrodynamic containment means that the volume around the pressure zone is saturated with pressurized water, therefore effectively preventing air leakage. However, a final conclusion is still to be made.

Q: How does the TES perform in a pressurized environment and how does it compare to ambient pressure applications?

A: The elevated pressure did not have any negative effect on the TES performance. This was anticipated because the TES does not have any pressure-sensitive components. ALACAES’ proprietary and patented solution to place the TES in the pressure zone also eliminates any stress on the TES walls thanks to the pressure equilibrium in and around the TES. Using a mathematical model developed by ETH Zurich, the TES performance was compared to ambient pressure performance and showed no significant difference.

Q: Can the TES effectively cool down the hot pressurized process air and avoid temperature increase in the cavern while also having an acceptable round-trip efficiency?

A: Clearly, as shown in the experimental campaign, the TES effectively and efficiently cools down the incoming air and releases the cooled pressurized air into the pressure zone. During the entire operation of the plant, despite having temperature sensors installed in the TES' vicinity, the chamber temperature was not affected by the TES, which was filled with 550 °C hot stones and air. During discharging, the TES effectively returned the stored heat to the outflowing air leaving the plant, and achieved round-trip efficiencies of 75-89%. The relatively low thermal efficiency is only due to the small size of the TES. As it will be shown in the Outlook, a commercial-size TES installed in a scale-up AA-CAES plant will achieve round-trip efficiencies of over 99%.

Q: How do the critical plant components perform in the pressurized zone (pipelines, flanges and connectors, instruments)?

A: All other plant components worked without any problems for the whole duration of the tests:

- The temperature of the pipelines carrying water and signal cables were monitored and stayed within acceptable limits. Strong temperature variation could have caused strong deformations which could have led to a catastrophic failure.
- The feeding pipe through the plug that carries the hot pressurized air was effectively cooled down using the combination of passive insulation and active air cooling, thus preventing heating up of the surrounding concrete that could have led to additional fissures in the concrete and therefore leakages.
- All instruments in the pressure zone worked without any problems including the signal connectors, a crucial component that is the interface between the pressure zone and the ambient.
- The temperature drop between the TES in the pressure zone and the heater outside the pressure zone was about 50 °C. While this would reduce significantly with higher mass flow rates in a commercial plant, the distance to the TES should be minimized and the piping insulation optimized.

The general conclusion of the project is highly favorable for ALACAES' proprietary technologies, i.e. the thermal energy storage and its performance when placed in the pressure zone, as well as the adequacy of unlined rock cavern for compressed air storage. The main problem with the plant, i.e. the losses through the main plugs, was of civil engineering nature and not a patented or proprietary technology. ALACAES is currently investigating further steps to solve this problem (See Outlook below).

10. Outlook

10.1. Mandate to Investigate Cause of Leakages

In order to understand the leakage problems that hindered the plant to achieve the designed 33 bar, ALACAES has given a mandate to the Geostock Group[14]. Geostock, founded in 1965 and part of the French Vinci Group, is a world-leader in underground storage of liquid, liquefied and gaseous hydrocarbons. It has offices in 7 countries around the globe and dozens of reference plants. After the site visit and initial analysis of the documents, their preliminary conclusion was that the technology used for the containment of air (i.e. concrete plugs with consolidation grouting) is necessary, but not sufficient for gaseous fluids, and that additional "hydrodynamic containment" using water curtains is required.

The final report is soon due and the results will be communicated to the SFOE.

Further, Geostock has also expressed interest in the technology. ALACAES and Geostock are currently evaluating possible ways of cooperation.

10.2. Suggested Modification to Plant to Reduce Leakages

Amberg Engineering has suggested modifications to the plant in order to reduce the leakages and be able to achieve the 33 bar. As part of the mandate, Geostock will also suggest certain modifications in their final report that will be communicated to SFOE. Some of the suggestions are:

- pre-stressing/sealing of the joints at the rock/concrete-interface by placing circumferential tubes between rock and plug which facilitate follow-up injections after the concrete has set and possibly again later (increase resistance to escaping airflow)
- place several identical plugs in series (further extend distance/reduce acting pressure gradient between pressurized chamber and ambient conditions)

However, their conclusion is that these measures are likely to be rather costly while there is no guarantee that they actually will succeed in sealing the plug leakage.

Upon receiving Geostock's final report and evaluating all the possible options, the ALACAES board of directors will make a decision on how to proceed and communicate the results to SFOE.

10.3. Scale-Up Plant Models

As mentioned in Section 4, two nation-wide research projects are currently ongoing about the AA-CAES technology in which ALACAES is the main industrial partner: a project of the Swiss Competence Center for Energy Research (SCCER) in collaboration with ETH Zurich, EPFL in Lausanne, PSI

[14] http://www.geostockgroup.com

and SUPSI, as well as an NFP 70 project with the same academic partners. While both projects are still ongoing, preliminary results have been produced and communicated to ALACAES for inclusion in this report.

Thermal Energy Storage Analysis for a Commercial Plant

The Professorship of Renewable Energy Carriers (PREC) at ETH Zurich developed a model to simulate the performance of an ALACAES type Thermal Energy Storage (TES) in a commercial AA-CAES plant. The model is developed by Lukas Geissbühler in cooperation with Viola Beccatini, under the supervision of Dr. Andreas Haselbacher in the PREC lab of Prof. Aldo Steinfeld. It uses a quasi-one-dimensional model for the TES with temperature-dependent air, rock, and insulation properties linked to a cavern model to simulate the thermodynamic behavior of the pressure chamber. So far the model calculates only the TES performance indicators such as TES efficiency values and losses as well as the pressure chamber temperatures. The model has been validated with the experimental results from the pilot plant during the course of the tests, therefore ensuring a high reliability of the model results with respect to real-life conditions.

The main plant data is summarized in Table 10.1.

Plant Rated Power [MW]	100	Plant Rated Capacity [MWh]	500
Cavern Volume [m^3]	226‘000	Max/Min plant pressure [bar]	90/70
TES Volume [m^3]	9‘500	Insulation Thickness walls/lid [m]	0.1/0.15
TES Bottom Radius [m]	12.26	Charging/Discharging Duration [h]	4.8
TES Top Radius [m]	16	Charging/Discharging Mass Flow Rate [kg/s]	200
		TES charging Temperature [°C]	550

Table 10.1: Plant data used for the TES simulation in an AA-CAES plant by ETH Zurich.

The simulation consisted of a pre-charging period followed by 100 cycles of 4.8 h charging/discharging and finally a 10 day idle period.

The results are shown in the following graphs.

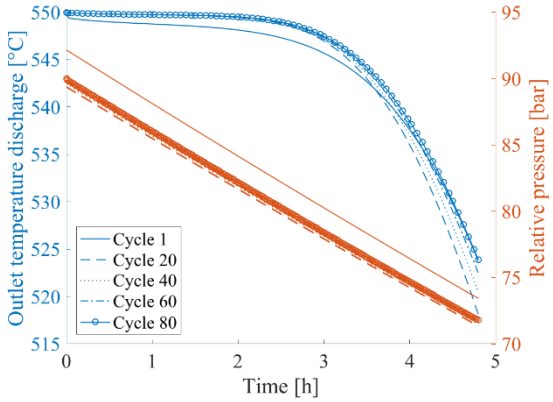

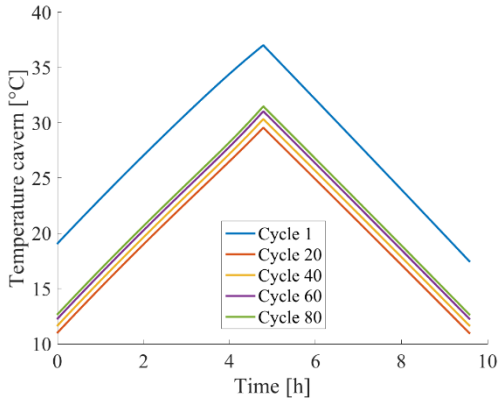

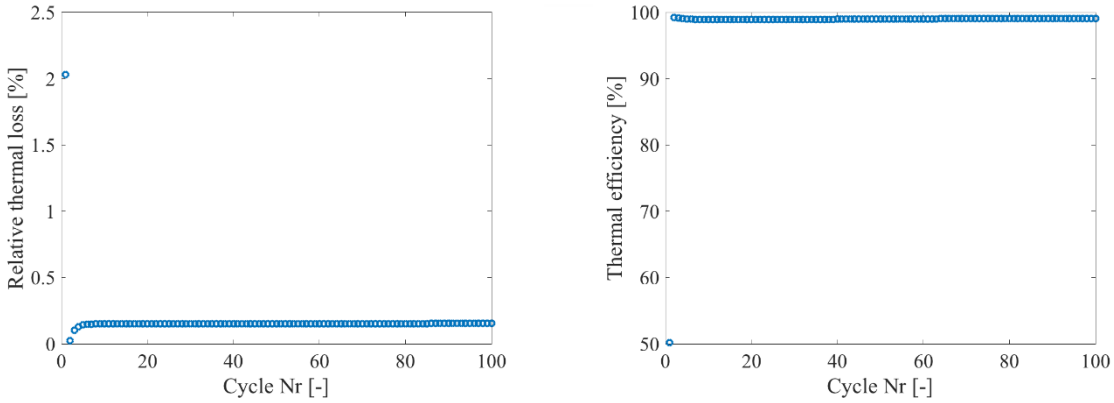

Fig. 10.1: TES and cavern performance data for a 500 MWh scale-up AA-CAES plant: Top left: The TES outlet temperature and cavern pressure variation during discharging runs. Top right: Cavern temperature variation during cycling. Bottom left: TES thermal losses per cycle as a percentage of incoming energy. Bottom right: TES thermal efficiency as a function of cycle number.

The above graphs give crucial and important information about the thermodynamic performance of the TES and pressure cavern for a commercial plant:

- The TES outlet temperature during discharging stays above 520 °C which is crucial for the operation of the downstream turbine.
- The cavern temperature does not exceed 30 °C during cycling which is important for the structural integrity of the cavern and to avoid thermal effects on the rock.
- The thermal losses of the TES per cycle as a percentage of incoming energy per cycle are below 0.2%, demonstrating the adequacy of the TES to store and release heat.
- The thermal efficiency of the TES, defined as the ratio of output energy during discharging to input energy during charging, is above 99%.

Further, the idle time losses were about 0.2% per day. These results support the assertions made in Section 7.2 that the TES performance significantly increases with size.

Overall Plant Analysis for a Commercial Plant

The Mechanical Engineering and Materials Technology Instititue (MEMTI) at SUPSI developed a model that incoporates the TES model by ETH Zurich in a comprehensive plant model that takes into account real-world compressor and turbine data and accounts for auxiliary and parasitic losses as well as turbine and compressor ramping times. The model is being developed by Jonathan Roncolato in cooperatin with Marco Fossati and Simone Zavattoni under the supervision of Prof. Maurizio Barbato. It uses Mathworks' Simscape coupled with the TES model from ETH with temperature dependent air properties. This model allows to optimize the plant configuration and operating conditions and to obtain the overall plant performance parameters.

The schematic plant layout is shown in Fig. 10.2 and the plant data is summarized in Table 10.2. While the plant layout details are out of the scope of this report and subject to optimization, it gives an overview of how a commercial plant might look like.

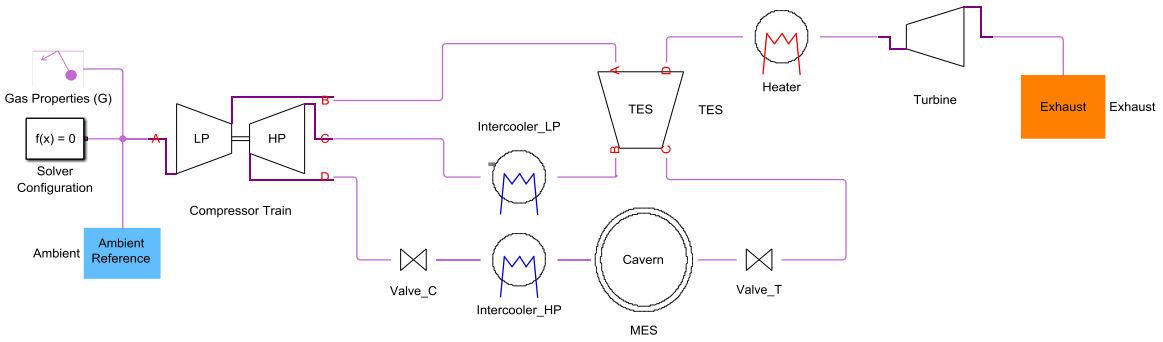

Fig. 10.2: Schematic plant layout of the scale-up AA-CAES plant simulated by SUPSI.

Plant Rated Power [MW]	145	Plant Rated Capacity [MWh]	650
Cavern Volume [m^3]	170‘000	Max/Min plant pressure [bar]	70/40
Compressor Efficiency [%]	0.85	Charging/Discharging Duration [h]	4.8
Turbine Efficiency [%]	0.9	Charging/Discharging Mass Flow Rate [kg/s]	185/255

Table 10.2: Plant data used in the scale-up simulations by SUPSI.

The following graphs summarize the plant performance.

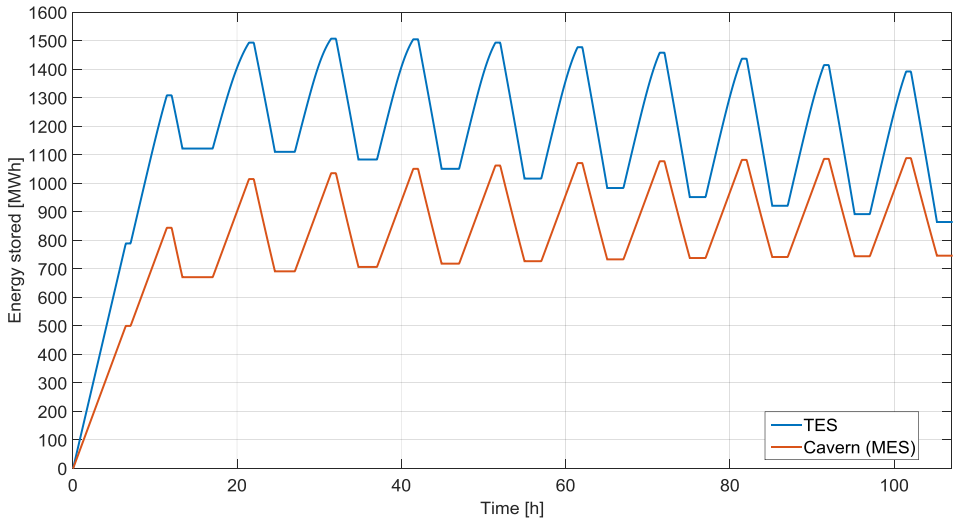

Fig. 10.3: Energy Stored in the TES and in the cavern during plant operation.

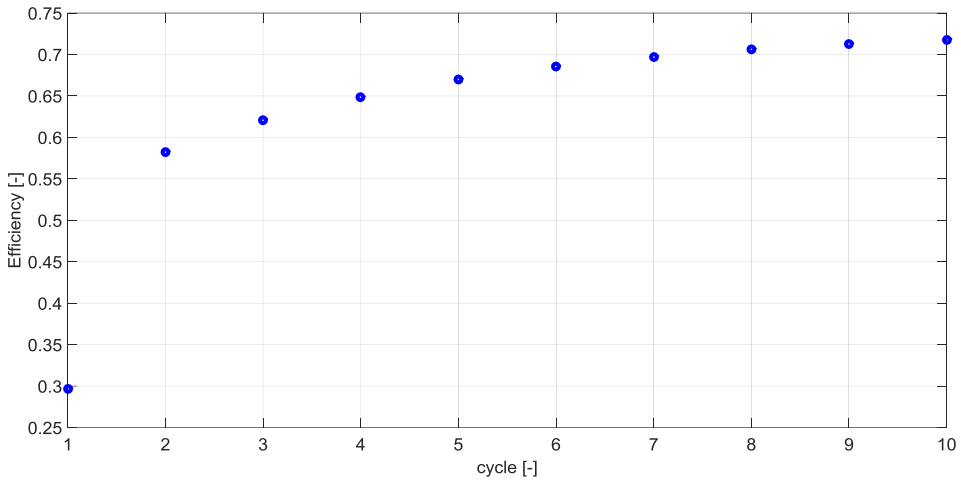

Fig. 10.4: Overall plant cycle efficiency, taking into consideration all auxiliary power and parasitic losses.

It can be extracted from the above graphs that:

- Around 60% of the energy stored in an AA-CAES plant is stored in the form of heat in the TES
- The cycle efficiency at steady state operation (after 8-9 cycles) approaches 72%.